(12) LEVEL I

# Semiannual Technical Summary

## Seismic Discrimination

31 March 1981

Prepared for the Defense Advanced Research Projects Agency
under Electronic Systems Division Contract F19628-80-C-0002 by

**Lincoln Laboratory**
MASSACHUSETTS INSTITUTE OF TECHNOLOGY
*Lexington, Massachusetts*



Approved for public release; distribution unlimited.

The work reported in this document was performed at Lincoln Laboratory, a center for research operated by Massachusetts Institute of Technology. This research is a part of Project Vela Uniform, which is sponsored by the Defense Advanced Research Projects Agency under Air Force Contract F19628-80-C-0002 (ARPA Order 512).



The views and conclusions contained in this document are those of the contractor and should not be interpreted as necessarily representing the official policies, either expressed or implied, of the United States Government.

The Public Affairs Office has reviewed this report, and it is releasable to the National Technical Information Service, where it will be available to the general public, including foreign nationals.

This technical report has been reviewed and is approved for publication.

FOR THE COMMANDER

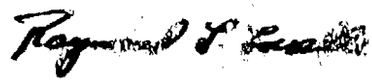

Raymond L. Loiselle, Lt. Col., USAF
Chief, ESD Lincoln Laboratory Project Office

MASSACHUSETTS INSTITUTE OF TECHNOLOGY

LINCOLN LABORATORY

# SEISMIC DISCRIMINATION

## SEMIANNUAL TECHNICAL SUMMARY REPORT TO THE DEFENSE ADVANCED RESEARCH PROJECTS AGENCY

1 OCTOBER 1980 – 31 MARCH 1981

ISSUED 28 SEPTEMBER 1981



Approved for public release; distribution unlimited.

LEXINGTON



MASSACHUSETTS

## ABSTRACT

This Semiannual Technical Summary describes the Lincoln Laboratory Vela Uniform program, ~~for the period 1 October 1980 through 31 March 1981~~, Section I describes progress in the development of a prototype Seismic Data Center. This development is on schedule, and a first version of the prototype will be operational during the next six months. Section II describes a series of activities in the development and implementation of the seismic processing techniques that will be utilized in the prototype system. Section III describes a series of investigations in General Seismological Research.

CONTENTS


| | | |
|---|---|---|
| | Abstract | iii |
| | Summary | vii |
| I. | SEISMIC DATA CENTER DEVELOPMENT | 1 |
| | A. Progress in Seismic Data Center (SDC) Development | 1 |
| | B. Seismic Processing in the Prototype SDC | 1 |
| | 1. DP – Detection Processing | 2 |
| | 2. ABAR – Arrival Based Analyst Review | 2 |
| | 3. MERGE – Merge Parametric Data Sources | 2 |
| | 4. AA – Automatic Association | 3 |
| | 5. EBAR – Event Based Analyst Review | 3 |
| | 6. BUL – Bulletin Preparation | 3 |
| | C. Waveform Display on the SAS | 4 |
| | D. Waveform Database Subsystem | 5 |
| | 1. Waveform Database Sizing Requirements | 5 |
| | 2. Reliability Requirements | 6 |
| | 3. The Initial Prototype | 6 |
| | 4. Final Prototype | 7 |
| | E. Access Routines for the Parameter Database | 7 |
| | F. Application of the MUMPS System to the Parameter Database | 8 |
| | G. Remote Seismic Terminal | 8 |
| | H. VAX UNIX Installation | 11 |
| II. | SEISMIC PROCESSING TECHNIQUES | 13 |
| | A. Seismic Algorithm Development: Overview | 13 |
| | B. IDCE Database | 13 |
| | C. Detection Algorithm | 15 |
| | D. Detector Evaluation With IDCE Data | 17 |
| | E. Automatic Timing and Analysis of Digital Data | 22 |
| | F. Use of the Multiple-Arrival Recognition System (MARS) for Timing and Identifying Seismic Body Waves | 26 |
| | G. Syntactic Analysis of Regional Seismic Signals | 27 |
| | H. Rayleigh-Wave Azimuth Detector | 30 |
| | I. Association of Rayleigh Waves | 33 |
| | J. SRO/ASRO Rayleigh-Wave Detections | 35 |
| III. | GENERAL SEISMOLOGY | 47 |
| | A. Further Surface-Wave Analysis of Eastern Kazakh Presumed Explosions | 47 |
| | B. Induced Thrust Faulting at NTS? | 52 |
| | C. Crust and Upper-Mantle Structure of the Middle East and South Central Asia | 55 |
| | D. Numerically Stable Calculation of Mode Eigenfunctions | 56 |
| | E. The Waveguide of Lg | 57 |
| | F. Inversion for Multiple Sources | 59 |
| | G. Routine Determination of Source Parameters from the Analysis of Waveforms Recorded by the Global Digital Network | 61 |

H. Exact Numerical Solution for a Propagating Line Source and the Method of Centroid Location 64

I. The Excitation of Seismic Waves by a Source Spanning a Surface of Discontinuity 68

J. A Linear Approximation to the Effect of Finite Rupture Length and Rupture Velocity on the Radiation From Seismic Sources 72

K. The Calculation of the Complete Normal-Mode Spectrum of the Earth Using Finite Difference Methods 73

Glossary 95

## SUMMARY

This is the thirty-fourth Semiannual Technical Summary (SATS) report describing the activities of Lincoln Laboratory funded under Project Vela Uniform. This report covers the period 1 October 1980 through 31 March 1981. Project Vela Uniform is a program of research into the discrimination between earthquakes and nuclear explosions by seismic means. An important recent emphasis of the project is in the development of data-handling and analysis techniques that may be appropriate for the monitoring of a potential Comprehensive Test Ban Treaty. The FY 1981 program consists of the development of a prototype Seismic Data Center (SDC), which will fulfill U.S. obligations that may be incurred under such a Treaty, and which will also provide a data resource to the seismological research community. The program also contains an element of seismic research, with emphasis on those areas directly related to the operations of the SDC.

Substantial progress has been made in the development of the first version of the prototype SDC. In the absence of a Local Computer Network, which will be delivered during the next quarter, the Seismic Analysis Station (SAS) and database subsystems are being developed as stand-alone systems. Seismic processing techniques are being developed on our general-purpose computers. We have now demonstrated the capability to read input seismic data, carry out signal detection and the automatic extraction of a variety of signal parameters, and display the detected waveforms for analyst review. A variety of additional analyst software tools will be installed soon on the SAS. The waveform and parameter database systems are being developed on the SAS as local facilities, and they will be expanded to system-wide databases at a later stage. A Remote Seismic Terminal, capable of limited waveform display and analysis and remote interaction with the SDC over dial-up lines, has been demonstrated.

An important effort during this period has been the development and implementation of a variety of seismic processing algorithms for automatic signal analysis, and analyst interactive review. A package of programs for automatic analysis of incoming data has been installed on our VAX 11/780 computer. These include programs for signal detection, onset time measurement, amplitude and period measurement, and discrimination between local and teleseismic events. In the prototype SDC, provision is made for analyst review and modification of each of these measurements. The output sets of arrival parameters are then merged with any external arrival data into a local parameter database. This is followed by automatic association into a preliminary event list, analyst review of the output using available waveform data, and final event bulletin preparation. We are continuing to evaluate and develop a series of additional algorithms for phase identification, azimuth measurement, and association of long-period arrivals with events determined from short-period data.

Other seismological research has continued in several areas. Previous work on anomalous surface-wave excitation by presumed explosions in the Eastern Kazakh region has been extended. A variety of evidence is given in support of the hypothesis that thrust faulting accompanies these unusual events, and that at least some observed tectonic strain release by Nevada Test Site events can also be attributed to this type of faulting. Other studies include: an inversion of Rayleigh-wave phase and group mantle structure in the Middle East and South Central Asia; a method for the evaluation of mode eigenfunctions for P and SV motion in a layered medium, which is numerically stable; and an application of this technique to the study of the excitation of the Lg phase as a function of source depth. A generalization of the method

of centroid location to the estimation of source parameters (particularly moment and hypocenter) for events close in time is described and applied to the resolution of explosion and earthquake sources, and to the modeling of finite seismic sources. In another investigation, the effect of a boundary on the radiation from seismic sources is evaluated, with particular emphasis on contributions to the moment tensor. It is shown that assumptions about the boundary are necessary if a proper interpretation of the moment tensor is to be obtained. The application of finite difference methods to the calculation of normal-mode eigenfrequencies and eigenfunctions so that seismogram synthesis may be performed at higher frequencies is discussed.

M. A. Chinnery

# SEISMIC DISCRIMINATION

## I. SEISMIC DATA CENTER DEVELOPMENT

### A. PROGRESS IN SEISMIC DATA CENTER (SDC) DEVELOPMENT

During this report period, development has continued on the various subsystems of the prototype SDC.[1] Particular emphasis is being placed on the development of the Seismic Analysis Station (SAS), the waveform database, and the parameter database. Hardware acquisition for these subsystems is now complete. The Local Computer Network, which will link these subsystems, is being built by a subcontractor and is scheduled for delivery within a few months.

The first operational version of the SDC is being built up around a combination of the SAS and a general-purpose (VAX 11/780) computer, with local waveform and parameter databases. This early version will provide both a test bed for the refinement of the man-machine interface and will also help to define the structure of the databases for implementation on a system-wide basis early in FY 82. The VAX also performs all seismic processing tasks, and is therefore acting as a test bed for the Automatic Processing Subsystem.[1]

Initial software implementation on the VAX and SAS is essentially complete. Seismic data received as part of the International Data Collection Experiment (IDCE) can now be processed using a variety of algorithms (see Sec. II of this report). The local waveform database is a development of the "gram file" concept,[2] and the local database is an improvement on the "Mod I system."[3] Each of these will be available to the analyst using the SAS. Display software for the SAS has been based on a "display" system evolved previously.[2] Each of these components is described in the contributions that follow.

During the past six months, substantial effort has also been expended on the development of a Remote Seismic Terminal (RST), which will form a low-cost remote facility for limited waveform analysis and interaction with the SDC. This unit was demonstrated to the UN Committee on Disarmament in February 1981.

Specifications for the Communications Interface Subsystem, which will link the SDC to incoming data streams, are being formulated on the basis of discussions with DOE. This will be built by a subcontractor during the next six months.

We continue to interact with DOE, DARPA, and various DARPA subcontractors to ensure that our approach to the prototype SDC is state-of-the-art.

M. A. Chinnery
A. G. Gann

### B. SEISMIC PROCESSING IN THE PROTOTYPE SDC

This section describes the seismic processing steps that will be performed in the Version 1 of the Seismic Data Center prototype, SDC-V1. The goal of SDC-V1 is to provide many of the capabilities of the SDC as quickly as possible so that operational experience with SDC-V1 can lead to rapid improvements in later versions. The capabilities of SDC-V1 will include:

(1) Automatic detection of arrivals using waveform data from various sources.

(2) Analyst review and refinement of automatic detections using interactive graphics.

(3) Combining automatic detections and external arrival times to produce an arrival database.

(4) Combining external event bulletin information into a parameter database.

(5) Automatic association of arrivals to produce a preliminary bulletin.

(6) Analyst review and refinement of the preliminary bulletin.

(7) Production of final-event bulletins based on several event-selection criteria.

Routine analysis will have the following major steps:

| | |
|---|---|
| DP | Detection Processing |
| ABAR | Arrival Based Analyst Review |
| MERGE | Merge Parametric Data Sources |
| AA | Automatic Association |
| EBAR | Event Based Analyst Review |
| BUL | Bulletin Preparation |

Normally, processing will proceed from one stage to the next, but circumstances occasionally will require that one or more stages must be redone.

The following subsections briefly describe the processing and software involved in each stage.

1. DP – Detection Processing

Inputs: Continuous waveform data stored in GRAMFILE format. Waveform data are currently received on magnetic tape in various formats. Programs which read the tapes and store the waveforms in a GRAMFILE database are available.

Outputs: A GRAMFILE database which contains waveform segments of the interval around the arrival time, and a time-ordered list of detected arrival times and related parameters.

Processing: The detection processing is done in two steps. First, a detection algorithm is run on the continuous waveforms to detect arrivals and produce waveform segments. A second process is run on the segmented data to refine the onset time and measure other parameters.

2. ABAR – Arrival Based Analyst Review

Inputs: The outputs of the previous step.

Outputs: The arrival list and waveform database are revised to reflect improvements made by the analyst.

Processing: Using the DISPLAY command, the analyst inspects the waveform data corresponding to each pick, one at a time, and makes any adjustments and additional measurements that might be required. Waveform data which have been provided to the SDC in segmented form, such as from SRO stations, can be inspected in this way also. Once the analyst is finished, the second stage of the DP is run to redo any automatic measurements as necessary.

3. MERGE – Merge Parametric Data Sources

Inputs: Internal arrivals from the previous step and arrival data from external sources such as the WMO/GTS.

Outputs: A uniform parametric database for a given time interval. This database will contain at least a time-ordered arrival list, and a time-ordered event list if event information is available from external sources. Currently, this database is in MOD1 PARAMETERFILE format.

Processing: To date, the parametric data created by the previous steps have been kept in a form convenient for the detection and arrival review process, in separate databases for each station for example. These data will be merged with any external arrival or event information to produce a parametric database. External data may require extensive preprocessing and editing. The sorting and editing tasks are performed using standard UNIX commands, and EDPF – the PARAMETERFILE editor.

4. AA – Automatic Association

Inputs: The parametric database produced in the previous step.

Outputs: A parametric database augmented with event locations, and GRAMFILE databases for each event for use with DISPLAY during EBAR.

Processing: An Automatic Association (AA) algorithm is run on the parametric database. AA searches the arrival list and identifies group arrivals that belong to an earthquake. The arrivals are then used to locate the event, and the event is added to the database. This process is repeated for the entire arrival list. The resulting database can be used to produce a preliminary event bulletin.

After association, the waveform data are grouped by event for use in the following step.

5. EBAR – Event Based Analyst Review

Inputs: Outputs from the previous step.

Outputs: A refined parameter database.

Processing: An analyst is again given an opportunity to review the results of automatic processing, using DISPLAY in conjunction with the parameter database editor, DEV. However, at this point he has much more information to go on, namely the event hypotheses produced by AA. The analyst may need to do many operations on the waveform and parametric data. For example, to refine an event location an analyst may need to display the waveforms corresponding to a subset of the arrivals associated with this event, adjust picks or other parameters, alter associations, and relocate the event. This process may have to be iterated several times for each event.

6. BUL – Bulletin Preparation

Inputs: The parametric database from the previous step.

Outputs: Various event bulletins.

Processing: Once the parameter database has been processed to the satisfaction of the analyst, event bulletins can be produced as needed. This task will be done by a senior analyst who is responsible for bulletin preparation and ensuring that the parameter database is complete, consistent, and that its analysis is complete.

K. R. Anderson

## C. WAVEFORM DISPLAY ON THE SAS

The SAS is the principal user terminal for performing the operational and research functions of the SDC. The current prototype consists of a PDP-11/44 computer, Megatek 7000 graphics display, two Datagraphix 132-A alphanumeric displays, disks, and tapes. This subsystem will be linked to the rest of the SDC subsystem through the local computer network when it is installed. The current prototype is being used to evaluate display techniques for waveform data, the integration of waveform and parameter data processing, and the development of enhanced software for the SAS subsystem itself.

A program called DISPLAY was developed several years ago on the PDP-11/50 to allow seismologists to interactively analyze a waveform database on the Tektronix 4014 graphics terminal. DISPLAY plots a subset of the waveforms in a database, and then allows the user to interactively set and delete markers, change vertical and horizontal scaling, post amplitude and time scales, and move the waveforms left and right. We have converted DISPLAY to run on the prototype SAS. The graphics primitives originally in DISPLAY were replaced by calls to Graphpac, a faster set of graphics routines which originally were also used on the Tektronix. Conversion of DISPLAY to the Megatek was completed by using a set of device specific graphics routines developed by Purdue University. As it now stands, DISPLAY calls Graphpac which, in turn, calls the Purdue routines to display information on the Megatek graphics terminal. All the options available in the original DISPLAY program designed for the Tektronix 4014 graphics terminal can now be used with the Megatek 7000 graphics terminal on the PDP-11/44.

Complementing this approach, we are working on a variety of performance enhancements. Here, software at the device specific, function primitive, and system levels will be designed and implemented to facilitate new waveform manipulations, for which the original software is too deficient structurally to be modified appropriately.

Intrinsic in this dual approach is a layered, or fine-grained approach to software development. Conceptually, three levels or layers of software are involved: (1) a command level; (2) the function primitive level; and (3) the device specific or system levels. The command level is a user interface accepting input from the user and dividing his commands into more elementary function primitives related to display and database tasks. The function primitives retrieve and process data necessary for display tasks and create various device specific and system level function calls necessary to drive the graphics and other hardware.

This layered structure underlying the software permits separation of the user interface from device specific and lower-level data-handling considerations. As later generations of graphics and device specific primitives emerge, permitting, for example, increasingly complex waveform scrolling, overlaying and geometric transformation functions, they may be implemented in terms of existing or slightly modified upper layers operating with a new bottom level to the system. As experience is gained with command languages and user interfaces, increasingly facile ones can be implemented while retaining existing lower levels to the system. At any time, as at present, a working system is available which can be utilized for seismic analysis and as a laboratory for discovering improved graphics techniques for seismic analysis.

P. T. Crames
J. Hirsch

## D. WAVEFORM DATABASE SUBSYSTEM

The Database Subsystem of the SDC consists of two conceptually separate parts, the waveform database and the parameter database. The waveform database must receive the telemetered waveform data from the communications interface subsystem, store it in the on-line working set, archive it in permanent storage, and process retrieval requests for specific blocks of waveform data. The parameter database receives parametric data from various subsystems in the SDC, updates the database, and processes retrieval requests for parametric data for other subsystems in the SDC.

This section describes a preliminary specification for the waveform database component of the SDC. Two systems are mentioned: the initial prototype, which should be completed by October 1981; and the final prototype, which is projected for FY 1982. The initial prototype is a simple system that stores only waveform data; parametric data will be stored locally at the Seismic Analyst Station. The final prototype will integrate both waveform and parametric data storage and retrieval.

### 1. Waveform Database Sizing Requirements

The final prototype must be able to absorb incoming data at a rate of 200 kbps. This figure is double the expected 100-kbps nominal data rate from 30 National Seismic Station (NSS) instruments. Doubling the expected rate allows for retransmission after perious of Data Center shutdown or communications failure. Also, it will allow moderate increases in the nominal data rates caused by additional NSSs and other data sources, such as Seismic Research Observatory (SRO) data on magnetic tape. The design should permit expansion beyond this data rate since additional NSSs and other data sources may be added to the system. However, the desire for expandability should not drive the design to unrealistically ambitious aims.

The requirements for the initial prototype will be much less demanding. The data source will be five NSSs of the Regional Seismic Test Network (RSTN). Each station provides roughly 2.4 kbps, so the incoming data rate will be about 12 kbps. There are no initial reliability requirements, so a guideline data rate of 20 kbps should allow for adequate expansion.

Both the initial and final prototypes should be able to retain all incoming data on-line during a 5-day bulletin preparation period. The resulting capacity requirements for unprocessed data during various time periods are displayed in Table I-1. Note that these calculations assume no data conversion or data compression since disk formats have not yet been defined. In addition,

TABLE I-1
WAVEFORM SIZING REQUIREMENTS

| Data Rates | Initial Prototype | Final Prototype |
|---|---|---|
| Kilobits/second | 20.0 | 200 |
| Kilobytes/second | 2.5 | 25 |
| Megabytes/day | 216.0 | 2,160 |
| Megabytes/5 days | 1,080.0 | 10,800 |

space will be required for indices and other system-controlled areas, and for parametric data in the final prototype.

### 2. Reliability Requirements

The following reliability requirements apply to the final prototype system. They are not required for the initial prototype.

In general, data should continue to be stored somewhere within the Data Center during routine maintenance and small-scale component failures. Retransmission from external sources should be required only for recovery from extensive failures. This means that either the waveform database must use a non-stop implementation or the Communications Interface must be able to retransmit data. Details of these approaches will be examined and the choice of approach will be made during the design of the final prototype.

Authentication of the incoming data is performed by the Communications Interface. Therefore, all data reaching the waveform database are assumed to be valid. Some data may be retransmitted to the Data Center after failure of the data network supplying the data, or complete failure of the Communications Interface. Multiple transmissions of data should match the original transmission. Mismatches should be detected and some technique, perhaps manual, should be employed to determine what data are valid.

### 3. The Initial Prototype

The goal of the initial waveform database prototype effort is to quickly develop an implementation of the waveform database that supplies the functionality essential to the analyst's work. This approach will provide a foundation for developing and refining functions that the automatic processing tasks and analysts require the waveform database to perform. This early experience with an operational Data Center is essential to determine what features are really required, and will guide the design of the final prototype.

The initial prototype waveform database will be implemented using the UNIX† operating system on a single DEC VAX 11/780 processor with 4 Mbytes of primary memory. The configuration will include four 600-Mbyte disk drives for waveform storage during bulletin preparation. Received data will be archived on 6250-bpi density magnetic tape.

The Communications Interface will supply authenticated data to the waveform database using magnetic tapes. Alternate approaches include a connection to the Communications Interface via a direct point-to-point data connection or the local network. The final approach we use will depend on availability of the Sytek Local Network Interfaces.

A high-speed point-to-point data connection will be used to connect the Seismic Analyst Station and the waveform database since the Sytek Local Network Interfaces will not be available soon enough to be used for this application. Magnetic tape was ruled out for this connection because the extra manipulation required to transfer data via magnetic tape would limit the implementation to batch-style strategies and require undesirable analyst action to manipulate the tapes.

Existing software will form the basis of the waveform database implementation. This approach simplifies transporting existing programs to the VAX, since these programs already use a consistent database format and access subroutine library. It also simplifies implementation

† UNIX is a trademark of Bell Laboratories.

of new programs since our seismic research personnel are already familiar with the existing database formats and access routines. Also, the maturity of the existing routines makes them far more reliable than new software would be.

The remaining development of the initial waveform database involves enhancements to the existing database software and interfacing the waveform database with the Seismic Analyst Station and the Communications Interface. The level of effort required will depend on how difficult hardware installation and software performance and functional enhancement prove to be.

We are just completing the hardware procurement. The disk and tape peripherals have arrived and are being installed. We expect the intercomputer links to arrive during the first week of April 1981. Software for these devices has been developed at other installations and we are in the process of acquiring copies. We expect installation to be finished by the end of April.

The file system performance of UNIX should be adequate for the 2.5-Mbyte/s design data rates required by the initial prototype. Additional benchmarks must be done under varying load conditions when the large disks and high-density tapes have been installed to determine whether performance issues will require special index structures not supplied by the UNIX file system.

4. Final Prototype

We are beginning the specification of the final prototype. The design will encompass both the waveform and parametric databases. Several critical design areas such as user interface, reliability, extensibility, and data compression have been identified. We plan to elaborate and refine the design during the next few months using our experience with the initial prototype to guide our efforts. The design should be completed and implementation started by October 1981.

K. J. Schroder

## E. ACCESS ROUTINES FOR THE PARAMETER DATABASE

Work has progressed on our parameter database access routines, a set of file management subroutines which enable the user to create and modify files of fixed-length records flexibly. The access routines have been used by applications programs during the Mod I project, and will be used, in enhanced form, in the development of the SAS. Briefly, records may contain parameters of several different types; the user describes the layout of a typical record in a C structure, and then calls routines to add, delete, change, and find records. To date, we have been able to access these records by two slow methods: physically sorting the file on a desired key and then using binary searches to locate the desired record, and sequentially searching through all the records until the desired key is found. These access methods were developed so that we could test the user interface of the access routines as soon as possible, without special regard for speed or operating efficiency. The sorting of records is not efficient since we can only sort on one parameter at a time. Even though fast searches can be made on the order of $\log_2 N$ (where N equals the number of records in the file), insertions and deletions require that, on the average, N/2 records be physically moved. The sequential searches are not efficient because, on the average, N/2 records must be read before the desired record is found.

We have now developed a third method of accessing records, B+ trees. This method is very fast, but somewhat more disk storage space is required than with the other two methods.

B+ trees, developed by R. Bayer and E. McCreight,[4] allow retrieval, insertion, and deletion in time proportional to $\log_k N$, where N is the number of elements in the index. In our scheme, the value of k depends on the indexed variable's type, as follows: k is 30 for variables typed as double, 60 for floats, and 120 for integers because they are 8-, 4-, and 2-byte-long variables, respectively, in a 240-byte fixed-length record. Using floats as an example, we can access any of 60 keys with one disk access, 3,600 keys with two disk accesses, and 216,000 keys with three disk accesses. A penalty is paid in terms of disk storage space, because a B+ tree must be built for each variable indexed. Besides their fast random-access speed, B+ trees allow even faster sequential accesses. Once the desired key is located in the tree, the next higher or lower key can be accessed directly because a pointer to each is present.

P. T. Crames

## F. APPLICATION OF THE MUMPS SYSTEM TO THE PARAMETER DATABASE

A sample parametric database and associated query capability were developed using the MUMPS language and operating system available on the PDP-11/44. This implementation of MUMPS is a stand-alone system optimized for database applications. The system includes the operating system, data management system, and query language. Since the query language is interpreted, and not compiled, and the basic primitives are aimed at string manipulation, it was possible to develop a prototype system very quickly, in less than two weeks.

The database was transferred from a UNIX system via magnetic tape, and loaded into a MUMPS database structure which had been designed for query access efficiency (the basic data structure in MUMPS is Multi-way trees[5]). Query capability included selection of stations, time intervals, latitude and longitude ranges, magnitude, and arrival type. In addition, the bulletin, arrival, and event print functions of the Mod I library were duplicated within MUMPS.

Comparison of this implementation with the implementation of Mod I under UNIX in C revealed comparable storage efficiency and superior access efficiency. Specifically, the bulletin and arrival print functions, running on the same day's worth of data, with identical environments (same hardware, single-user mode), ran approximately 30-percent faster with MUMPS than with UNIX. In terms of storage, the MUMPS file handler required approximately 65 kbytes for the sample database, compared with 72 kbytes on the UNIX system. The MUMPS figure also includes ancillary inverted files created for the query capability which did not exist in the UNIX file structure.

The interpretive character of the MUMPS language makes it likely that, given equal levels of skill in the two environments, it would be easier and faster for developing the parametric database. The main issue is the network interface. Because the available implementations of MUMPS for the PDP-11 are stand-alone systems, they would have to be modified to handle the network interface as developed by Sytek. Neither of the two vendors (InterSystems and DEC) is interested in performing this work. For this reason, it is apparent that, although MUMPS is an attractive environment for the parametric database, it would not be possible to use it in the networked environment planned for the SDC.

H. Lison

## G. REMOTE SEISMIC TERMINAL

The Remote Seismic Terminal (RST) is a microcomputer-based display and communication system designed to support the analyst faced with the processing of data from a seismic station,

the communication of seismic data to the SDC, and the receipt of the SDC bulletin at a remote location. It is an alternative to the manual processing of seismic data and will provide computer-assisted communication with the SDC. In its basic form, the RST will provide support to the analysis of digital waveform data and will partially automate the measurement and extraction of seismic parameters. In expanded versions, the RST can digitize waveform data and provide a variety of tools for the analysis of digital data. An overview of the design of the RST and a discussion of its capabilities are given.

The RST is a modular microcomputer and peripheral system plus a modular suite of software designed to provide communications with the SDC, waveform display capability and support for creation of International Exchange of Seismic Data (IESD) Level I (parametric data) data reports.

The RST hardware consists of a chassis containing a microcomputer and associated memory and peripheral boards, an alphanumeric terminal, a graphics terminal, a floppy disk, and a modem for communications. The main chassis provides power supplies and the means for interconnection of the other boards via the standard S-100 bus.

In the main chassis are four boards plus the memory boards. The first is a California Computer Systems (CCS) CPU board, which is a Z80 CPU. Second, the Morrow disk controller board operates the floppy disks. Third, the Scion graphics display is controlled by a separate board which has its own Z80 and memory connected to an internal bus. Communication with the system is via I/O ports, and the board produces video for driving the monitor. The final mainframe board is a Morrow Designs "Switchboard" which incorporates two serial and four parallel ports plus a status port.

There are four memory boards in the RST. The Z80 can only address 64K of memory but the S-100 bus allows the switching of multiple, independent memory banks into the Z80 address space. A 16K static RAM is used for the stack and for communication between programs in the other memory banks. Next, there are three CCS 64K dynamic RAMs, assigned to banks 1, 2, and 3, respectively. On these boards, the 16 kbytes of each are disabled, leaving 48K of each board active. The bank 1 board is configured to become active on power on/reset, and thus in "normal" mode the entire collection looks like 64K of contiguous memory. By exercising the bank switching logic, the 48K bank can be replaced by one of two other completely independent sets.

The rest of the hardware consists of independently packaged units interconnected with cables. The dual-disk drive is a Morrow Designs Discus 2+2D and is capable of reading both single- and double-density diskettes. The alphanumeric terminal is a standard Hazeltine 1421, which communicates with the system through a serial I/O port. A Racal Vadic modem is used. It is capable of 300- or 1200-baud operation, the latter with the Bell 212A (industry standard) protocol or with the older Vadic protocol.

The software suite of the RST includes the CP/M (CP/M is a registered trademark of Digital Research) operating system with its file management system, editor, compilers, etc. This supports the preparation of Level I reports and the printing of bulletins. It also supports the generation of analysis programs and the analysis of data. The communications function is supported by specialized programs which observe a communications discipline and allow the transfer of files of data to and from the Data Center. Finally, the analysis of waveform data is supported by a display program which allows the display of and measurement from waveform data stored on the local floppy disks.

The RST has three different "operating modes." First, it is or can be a normal CP/M-based microcomputer with all of the CP/M features such as editor, assembler, debugger, peripheral interchange processor, and so on; extra features are a BASIC compiler and a complete relocatable macro assembler package (Microsoft M80).

Next, the RST can be configured to be an intelligent terminal for use in communicating with another device via a modem supplied. This operating mode is entered from the CP/M mode by activating an appropriate software package.

Finally, the RST has a graphics display mode, again entered from the CP/M mode via a call to DISP. DISP is a self-contained software package which prompts the operator to perform various waveform display and analysis operations. DISP takes commands from the terminal keyboard and allows the use of a graphics cursor controlled by the operator to extract amplitude and period measurements from the waveforms.

A number of different enhancements have been suggested by potential users who have had an opportunity to see the RST demonstrated and to try using it themselves. They group into five categories: arithmetic enhancement through the addition of a Pascal processor; addition of a hard disk for increased storage capacity and access speed; software enhancements including hard copy of graphics display, display of maps, and improved communications protocol; addition of a plotting board for digitization of analog seismic records; and real-time operation including direct digital data acquisition from a seismometer. These enhancements are being planned and should be accomplished in the next reporting period.

Considerable interest was expressed in the extent to which the demonstration RST configuration could be "cut down." In Table I-2, five systems of increasing complexity are given with their costs. Three columns of cost data are included: the first column is the incremental cost of adding the capability described; the second column is the accumulation of these increments, and represents the cost of a system at this level in a form that allows future expansion; the third column shows the cost of an all-in-one system at the desired level – such a system will be cheaper but will have no growth capability.

TABLE I-2
LEVELS OF COMPLEXITY AND COSTS

| Level of Capability | Incremental Cost | Total Cost | Minimum Cost Alternative |
|---|---|---|---|
| Video Terminal + Modem + Printer | 3,000 | 3,000 | 2,000 |
| + Disk + CPU + Compiler | 4,500 | 7,500 | 5,000 |
| + Graphics Display and Cursor† | 2,500 | 10,000 | (5,000)‡ |
| + Plotter + Hard Disk§ | 5,000 | 15,000 | (9,000)‡ |
| + Seismometer Hookup | 21,000 | 36,000 | N/A |

† Model demonstrated at the Group of Scientific Experts Meeting.
‡ Limited resolution graphics, limited arithmetic capability.
§ Current level of capability.

The first system allows simple communication of text, it has no computing or graphics capability. An even smaller system is possible if one dispenses with the lineprinter, but nobody was willing to do without hard copy. The next increment adds a computing capability (hardware and software) and produces a viable small computer. Addition of high-resolution graphics comes next; the (5,000) in the third column is intended to indicate that generally the preceding system will have some graphics capability, perhaps 190 × 280 or better. This is the level of the present RST. The next two increments provide, respectively, a realistic database capacity with analog data reduction capability, and a true seismic station.

R. M. Moroney
A. G. Gann

## H. VAX UNIX INSTALLATION

In December 1980 we installed the Fourth Berkeley Release of Software for the VAX† on our VAX 11/780 after experimenting for a short time with VMS† and an earlier release of the Berkeley material. The Fourth Berkeley Release is distributed by the Computer Systems Research Group of the University of California at Berkeley, and consists of modifications and extensions to Western Electric's UNIX/32V‡ operating system. The Fourth Berkeley Release is largely compatible with the Version 7 UNIX‡ operating system which is currently running on our PDP-11/50† and PDP-11/44.

Despite somewhat lower performance in particular areas, UNIX was selected in preference to VMS, the operating system supplied for the VAX by Digital Equipment Corporation (DEC), because it offers greater ease of modification for special functions, a more complete development environment, and compatibility with our existing systems. UC Berkeley has been funded by DARPA to develop a standard VAX UNIX system for Government contractors, and to enhance the performance of UNIX for large applications. We anticipate that the system to be produced from this project will make UNIX even more desirable.

The only substantial obstacle encountered in installing this system was a lack of software support for our UNIBUS† interface magnetic tape controller. This was overcome by obtaining, from UC Berkeley, an experimental software driver which we are using successfully.

Initial execution speed of FORTRAN code compiled under UNIX was disappointing when compared with FORTRAN compiled and run under VMS. Installation of a hardware floating-point accelerator, however, resulted in a dramatic improvement in the speed of UNIX FORTRAN relative to that of DEC's. We are currently awaiting software from UC Berkeley which should improve the performance of UNIX FORTRAN even further.

D. A. Bach

† VAX, VMS, PDP, and UNIBUS are trademarks of Digital Equipment Corporation.
‡ UNIX and UNIX/32V are trademarks of Bell Laboratories.

## REFERENCES


1. M. A. Chinnery and A. G. Gann, "Design and Development of a Seismic Data Center," Technical Note 1980-39, Lincoln Laboratory, M.I.T. (11 August 1980), DTIC AD-A091621.
2. Seismic Discrimination Semiannual Technical Summary, Lincoln Laboratory, M.I.T. (31 March 1978), DDC AD-A057279.
3. Ibid. (30 September 1980), DTIC AD-A097999.
4. R. Bayer and E. McCreight, "Organization and Maintenance of Large Ordered Indexes," Acta Informatica 1, 173-189 (1972).
5. D. E. Knuth, The Art of Computer Programming, Vol. 3 (Addison-Wesley, Reading, Massachusetts 1973), pp. 471-479.

# II. SEISMIC PROCESSING TECHNIQUES

## A. SEISMIC ALGORITHM DEVELOPMENT: OVERVIEW

Substantial progress has been made in the development of the seismic algorithms required for Data Center operation. Throughout this task, the emphasis is upon replacing the functions currently performed by the human analyst by automatic algorithms, while retaining the capability to permit analyst intervention for the revision and addition of the automatically determined parameters at several points during the data flow from continuous digital data to final-event bulletin.

We have previously been hampered, particularly with respect to detection, by the lack of readily available data for testing purposes. This problem is now resolved by data from the International Data Collection Experiment (IDCE), described below, which provides large amounts of data suitable for testing not only the seismic algorithms but also many other aspects of SDC development. Several changes have been made to the detection algorithm which is described in some detail, and a description of its performance upon one day of IDCE data is given. A process to revise the signal onset times provided by the detector and, additionally, to identify source character and measure magnitude-related parameters is described and evaluated. A multiple-filter technique to time and identify body waves is also outlined and applied to local data. We emphasize that any application of the above algorithms for short-period data may well require substantial modification when the broader-band high-frequency RSTN data become available. A proposed method for "synoptic" analysis of seismograms, designed to recognize and use the features of seismic data employed by the analyst, is described and its possible applications are discussed.

The low noise characteristics of the SRO/ASRO long-period data imply that surface-wave detection capability may be superior to that given by short-period body waves, particularly for regions with poor station coverage such as the southern hemisphere. Techniques for the detection, azimuth determination, and association of Rayleigh waves to provide a location based upon long-period data only are described and tested using IDCE data.

R. G. North

## B. IDCE DATABASE

From 1-15 October 1980, several countries cooperated in the International Data Collection Experiment proposed by Sweden to provide experience in

(1) the mechanics of an international exchange of seismic data,

(2) the extraction of Level I parameter data, and

(3) the handling of Level I and II data at Data Centers.

Parameter and, where available, waveform data were recorded at many stations worldwide and sent to Sweden where the data will be collated and a bulletin prepared. The data from this experiment will be invaluable for testing all functions of the SDC, and will be the only data available for this purpose until the RSTN starts operation.

The U.S. contribution to the IDCE consisted of digital data recorded at 25 stations whose locations are shown in Fig. II-1. This network includes the Global Digital Seismograph Network (GDSN) comprising the SRO, ASRO and DWWSSN sites operated by the USCS. Additional stations

include: USGS Seismic Network sites ADK, BDW, PMR, and SMY; SDCS sites P'-WY and HN-ME; and the prototype RSTN station at CPO. Twenty of the stations (9 of which are 3-component) recorded continuous short-period data, while the remaining 5 used an on-site detector to select event waveforms. All stations recorded continuous 3-component long-period data. While the inevitable data transmission dropouts and occasional station failures occurred, to our knowledge this is the largest digital database yet collected from a global network. Further data contributed by other nations will eventually become available and augment this database.

In addition to the Level II waveform data, Level I parameters were also supplied to Sweden by the U.S. These consist of analyst measurements for most of the 25 digital stations, made from the analog seismograms which are recorded at each site. For each time pick, the maximum amplitude and dominant period were measured by USGS analysts, and a special effort was made to identify secondary phases and corresponding arrivals on the long-period components and, where available, the horizontal component short-period data. These analyst picks will be invaluable in evaluating automatic detection and signal measurement algorithms for the SDC. On 2 and 4 October the time, amplitude, and period measurements were repeated with the digital data in order to compare these with analog determinations.

The above is a brief summary of a detailed report[1] prepared by the USGS for presentation at the February 1981 meeting in Geneva of the Group of Scientific Experts of the Committee on Disarmament. We have received from SDAC copies of the digital data tapes and, from USGS/Golden, the parameter database. A major advantage of the digital data is their standardization to the SRO tape format. While some minor modifications to this format were unavoidably required to accommodate the range of data types, we have, with gratefully acknowledged assistance from both USGS/Golden and SDAC, been able to read digital data from all the stations with small changes to our program to read the SRO network day tapes. This program converts the data into the waveform database structure which we have developed, and for which we have written much special-purpose software for the display and analysis of digital data. We are thus able to immediately start data analysis and testing of the SDC seismic algorithms using this large database.

The digital data consume over 100 tapes at 1600 bpi, and data volumes are ~70 million samples/day, or ~280 Mbytes when stored in the floating-point representation used by the waveform database structure. This exceeds by nearly 25 percent the data rates anticipated from the 5-station RSTN, and its processing will enable reliable estimates to be made of the computational requirements and special hardware needs, such as array processors, necessary for an operational version of the SDC.

We have prepared sample databases in the waveform database format for the 2 and 4 October data. At present, we do not have the disk storage capacity to maintain one day of continuous data from all stations in on-line storage, though we anticipate possessing the capability to store several-day's worth on-line in the very near future. The continuous data have thus been initially stored on UNIX Tar (Tape Archive) tapes, from which retrieval is much more rapid than from the original dat. tapes. We have run our detection algorithm on all the continuous data for the two days selected and intend to maintain the detected waveform segments, together with the Level I parameters, on-line indefinitely. This will constitute the major data source for testing analyst procedures such as detection review and revision of automatically measured parameter determinations upon the SAS.

The data quality is generally good, particularly at the GDSN sites. Stations whose data were telemetered from the site, such as the Alaskan USGS stations and the SDCS sites, include numerous data dropouts and glitches. We have encountered some timing problems at CPO and some of the telemetered stations. At BDW (Boulder, Wyoming) there is apparent data quantization due presumably to partial failure of the A/D converter. While these assorted features are undesirable, they are representative of the problems with which the SDC, and the seismic algorithms in particular, must be able to cope. Later in this report we describe some preliminary results of analysis of these data, particularly in the areas of detection and parameter measurement.

R. G. North

## C. DETECTION ALGORITHM

The detection algorithm which we have implemented and described very briefly in previous SATSs[2,3] is basically the Z-statistic detector[4] with a few additions. We have recently generalized the detector to permit rapid change of parameters, added a glitch remover, and included the recursive bandpass prefilter in the detection program itself. While the Z-statistic detector has been described and evaluated in some detail by its original developers,[4] we present here a summary of its implementation by this group.

A sample input parameter file is given below:

| | | | |
|---|---|---|---|
| 0.50 | low corner freq | (hz) | (1) |
| 4.00 | high corner freq | (hz) | (2) |
| 0.00 | mu | <log<x**2>> | (3) |
| 0.00 | sigma | (var)**.5 | (4) |
| 60.00 | LTA window | (sec) | (5) |
| 3.00 | STA window | (sec) | (6) |
| 1.50 | STA increment | (sec) | (7) |
| 20.00 | STA to LTA lag | (sec) | (8) |
| 50.00 | coda reset | (sec) | (9) |
| 3.75 | detection threshold | | (10) |
| 1 | minimum detection votes | | (11) |
| yes | freeze LTA during detections? | | (12) |
| yes | de-glitch? | | (13) |
| szr | component | | (14) |

In the above, (1) and (2) are the 3-dB low- and high-frequency cutoffs of the prefilter bandpass. The present filter is a 3-pole Butterworth; faster roll-off than this seems desirable and will be implemented shortly. Lines (3) and (4) are initial values of $\mu$ and $\sigma$ for log (STA), where STA is the short-term power over a time window of given length (here 3.0 s). The statistics $\mu$ and $\sigma$ are here set to zero for a "cold start," but in routine operation use of previous values for the same site would eliminate the warmup time which this choice requires. Line (5) gives the long-term averaging time constant which determines how rapidly new values of STA are incorporated in the update of $\mu$ and $\sigma$.

The STA need not be updated nor its Z tested against the threshold for every sample point, here [line (7)] it is shifted by 1.50 s or half its window length each time. It could be shifted by the entire window length, but this raises the possibility that a small signal may be split between successive windows, neither of which has sufficient power to trigger the detector. The STA to LTA lag [line (8)] was introduced to assist detection of emergent arrivals, which would slowly pollute $\mu$ and $\sigma$ so that the threshold would never be exceeded. The lag here (20 s) is the time between the STA being tested and the STA to be used in LTA update. Lags of 10 to 20 s have been found to optimize performance for most emergent arrivals. The coda reset time [line (9)]

TABLE II-1

SAMPLE OUTPUT OF DETECTION LOG

```
#   DETECTOR LOG     anto4                #
#                                         #
#   low corner freq =     .50 hz          #
#   high corner freq =   4.00 hz          #
#   mu =     .00                          #
#   sigma =     .00                       #
#   LTA window =  60.00 sec               #
#   STA window =   3.00 sec               #
#   STA increment =   1.50 sec            #
#   STA to LTA lag =  20.00 sec           #
#   coda reset = 50.00 sec                #
#   detection threshold =   3.75          #
#   minimum detection votes =  1          #
#   freeze = yes                          #
#   de-glitch = yes                       #
#   component = szr                       #
#                                         #
#    Gram   1    23:59:59.960             #
    1   10/ 4/80   1:21:46.410  start DETECTOR
    1   10/ 4/80   1:22:38.910  end   Zmax =  4.0
    1   10/ 4/80   2:28:14.910  start DETECTOR
    1   10/ 4/80   2:29: 8.910  end   Zmax =  4.7
    1   10/ 4/80   3:42:20.910  start DETECTOR
    1   10/ 4/80   3:43:20.910  end   Zmax =  4.3
    1   10/ 4/80   4:57:20.910  start DETECTOR
    1   10/ 4/80   5: 0:23.910  end   Zmax =  9.4
    1   10/ 4/80  12:22:11.911  start DETECTOR
    1   10/ 4/80  12:23: 4.411  end   Zmax =  4.1
    1   10/ 4/80  15:13:11.911  start DETECTOR
    1   10/ 4/80  15:20:44.911  end   Zmax = 32.4
    1   10/ 4/80  16: 6:47.911  start DETECTOR
    1   10/ 4/80  16:10:50.911  end   Zmax = 17.4
    1   10/ 4/80  16:29:17.911  start DETECTOR
    1   10/ 4/80  16:30:19.411  end   Zmax =  7.9
    1   10/ 4/80  16:38:29.911  start DETECTOR
    1   10/ 4/80  16:39:23.911  end   Zmax =  4.6
    1   10/ 4/80  19: 2:41.911  start DETECTOR
    1   10/ 4/80  19: 3:34.411  end   Zmax =  4.5
    1   10/ 4/80  19: 6:25.411  start DETECTOR
    1   10/ 4/80  19: 7:37.411  end   Zmax = 12.4
    1   10/ 4/80  20:11:22.411  start DETECTOR
    1   10/ 4/80  20:12:14.911  end   Zmax =  3.8
    1   10/ 4/80  23:54:50.911  start DETECTOR
    1   10/ 4/80  23:55:43.411  end   Zmax =  3.8
#    EOF          0: 0:35.861             #
#    mu = 18.15                           #
#    sigma =     .35                      #
```

is the minimum amount of time allowed between detections, and inhibits multiple detections within a coda. For windowing purposes, this time is considered part of the detection interval.

The minimum detection votes [line (11)] may be used in an attempt to prevent detection of glitches and anomalously short-lived arrivals. If set to 3, for example, then it requires that the threshold be exceeded at least 3 times in succession before a detection is declared. We have found its usefulness to be low. The LTA (i.e., $\mu, \sigma$) may be "frozen" [line (12)] when a detection is declared; this prevents their contamination by signal characteristics and reduces the number of multiple detections during a given arrival. On the negative side, freezing may inhibit detection of signals from another event during a detection interval, but this function may be best performed by the analyst during detection review.

The de-glitch option [line (13)] permits application of a simple technique to remove large single-point excursions. Prior to prefiltering, the mean is removed and the absolute value of each point is tested against that of its immediate neighbors. If the former exceeds the latter by more than a factor of 10, it is deemed a glitch and set to the average value of its neighbors. We plan to test some ideas for a more sophisticated post-detection multipoint de-glitch routine, and candidates include checks for excessively one-sided arrivals and large ratios of the maximum Z during detection to the detector on time.

The ability to set all these relevant parameters permits rapid implementation of changes to improve performance. A sample output detection log for the detector running with the parameters given above for 24 h of short-period vertical data at station ANTO is given in Table II-1. The chosen detector parameters are given, together with the start and end times of the detections. For each detection, the maximum value of Z within the detection interval is given. This permits rapid identification of the signals which would no longer be detected if the threshold were raised by a specified amount. This sample run, including glitch removal and prefiltering, took only ~10 min. on the VAX computer and, thus, the effects of parameter changes can be rapidly investigated.

A special-purpose windowing program has been written to read the detection log and extract windows corresponding to the detection intervals. A selectable additional amount of time is added before and after the start and end times indicated when the window is extracted. This is currently set at 60 s. Waveforms corresponding to the above intervals are shown in Fig. II-2.

An evaluation of the detection algorithm using IDCE data and a discussion of the scope for improvements which this experiment has revealed are presented in Sec. D below.

M. A. Tiberio

## D. DETECTOR EVALUATION WITH IDCE DATA

We have applied the detection algorithm described above to continuous short-period vertical component data at 19 stations provided by the IDCE for 4 October 1980. A valuable check upon its performance is provided by the analyst picks made for this period and the NEIS bulletin which gives 16 events located for this day.

Table II-2 lists the detection parameters used – these are described in more detail in Sec. C above. We decided to apply the same detector parameters to all stations for consistency, though in practice different prefilters and short-term power windows, selected on the basis of experience, will provide optimum performance at each site. We initially selected the band 1 to 4 Hz for the prefilter bandpass, but discovered that this choice resulted in a failure to detect some

TABLE II-2

DETECTOR PARAMETERS USED FOR ALL STATIONS

| | |
|---|---|
| 0.50 | low corner freq (hz) |
| 4.00 | high corner freq (hz) |
| 0.00 | mu <ln<x**2>> |
| 0.00 | sigma (var)**.5 |
| 60.00 | LTA time constant (sec) |
| 3.00 | STA window (sec) |
| 1.50 | STA increment (sec) |
| 20.00 | STA to LTA lag (sec) |
| 50.00 | coda reset (sec) |
| † 3.85 | detection threshold |
| 1 | minimum detection votes |
| yes | freeze LTA during detections? |
| yes | deglitch? |
| szr | component |

† Adjusted for optimum performance at each station.

signals (particularly PKP) from the largest event on this day. This failure may not be particularly serious since the number of P signals detected from this event would still be adequate for location purposes, but we decided to change the prefilter bandpass to 0.5 to 4 Hz. This, in its turn, resulted in a failure to detect some smaller high-frequency signals from local events without setting the threshold for detection so low that unacceptably large false-alarm rates resulted. We believe that this may indicate a need to run the detector several times upon the same data, with perhaps as many as three different bandpass prefilters; and while this can easily be carried out with the current detection algorithm, the logic for combining detections in a number of such bands into a final detection log is not straightforward and will be investigated in the near future.

Detector performance proved to be relatively insensitive to short-term power window lengths in the range 1 to 3 s and also to long-term averaging times in the range 20 to 60 s. The detection threshold was adjusted for each station to provide optimum detection of the analyst-picked signals combined with a moderate false-alarm rate which was chosen to result in ~30 detections/day at most stations. Fewer detections were made at the high-noise stations CTAO, GUMO, and KONO. A very large number of detections were made at CPO, but these are, without exception, signals from presumed mine and quarry blasts at distances of up to 300 km. No teleseisms were detected at this station due to a combination of this almost-continuous local activity and extremely high background noise levels.

The results of the detection processing and its comparison with analyst performance are summarized in Table II-3. For each station the number of detections and the percentage of time the detector was on during the 24-h interval are given. This exceeds 4 percent only at CPO. The total percentage of data saved is larger, since we decided to window the detections for analyst review with an additional 60 s before and after the detector start and end times, respectively. This is necessary to ensure that P is included for local arrivals since the detector often triggered on the stronger S phase at these distances, and the extension of the window

TABLE II-3

DETECTION STATISTICS AND COMPARISON WITH ANALYST PICKS

| Station | Pick | Detections | Miss | Total Detections | Extra | Real | False Alarm | Glitch | Percent On | Percent Save |
|---|---|---|---|---|---|---|---|---|---|---|
| ANMO | 13 | 12 | 1 | 25 | 13 | 8 | 5 | 0 | 2.3 | 5.5 |
| ANTO | 6 | 6 | 0 | 13 | 7 | 4 | 3 | 0 | 1.7 | 3.0 |
| BCAO | 9 | 8 | 1 | 26 | 18 | 15 | 3 | 0 | 3.1 | 5.9 |
| BOCO | 2 | 2 | 0 | 13 | 11 | 10 | 1 | 0 | 1.2 | 2.5 |
| GRFO | 6 | 6 | 0 | 22 | 16 | 8 | 8 | 0 | 2.0 | 4.3 |
| GUMO | 4 | 3 | 1 | 24 | 21 | 16 | 5 | 0 | 2.2 | 4.7 |
| JAS† | 1 | 1 | 0 | 8 | 7 | 6 | 1 | 0 | 0.3 | 0.7 |
| NWAO | 1 | 0 | 1 | 3 | 3 | 0 | 3 | 0 | 0.2 | 0.5 |
| ZOBO | 17 | 14 | 3 | 31 | 17 | 10 | 7 | 0 | 3.5 | 6.7 |
| | 59 | 52 | 7 | 165 | 113 | 77 | 36 | 0 | 1.8 | 3.8 |
| ADK | 25 | 3 | 22 | 31 | 28 | 1 | 7 | 20 | 2.3 | 5.5 |
| BDW | 18 | 15 | 3 | 35 | 20 | 3 | 6 | 11 | 3.8 | 7.5 |
| PMR | 21 | 18 | 3 | 43 | 26 | 7 | 3 | 16 | 3.7 | 8.2 |
| SMY | 1 | 1 | 0 | 33 | 32 | 10 | 7 | 15 | 2.6 | 6.1 |
| | 65 | 37 | 28 | 142 | 106 | 21 | 23 | 62 | 3.1 | 6.8 |
| CPO | 2 | 1 | 1 | 92 | 91 | 80 | 11 | 0 | 8.6 | 18.2 |
| CTAO | – | – | – | 13 | 13 | 9 | 4 | 0 | 1.2 | 2.1 |
| KONO | – | – | – | 2 | 2 | 2 | 0 | 0 | 0.1 | 0.3 |
| MAJO | – | – | – | 17 | 17 | 14 | 3 | 0 | 1.8 | 3.6 |
| | | | | 32 | 32 | 25 | 7 | 0 | 1.0 | 2.0 |
| CHTO | 18 | 18 | 0 | 46 | 28 | 3 | 25 | 0 | – | 5.6 |
| KAAO | 15 | 10 | 5 | 30 | 20 | 15 | 3 | 2 | – | 6.1 |
| LON | 10 | 9 | 1 | 22 | 13 | 13 | 0 | 0 | – | 5.1 |
| SNZO | 1 | 0 | 1 | 3 | 3 | 0 | 3 | 0 | – | 2.6 |
| TATO | 3 | 1 | 2 | 3 | 2 | 0 | 2 | 0 | – | 0.5 |
| | 47 | 38 | 9 | 104 | 66 | 31 | 33 | 2 | | 4.0 |

†For JAS, continuous data were recorded only for the first 10.2 h and the statistics refer to this portion of the day only.

past the switch-off time of the detector is designed to include the pP depth phase for events up to 400 km in depth. While it might be desirable to increase the time saved past the end of the detection to include all conceivable depth phases (240 s required) for teleseisms, and Lg for regional events (300 s for up to 15° distance), this would greatly increase the amount of data saved. The continuous data are always available for rewindowing to enable the analyst to search for these additional later arrivals.

Table II-3 also gives the number of initial (P) arrivals picked by the analyst for each station, and the number of these detected and missed by the detector. The number of extra detections not picked by the analyst are also given: these include glitches and false alarms, but many are genuine signals. Detector performance was excellent at most of the SRO/ASRO stations, but less acceptable at USGS stations ADK, BDW, and PMR. In the latter case, much of this is due to the excellent analyst performance at these sites. Many of the signals missed by the detector can be captured by tailoring the prefilter bandpass to each individual station. Figure II-3 shows examples of the analyst-picked signals which evaded the detector with the standard (0.5 to 4 Hz) prefilter bandpass. Analyst picks for signals 5, 6, and 10 are PKP arrivals from an $m_b$ 5.5 event in the Fiji region at noisy sites. At NWAO (6) and GUMO (10), the arrivals are only barely distinguishable from the noise and the onset time is difficult to identify. At CPO (5), we fail to see how a pick could have been made. Local arrivals 2, 3, 7, and 9 can easily be detected by changing the prefilter to the 1- to 4-Hz bandpass, with scarcely any increase in false-alarm rate. At BDW (4), it can be seen that the data are quantized, due presumably to either partial failure or incorrect setting of the A/D converter, and we are surprised that under these circumstances we have been able to detect 15 of the 18 signals picked at this station. The apparently disastrous failure to detect signal 8 at ZOBO can be explained by its occurrence only 100 s after the start of the day, before the noise statistics have been initialized. We shall attempt to correct this type of failure due to "warm-up" time. The worst performance is that for ADK, at which only 3 of the 25 picks were detected. Of the 31 detections made, 20 were small glitches which evaded the de-glitching algorithm. These glitches were not only small single-point data excursions, but also small one-sided pulses which were clearly not of seismic origin. Nearly all the signals missed were very high-frequency local events, and by changing the prefilter bandpass to be 2 to 6 Hz, 20 of the 25 picks were detected, but with about a 200-percent increase in false alarms which were again mainly glitches.

On the brighter side, many detections were made which did not correspond to analyst time picks. At the SRO/ASRO/DWWSSN stations, a large number of these (~70 percent) are, in our opinion, genuine seismic arrivals for which time picks can be made. At the stations ADK, BDW, PMR, and SMY nearly all were either false alarms or glitches. Figure II-4 shows some examples of detections of signals which were not picked by the analyst. For the stations in common between this figure and Fig. II-3 (undetected picks), we feel that the unpicked detections are in general stronger than the undetected picks. Four of the signals shown in Fig. II-4 in fact correspond to arrivals predicted by the PDE event list.

The last five stations given in Table II-3 were those for which continuous data were not recorded, and the statistics shown refer to the on-site detector at these sites. The performance of this detector compared with the analyst was exemplary at CHTO, but a large number of the unpicked detections were false alarms.

To give some indication of the ability to locate events using arrivals from an automatic detector only, with the analyst intervening only to revise the onset time given by the detector,

Table II-4 shows the number of detections made for each of the 16 events given in the PDE for 4 October. Of these events, 5 were recorded only at local stations and were assigned no magnitude. Of the remaining 11, it is our opinion that the azimuthal coverage of the detections made would have been sufficient for a preliminary location to be made in 7 cases. We are, to say the least, puzzled by the lack of detections (and analyst picks) for the $m_b$ 5.2 event in the Philippines. The only arrival corresponding to the predicted arrival times from this event is that at KAAO.

TABLE II-4

EVENTS GIVEN IN THE NEIS MONTHLY EVENT SUMMARY FOR 4 OCTOBER 1980

| Origin Time | Location | $m_b$ | Depth | Stations Detecting |
|---|---|---|---|---|
| 00:58:26.2 | Greece | 4.0 | 10 | PMR? |
| 02:08:43.8 | Tonga | 4.7 | 107 | ANTO, BCAO, CHTO, GFRO, BDW, PMR |
| 03:11:35.8 | Columbia | 0 | 167 | BOCO |
| 03:24:49.0 | Philippines | 5.2 | 33 | KAAO |
| 04:10:31.0 | Chile | 4.7 | 33 | AMMO, BCAO, BDW, ZOBO |
| 04:37:34.1 | Fiji | 5.5 | 33 | ADK, ANMO, ANTO, BCAO, CHTO, CTAO, GRFO, JAS, LON, MAJO, BDW, PMR, SMY, ZOBO |
| 06:09:03.3 | Italy | 0 | 10 | |
| 06:32:13.7 | Sumatra | 4.6 | 33 | |
| 12:56:59.6 | New Hebrides | 4.8 | 208 | BCAO, CHTO, CTAO, MAJO |
| 15:12:03.8 | Greece | 4.9 | 10 | ANTO, BCAO, CHTO, GRFO, KAAO, KONO, MAJO, PMR, SMY |
| 16:05:40.0 | Turkey | 3.8 | 10 | ANTO, BCAO, GRFO |
| 16:37:12.7 | India | 4.5 | 33 | BCAO, CHTO, KAAO |
| 16:38:22.6 | California | 0 | 4 | ANMO, BDW |
| 16:42:18.4 | California | 0 | 5 | |
| 22:46:16.3 | California | 0 | 5 | |
| 23:35:43.6 | Japan | 4.9 | 366 | ANMO, CHTO, GRFO, GUMO, KAAO, LON, MAJO, TATO, ZOBO |

From our experiences with these data, we have gained valuable insights into methods for improving detector performance. Specific changes which would improve detection include:

(1) Detection in several frequency bands,

(2) Prefilter optimized to station noise characteristics,

(3) Better de-glitcher,

(4) Special techniques during detector "warm-up" to avoid missing signals during this interval.

Additional changes which we plan to implement shortly include 3-component detection and methods tailored to arrivals of longer duration such as local S and regional Lg.

R. G. North
M. A. Tiberio

## E. AUTOMATIC TIMING AND ANALYSIS OF DIGITAL DATA

For each signal detected, the detector described in the previous report outputs a windowed seismogram containing the detected signal and 60 s of the time series preceding it, and a marker indicating the detector onset time. This is used as input to a second program which attempts to refine the signal onset time and measure other seismic parameters from the signal.

There are several advantages to this two-step approach. Since the detection and analysis steps can be developed independently, the software is less complicated and easier to develop. Also, each step can have different design goals. The detector can be designed to be simple and efficient. The analyzer can be designed to be more thorough. Since a large number of detected waveform segments can be kept on-line, the development of the analyzer is simplified.

The analysis program under development has three main steps. First, it uses the frequency content of the signal to choose an appropriate prefilter bandpass. Second, an arrival time picking algorithm similar to that of Allen[5] is used to estimate the onset time. Finally, the onset time is refined, the amplitude and period are measured, and the arrival time accuracy is estimated. Each of these steps will be described more fully in turn.

The ratio of high-frequency (3 to 8 Hz) to low-frequency (0.3 to 1.0 Hz) power in the 5 s following the detector's trigger time is used to filter the seismogram and decide if it is local or teleseismic. If the ratio is greater than 0.1, the trace is high-pass filtered using a 3-pole Butterworth filter with the low-frequency 3-dB point at 2 Hz. Otherwise, it is Butterworth bandpass filtered with 3-dB points at 0.667 and 3.0 Hz. The trace is only forward filtered. Forward filtering with this filter causes a phase delay that we avoid by forward and backward filtering. However, the sharper phase-free filtering that results pushes energy from impulsive arrivals backward in time, and causes the program to pick a first arrival that is too early.

For a population of events with known epicenters recorded at MAJO, North and Shields[6] found events with a ratio of 0.1 or greater to be local (< 500 km). Events with a ratio of 0.03 or less were found to be teleseisms. Adjustments to this test, if necessary for other stations, will be incorporated into the program as information becomes available.

Once the data have been filtered and the event roughly categorized by distance, a picker similar to that of Allen[5] is used to estimate the signal onset time. Allen defines the E function as

$$E(t) = f(t)^2 + [C_2 * f'(t)]^2$$

where f(t) is the seismic trace regarded as a time series. f'(t) is the first difference and $C_2$ is a weighting constant dependent on the sample rate and noise characteristics at the station. The initial long-term average (LTA) of the E function is calculated over 200 points near the beginning of the seismogram. It is then continuously updated with the short-term average (STA) as long as an event has not been detected. A 2-point STA is used.

The signal onset is recognized as the first time the ratio STA to LTA exceeds a threshold (~5). The algorithm then checks that the signal lasts at least 4.5 s and contains at least 4 large zero crossings before deciding that a signal has been found. If no signal is found or if the STA/LTA is less than 10, the trace is phase-free filtered and re-examined. (This avoids phase-free filtering strong signals.' If the STA/LTA is less than 5, the trigger threshold is reduced to 4 and the trace is re-examined. (This is to allow emergent signals to be picked earlier than it would with a higher threshold.)

After the trace is searched, once if a strong signal is found or twice for a weak signal, the program estimates the position of the first arrival. This is done by backing along the trace from the point where the program triggered to the first preceding inflection point. Here, a marker is put on the trace and the corresponding time is calculated.

The program's estimate of the quality of its pick is directly related to the power of the signal. If the STA/LTA is greater than 10, the first arrival is designated "iP." If the ratio is between 5 and 10, it is called "eP." A first arrival with a ratio less than 5.0 is considered poorly known and is labeled "e(P)."

After estimating the first arrival, the maximum amplitude in the first 5 s is located and the period calculated. The amplitude is measured from the raw trace and converted to displacement in millimicrons.

Finally, all the information obtained is written to a summary file, an example of which is shown in Table II-7.

Preliminary tests of the program have been run on three databases. One database comprises 230 seismograms, all the detections from all the SRO stations on 3 April 1980. From these detections the program picked 127 arrivals, and a human picked 141 arrivals. The program rejected 7 other seismograms because they were too short to process. Table II-5 shows

TABLE II-5
TEST RESULTS ON 3 APRIL 1980 DATABASE

| Time Difference (Human – Machine) | Machine Designated Categories (percent) | | |
|---|---|---|---|
| | iP | eP | e(P) |
| <0.5 s | 76 | 48.4 | 34.8 |
| <1.0 s | 90 | 77.4 | 50.0 |
| >2.0 s | 6 | 16.1 | 41.3 |
| Total number of picks | 50 | 31.0 | 46.0 |
| Total number of machine picks | 127 | | |
| Total number of machine possible picks | 134 | | |

the results of a comparison between the machine picks and the human picks. The program made a pick on 127 of 134, or 94.8 percent, of all possible first arrivals. The human and machine picks agreed to less than 1 s on 92 picks, and disagreed by more than 2 s on 27 picks. The program designated 19 of these 27 picks as e(P).

A second database used to test the program consists of all the arrivals at MAJO over a 10-day period for which epicenters are available from the JMSA, PDE, and SDAC bulletins. The database contains 65 seismograms and 65 hand-picked first arrivals. Results of a program test run are listed in Table II-6.

TABLE II-6
TEST RESULTS ON MAJO DATABASE

| Time Difference (Human – Machine) | Machine Designated Categories (percent) | | |
|---|---|---|---|
| | iP | eP | e(P) |
| <0.5 s | 65.0 | 66.7 | 33.3 |
| <1.0 s | 92.5 | 66.7 | 58.3 |
| >2.0 s | 5.0 | 16.7 | 16.7 |
| Total number of picks | 40.0 | 12.0 | 12.0 |
| Total number of machine picks | 64 | | |
| Total number of picks possible | 65 | | |

The program picked a first arrival on 98.5 percent of the seismograms. The human and machine picks agreed to less than 1 s on 52 of 65 possible picks, or 80 percent of the time. They disagreed by more than 2 s on 6 picks, or 9.2 percent of the time. Two of these six picks including the greatest disagreement (14.5 s) were designated e(P).

The third database examined, a set of 25 detections from ANMO on 4 October 1980, is part of the IDCE. The seismograms, shown in Fig. II-5, are detection windows provided by the algorithm discussed in Secs. C and D. In the figure, X is the program's estimate of the first arrival; U is the pick provided by an NEIS analyst; 0 is the detection time; A is the greatest peak (or trough) in the first 5 s of the signal; and B is the adjacent trough (or peak) used to calculate ground motion and period.

Table II-7 is the output of the program for this set of seismograms. There is no information for seismograms 1, 5, 6, 7 or 10 since the program did not identify them as seismic signals. The column of numbers following the onset times is the set of time differences between human- and machine-picked times (human – machine). The residual (–79.1 s) on seismogram 9 arises from the windowed seismogram not containing the event onset time.

An examination of the data reveals that the machine picks are probably more correct than the analyst picks on seismograms 3, 14, and 16 while the analyst picks are better on 8 and 13.

TABLE II-7

EXAMPLE OF PROGRAM OUTPUT

| Seismogram | Station | Confidence | Date | Arrival Time | Difference† | Ground Motion (mμ) | Period (s) | Distance |
|---|---|---|---|---|---|---|---|---|
| 2 | ANMO | ePD | 10/4/80 | 4:21:50.1 | +0.1 | 4.39 | 0.95 | TELESEISM |
| 3 | ANMO | e(P)D | 10/4/80 | 4:44:31.2 | +0.8 | 1.39 | 0.65 | TELESEISM |
| 4 | ANMO | iPC | 10/4/80 | 4:50:11.5 | −1.2 | 27.92 | 1.70 | TELESEISM |
| 8 | ANMO | e(P)C | 10/4/80 | 14: 3:56.9 | −2.4 | 1.21 | 0.90 | TELESEISM |
| 9 | ANMO | e(P)D | 10/4/80 | 16:41:39.7 | −79.1 | 3.50 | 0.95 | – |
| 11 | ANMO | e(P)C | 10/4/80 | 18: 4:15.1 | +0.4 | 0.94 | 0.35 | LOCAL |
| 12 | ANMO | e(P)D | 10/4/80 | 18:14:41.7 | −1.9 | 0.34 | 0.40 | TELESEISM |
| 13 | ANMO | e(P)D | 10/4/80 | 19: 2:46.2 | −2.2 | 3.59 | 0.55 | LOCAL |
| 14 | ANMO | e(P)D | 10/4/80 | 19:34:49.5 | +3.7 | 0.88 | 0.55 | LOCAL |
| 15 | ANMO | e(P)C | 10/4/80 | 19:57:36.6 | – | 1.57 | 0.90 | TELESEISM |
| 16 | ANMO | ePD | 10/4/80 | 20:16: 6.5 | +1.3 | 2.44 | 0.30 | LOCAL |
| 17 | ANMO | e(P)D | 10/4/80 | 20:28:20.8 | – | 1.05 | 0.40 | LOCAL |
| 18 | ANMO | e(P)D | 10/4/80 | 21: 9:24.1 | – | 0.87 | 0.25 | LOCAL |
| 19 | ANMO | e(P)C | 10/4/80 | 21:34:16.2 | – | 0.95 | 0.25 | LOCAL |
| 20 | ANMO | e(P)C | 10/4/80 | 21:36:26.1 | – | 0.46 | 0.40 | LOCAL |
| 21 | ANMO | ePD | 10/4/80 | 21:42:46.6 | −1.6 | 1.33 | 0.60 | – |
| 22 | ANMO | e(P)C | 10/4/80 | 21:47:35.8 | – | 0.86 | 0.45 | LOCAL |
| 23 | ANMO | ePC | 10/4/80 | 22: 5: 4.2 | – | 4.03 | 0.50 | LOCAL |
| 24 | ANMO | ePC | 10/4/80 | 22:10:33.6 | – | 3.54 | 0.45 | LOCAL |
| 25 | ANMO | iPC | 10/4/80 | 23:47:57.2 | −0.2 | 11.03 | 1.20 | TELESEISM |

†Time difference between human and machine picks (human – machine).

On seismogram 4, the analyst pick is probably a few tenths of a second early, and the machine pick about 0.5 s late. It is difficult to judge between the two on seismograms 11 and 12. Both picks may be several seconds late on seismogram 21. The events on 17, 18, 19, 20, and 22 may be caused by machinery near the station. Seismograms 23 and 24 contain events timed by the program but missed by the analyst. The program's pick appears about 1 s late on seismogram 23 and about 0.5 s late on seismogram 24. The detector onset time, which identifies only the time that the detector triggered and is not claimed to be the true onset, is usually inferior to that provided by this algorithm. Only for seismogram 13 is it better.

In summary, the program can, at present, provide an onset time within 1 s of what an analyst would pick about 90 percent of the time for events it designates as iP and about 60 to 80 percent of the time for events it calls eP. This is sufficient for the purpose of event association and preliminary location and should greatly ease the burden of the analyst. Furthermore, since it applies the same objective criteria to evaluating the arrivals on all seismograms, its picks should be more consistent than those of the analyst.

Research to improve the performance of the program is proceeding in three areas. First, signals so emergent as to be impossible for a human analyst to time more accurately than several seconds sometimes elude the program. A possible solution to this problem is to alter the up ing procedure for E (long-term average). Second, instead of merely backing along the trace to the first inflection point preceding the trigger point, a more thoughtful way of locating the exact position on the first arrival is being sought. Finally, the criterion for deciding if an event is local or teleseismic is being studied to make sure of its applicability at stations other than MAJO.

M. W. Shields

## F. USE OF THE MULTIPLE-ARRIVAL RECOGNITION SYSTEM (MARS) FOR TIMING AND IDENTIFYING SEISMIC BODY WAVES

The most general waveform containing body waves also contains Earth noise, source-gene surface waves at local and regional distances, and randomly scattered body waves genera y velocity inhomogeneities along ray paths and topographic irregularities at velocity disconti es. Masso et al.[7] have described a method of waveform processing that exploits the nondispersive property of body waves to separate them from the dispersive components of a waveform. The MARS applies a series of Gaussian filters F having different center frequencies $f_k$ to a s mal S, where

$$F = \sqrt{\frac{\alpha}{\pi}} \exp[-\alpha(f - f_k)^2] \quad . \tag{II-1}$$

The parameter $\alpha$ is related to the center frequency and Q of the filter by

$$\alpha = \frac{\ln 2 Q^2(f_k)}{f_k^2} \quad . \tag{II-2}$$

The envelope function of the filter output in the time domain can be formed from the output spectrum and its Hilbert transform (Dziewonski et al.[8]). The Q of the narrowband filters is chosen to compromise between frequency resolution of the filters and time resolution of the envelope function. Peaks in the envelope function for each narrowband filter are then displayed in a group arrival-frequency ($t_g$-f) plane. Whenever a sufficient number of peaks line up within a narrow time band, a nondispersed (body wave) is detected.

Figure II-6 shows the $t_g$-f plane for a presumed quarry blast recorded by the vertical component of the NSS station CPO. Before application of the narrowband filters, the spectrum of the waveform is corrected for the velocity response of the short-period band of an NSS response. The waveform is corrected for velocity rather than displacement in order to emphasize the seismic energy radiated near the corner frequency of body waves. (An optimal spectral correction should generally be based upon body-wave spectral characteristics at a given distance as well as the instrument response.) Q is taken to be 8.5, giving an $\alpha$ of 50 at 1 Hz. The theoretical time uncertainty of the envelope function at a center frequency f is given by

$$\Delta t \geq \frac{1}{4\pi(Q/f)} \qquad \text{(II-3)}$$

Thus, at 2 Hz $\Delta t \geq 0.3$ s. The threshold at which a peak in a time envelope should be considered significant should be based upon the level of noise in the envelope. Here, the threshold is simply taken to be twice the LTA. The lineup of envelope peaks in the $t_g$-f plane shown in Fig. II-6 clearly reveals the Pn, Sn, and S arrivals as well as some unidentified body waves. The first three body waves following Pn may be associated with the P*, Pg, and P phases. From the Pn, Sn, and S phase identifications the distance is estimated to be 244 ± 10 km. Note that the Pn arrival has some dispersive character visible in both the seismogram and in the $t_g$-f plane. The apparent dispersion of Pn may reflect its character as an interference head wave along the Moho, a ray that penetrates below the Moho forming the first arrival with lower relative frequency content, and an infinite series of multiply reflected and scattered rays along the underside of the Moho forming the higher-frequency coda.

Preliminary results of applying MARS processing to teleseismic and regional data indicate it to be a valuable aid to the seismic analyst when automatic detections are refined and reviewed. The value of MARS processing lies in its ability to detect arrivals in the disturbed portion of the waveform following a strong arrival. By aiding the identification of multiple body-wave arrivals, processing improves distance estimates of regional data recorded at a single station and improves detection of depth phases associated with regional and teleseismic body waves.

V. F. Cormier

## G. SYNTACTIC ANALYSIS OF REGIONAL SEISMIC SIGNALS

Although many signal-processing techniques are used in seismic analysis, application of these techniques still requires human intervention. For example, to compute the group-velocity curve from a surface-wave seismogram, a seismologist must first identify the interval containing the surface wave.

In the detection of seismic signals, attempts to use advanced techniques – such as polarization filtering or prediction-error filtering – have not been shown to be superior to simpler methods because, although these methods are powerful, they require the skilled eye of a seismologist to be applied and interpreted properly. Thus, if an automatic system is to use these methods to advantage, it must use many of these same seismological skills.

Most detectors make one pass over the data, declaring a detection if a simple threshold test is satisfied. Unfortunately, seismic signals are often ambiguous and cannot always be correctly identified by a simple one-pass detector. A better approach is to analyze the entire waveform and identify its prominent structures before making a decision about it, much as a seismologist does.

As a first step toward this, a computer laboratory known as SEISMOGRAMMAR is under development. This laboratory is being used to investigate techniques for syntactic structural analysis of seismic waveforms. The structural analysis of a waveform is analogous to the analysis performed by a compiler on a statement of a computer programming language. The waveform is broken up into features of morphological significance or "words." Such features might include peaks, inflection points, or segments of constant slope. Grammar rules are then given that describe how these words may be combined to form "sentences." Simple descriptions can be combined to form more complicated descriptions.

Although the analogy between computer language analysis and waveform analysis is compelling, the two domains are distinctly different. The techniques used in computer language analysis cannot be transferred to the waveform domain directly. There are several reasons for this, namely:

(1) In the waveform domain, noise is always present and any parsing scheme must be tolerant of it. Thus, one important issue is how to identify the significant variations in the signal. This is not always easy since significant variations in a signal can be small, and the signal may have large variations that are not meaningful.

(2) Because of this, the recognition of words, or morphs, is often ambiguous. This can lead to very complicated grammars, or combinations of grammatical and nongrammatical analysis.

(3) The words used in waveform analysis have features which are continuous variables, such as slope or radius of curvature. This tends to make syntactic analysis more complicated by forcing semantic issues to be checked earlier than would be required in analyzing a computer language.

(4) The traditional left-right approach used in computer language parsing is not robust enough to work well in waveform analysis. A better approach is to identify reliable features first, and use them to guide further analysis.[9-11]

(5) Since a language which adequately describes a waveform, in a particular application, is usually not known a priori, a waveform parsing system must allow analyzers to be developed and tested easily.

Because of these problems, SEISMOGRAMMAR is based on the Augmented Transition Network (ATN) formalism.[11] The ATN approach provides the grammar designer with considerable freedom and power. Grammatical and nongrammatical methods can be combined in a number of ways, and grammars can be built, modified, and tested easily.

The parsing techniques being developed are being applied to the problem of recognizing the S-P interval on local and regional seismograms. Figure II-7 shows the variation of signal characteristics possible over a distance range of 6° to 10°. Although the S arrival is a prominent peak in the signal envelope, the P arrival is variable. It can manifest itself either as a peak or as a step beginning a relatively flat coda. Occasionally, both the Pn and Pg arrivals can be identified. Automatic detectors can miss a weak P arrival completely, thus further complicating the extraction of the S-P interval.

Before syntactic analysis, the seismic signal is high-pass filtered (to remove low-frequency background noise), rectified, and averaged into 5-s blocks. The 5-s averaging length removes most of the unnecessary detail from the signal, yet allows distance to be estimated to better than a degree.

The resulting envelope is used as an input sentence to the parser. The words of the sentence are simply the segments between consecutive points on the smoothed envelope. An alternative would be to use a preprocessing step to segment the envelope into a larger set of words of morphological significance.[9,12] The simpler approach was chosen since the appropriate morphs are currently not known, and the ATN formalism allows morphs to be built easily by the grammar designer as shown below.[10]

The ATN method of parsing was first developed by Thorne, Bratley, and Dewar[13] and Bobrow and Fraser.[14] Its current popularity as a parser for natural language is due to Woods.[15,16] ATN parsers were first applied to waveform analysis by Lozano-Perez.[10] The formulation given here is similar to one described by Charniak, Riesbeck, and McDermott[17] except that extensions for waveform analysis have been added. It is implemented in FRANZ LISP running under the UNIX operating system on a VAX 11/780.

The basic idea is to represent a grammar as a transition net. This is a set of nodes (or states) with arcs between them. Arcs are labeled according to their type, and an arc may be traversed only if tests appropriate for its type are satisfied by the current input word. The arcs may be augmented with actions that do useful functions such as building parse trees. Nodes may be grouped into subnets, each subnet being responsible for parsing one kind of constituent. These subnets can be called recursively by an arc. Figure II-8 gives an example of a simple ATN that divides an input waveform into a list of rising or falling segments.

The arc types are:

WORD — The arc is traversed if the current input word has the indicated feature. Before the arc is traversed, the current input pointer is advanced to the next word in the input. For example, (word +) checks that the current word has a positive slope. A feature is a predicate that the word must satisfy.

TEST — The arc is traversed if the arbitrary test is satisfied. For example, (test t) is a test which is always satisfied.

PARSE — The indicated subnet is called recursively and, if it succeeds, the arc is traversed. A subnet can return a value that is usually a description of the constituent it recognized.

DONE — This arc does a return from a subnet. The final action of the arc is returned as the value of the call.

Parsing proceeds as follows. Given an input sentence and an ATN grammar, the arcs emanating from the initial state are inspected in turn. The first successful arc is traversed, and the arcs at the new node are processed similarly. If a node is reached for which no arc can be traversed, the parser backs up to the most recent node that has an alternative arc and tries to continue the parse. This ability to back up and pursue another alternative is valuable in waveform analysis. This allows the ATN to use local and global information in its analysis, which would be difficult to do otherwise.

The ATN grammar shown in Fig. II-8 consists of three subnets. The SEG+ net accepts consecutive segments with positive slope. Arc actions (not shown) simply return the beginning and end points of the resulting segment. The SEG- net works similarly for negative segments. The SEG1 net alternatively calls the SEG+ and SEG- subnets and returns a list of the returned segments. In Fig. II-9(a), the effect of applying this grammar is shown. The dotted curve is the original envelope, and the solid one is the resulting segmentation.

One problem with this definition of SEG+ and SEG- is that a small segment of opposite sign will stop them. It would be better to look ahead slightly to see if the segment can be continued further on. This is what the SEG2 grammar in Fig. II-10 does. Its top level is the same as the previous one. It simply returns a list of segments. However, the SEG+ and SEG- nets have been expanded. The words used by this grammar are the segments produced by the SEG1 grammar. Four different word categories are recognized:

| | |
|---|---|
| S+ | A short segment with positive slope. |
| S- | A short segment with negative slope. |
| BIG+ | Either a sharply rising segment, or a long segment with positive slope. |
| BIG- | Either a sharply falling segment, or a long segment with negative slope. |

The SEG+ net is recursive. SEG+ will accept either a BIG+ or a BIG+ followed by an SEG+. It will also allow a segment to begin with a short segment of either sign. Thus, recursion and backtracking allow the parser to look ahead in the waveform before deciding on an interpretation. The results of applying this grammar are shown in Fig. II-9(b). The representation is more compact than that of the SEG1 grammar, though the general features of the envelope are still preserved. For a comparison, a 25-s running median filtered version of the envelope is shown in Fig. II-9(c).

The grammars shown so far have done a form of data compression. They returned a simple list of the constituents found, without trying to determine any higher-level description of the seismogram, or extract any features such as the S-P interval. Figure II-11 shows one way of building such a description. The dotted lines form a binary tree structure that represents the relationships between the dominant peaks and valleys in the envelope. This approach is similar to that of Ehrich and Foith[18] except that the ATN parser was used to remove minor peaks, eliminate noise and coda, and build the peak structure.

Although the grammars presented here are simple, they show the main features of the ATN approach to structural analysis. Too often, automatic seismic programs, such as detectors, develop into large ad hoc programs which are difficult to debug and test. Typically, a detector must perform a number of complicated checks and measurements on the signal before and after a detection. For example, the detector might check if the detected signal is of seismic origin or not (it could be a glitch or a noise burst), attempt to refine the origin time, or measure other parameters.[19] The ATN paradigm provides a convenient framework for developing such automatic processing systems.

K. R. Anderson

## H. RAYLEIGH-WAVE AZIMUTH DETECTOR

We have combined the work of Frasier,[20] Frasier and North,[21] and North[22] in the development of a simple but effective Rayleigh-wave detector. Unlike the more sophisticated Smart[23]

detector, this one operates in the time domain and on Rayleigh waves only. Unlike P-wave detectors that are based on some function of an amplitude ratio taken over short- and long-time windows, the Rayleigh-wave detector is tuned to retrograde particle motion from which the azimuth of the propagation path can be estimated.

The first step in the processing is to prefilter so as to isolate a band of energy toward the long-period end of the spectrum. This diminishes the effects of multipathing which is desirable, but also diminishes the dispersed character typical of shorter-period Rayleigh waves and, if taken to extremes, will result in a signal-to-noise problem. This will occur because noise levels increase toward long periods, beyond a spectral minimum in the passband from 0.02 to 0.04 Hz. Typical noise spectra at SRO/ASROs are shown in Fig. II-12 and in a Texas Instruments Report by Strauss and Weltman.[24] Most of the results discussed in this and subsequent reports come from data that have been bandpassed from 0.015 Hz (66 s) to 0.04 Hz (25 s). Those frequencies (periods) define the 3-dB points of a phaseless 3-pole Butterworth filter. The spectrum of the broadband record shown in Fig. II-13 is an illustration of data with significant signal strength in this passband. It should be pointed out that, rather than noise minima, the important detection parameter is signal-to-noise ratio which has not been studied in a systematic way.

After prefilter, the data are polarized and filtered for elliptical particle motion in the manner proposed by Frasier[20] and North.[22] Briefly stated, elliptical particle motion is detected by first applying a 90° phase advance to the horizontal components which for retrograde elliptical motion makes the horizontals in phase with the vertical component. The motion in a time window of fixed length is fit in a least-squares sense to an ellipse for a fundamental-mode Rayleigh wave. This ellipse will be elongated and the correlation coefficient between the vertical and at least one of the horizontal records should be high. The output of the detector is the long axis of the ellipse multiplied by the filter coefficient g(t) and projected onto the vertical and horizontal axes. The filter coefficient is either the correlation coefficient pertaining to a moving time window of fixed length[21] or an elliptical filter coefficient

$$g(t) = \left\{ \left[ 1 + \frac{e(t)}{e_o} \right]^n \right\}^{1/2} \qquad \text{(II-4)}$$

proposed by Frasier.[20] The time-dependent variable e(t) is the ellipticity, $e_o$ is a cutoff ellipticity (Frasier suggested a value of 0.2), and n is the order of the filter (Frasier suggested 3 to 6).

Azimuth Az(t) is then the

$$\arctan \frac{NS(t)}{EW(t)} \qquad \text{(II-5)}$$

where EW(t) and NS(t) are the horizontal seismograms passed through the bandpass and particle-motion filters.

Experience to date would suggest that the ellipticity and correlation filters can be made to work equally well. Table II-8 gives the detections with both filters at stations ANMO and CHTO for 4 October 1980. Rayleigh-wave trains with average amplitudes as low as a few tens of nanometers are detected. The ellipticity filter in this case gives fewer detections because an $e_o$ of 0.2 rejects as not elliptical enough waves that the correlation filter passes. The cutoff value for the correlation coefficient is 0.7, where unity is perfect correlation. More work needs

TABLE II-8

RAYLEIGH-WAVE DETECTIONS, 4 OCTOBER 1980

| | Correlation Filter† | | | | Ellipticity Filter‡ | | | |
|---|---|---|---|---|---|---|---|---|
| | Onset Time (h:m:s) | Duration (s) | Azimuth Station to Epicenter (deg) | Average Amplitude (nm) | Onset Time (h:m:s) | Duration (s) | Azimuth Station to Epicenter (deg) | Average Amplitude (nm) |
| ANMO | 1:03:53 | 292 | 61.3 | 27.01 | – | – | – | – |
| | 4:15:25 | 308 | 292.8 | 39.90 | 4:48:25 | 192 | 47.5 | 189.09 |
| | 5:15:25 | 440 | 247.3 | 9981.30 | 5:11:33 | 196 | 328.7 | 1230.84 |
| | – | – | – | – | 5:16:29 | 228 | 242.8 | 16868.56 |
| | 6:45:05 | 412 | 68.1 | 1391.87 | 6:47:21 | 76 | 66.2 | 1266.59 |
| | 6:53:25 | 772 | 74.0 | 1805.87 | 6:58:25 | 348 | 72.4 | 2804.04 |
| | 7:07:05 | 88 | 86.3 | 428.29 | – | – | – | – |
| | 7:09:01 | 112 | 106.6 | 291.18 | – | – | – | – |
| | 7:18:29 | 208 | 17.2 | 180.99 | – | – | – | – |
| | 7:29:09 | 180 | 29.0 | 169.03 | – | – | – | – |
| | 15:57:25 | 788 | 34.5 | 322.09 | – | – | – | – |
| | 16:44:01 | 164 | 240.5 | 54.57 | – | – | – | – |
| CHTO | 0:21:53 | 104 | 97.6 | 29.16 | – | – | – | – |
| | 1:16:21 | 116 | 157.9 | 19.41 | – | – | – | – |
| | 2:16:37 | 104 | 175.6 | 18.51 | – | | – | – |
| | 3:26:05 | 240 | 181.1 | 24.37 | – | – | – | – |
| | 3:37:29 | 256 | 105.2 | 77.28 | – | – | – | – |
| | – | – | – | – | 4:48:37 | 416 | 299.2 | 247.06 |
| | 4:49:37 | 120 | 297.4 | 283.82 | 4:59:33 | 68 | 71.5 | 44.51 |
| | – | – | – | – | 5:15:29 | 72 | 121.6 | 2809.09 |
| | 5:18:13 | 392 | 92.5 | 8533.05 | 5:19:37 | 276 | 91.3 | 10928.32 |
| | 6:33:53 | 72 | 313.3 | 628.09 | 6:49:01 | 196 | 266.4 | 1362.71 |
| | 6:44:25 | 1312 | 276.4 | 915.32 | – | – | – | – |
| | 8:17:29 | 96 | 111.4 | 94.95 | – | – | – | – |
| | 15:45:05 | 312 | 321.9 | 201.96 | 15:30:29 | 304 | 25.6 | 25.87 |
| | 16:47:29 | 324 | 288.6 | 73.19 | – | – | – | – |
| | 21:30:17 | 64 | 76.2 | 16.19 | – | – | – | – |
| | 21:32:53 | 248 | 100.4 | 34.28 | – | – | – | – |

† Half-length of correlation window 32 s.

‡ $e_o = 0.2$ and n is 3 [see Eq. (II-4)].

to be done to find an optimum bandpass for the prefilter and optimum values of $e_o$ and n for the ellipticity filter.

T. J. Fitch

## I. ASSOCIATION OF RAYLEIGH WAVES

Criteria have been tested for the association of Rayleigh-wave detections coming from the azimuth detector discussed in the two preceding SATSs (31 March 1980 and 30 September 1980). The basic criteria are applied to paired detections that are parameterized by pairs of onset times, average amplitudes, and azimuths. To be associated, the ratio of average amplitude must lie in the range 0.1 to 10.0. Amplitude ratios outside this range are unlikely to be consistent with the effects of anelasticity and spherical spreading on radiation from a single source.

Next, the azimuths are used to define an epicenter from which the path lengths can be estimated. Then, consistent with the onset and path lengths, apparent origin times are tested for consistency. The test is successful if an origin time lies within a time interval appropriate of group velocities in the range from 3.2 to 4.2 km/s. For mantle waves, the upper end of the group-velocity range would be more appropriate. If the amplitude ratio and origin time tests are successful, the paired Rayleigh waves are considered associated. Epicenters from a number of associated pairs are then compared to see if a particular source region is indicated.

Two sets of Rayleigh-wave detections have been analyzed in this way with the following results. Table II-9 shows epicenters from azimuth pairs pertaining to an $M_S$ 6.1 shallow earthquake in the Fiji Islands region. Azimuths at CHTO, BOCO, ANTO, and BCAO differ by more than 10° from the appropriate great-circle azimuth. In particular, the paths to CHTO and ANTO which are largely tectonic in nature are expected to produce multipathing which, in turn, will result in large discrepancies between apparent and great-circle azimuths. The apparent azimuth at CHTO is 90.2°, whereas the great-circle azimuth is 107.6°. At ANTO, the apparent

TABLE II-9

ASSOCIATED RAYLEIGH WAVES FROM FIJI ISLANDS EARTHQUAKE
(4 October 1980, 4:37:34.0)

| Station Pair (1) | Station Pair (2) | Epicenter Latitude (deg) | Epicenter Longitude (deg) | Origin Time† Difference |
|---|---|---|---|---|
| ANMO | GUMO | −17.6 | 178.2 | −80 |
| ANMO | TATO | −21.4 | 172.7 | −362 |
| CHTO | GUMO | 10.6 | 148.1 | −30 |
| GUMO | NWAO | −18.6 | 179.4 | −256 |
| NWAO | TATO | −21.6 | 173.0 | 304 |
| ANTO | BCAO | −7.5 | −123.2 | −368 |
| | | PDE epicenter −15.76 | 179.31 | |

†O.T. (station 1) − O.T. (station 2) where O.T. = onset time − distance/4.0.

TABLE II-10

ASSOCIATED RAYLEIGH WAVES FROM PRESUMED EARTHQUAKE IN WEST AFRICA†

| Station Pair (1) | Station Pair (2) | Epicenter Latitude (deg) | Epicenter Longitude (deg) | Origin Time‡ Difference |
|---|---|---|---|---|
| ANMO | ANTO | 15.2 | 0.1 | 42 |
| CHTO | NWAO | 6.7 | 8.7 | −204 |
| ANMO | BOCO | 6.9 | −3.7 | −542 |
| CHTO | ANTO | 12.8 | 29.0 | 464 |
| CHTO | BOCO | 8.9 | 15.4 | 366 |
| CHTO | BCAO | 7.6 | 12.2 | −158 |
| NWAO | TATO | 2.1 | −141.3 | 408 |
| NWAO | BCAO | 16.1 | −7.2 | 18 |
| TATO | BOCO | 9.0 | −156.2 | 454 |
| TATO | BCAO | 6.7 | 34.2 | 318 |
| ANTO | BCAO | 15.5 | 15.8 | −54 |
| BOCO | BCAO | 9.3 | 8.4 | −120 |
| ANTO | KONO | 19.8 | 4.6 | 104 |
| ANTO | KONO | 12.1 | 4.1 | 44 |

†No PDE location.

‡ O.T. (station 1) − O.T. (station 2) where O.T. = onset time − distance/4.0.

azimuth is 36.3° and the great-circle azimuth is 58.4°. In contrast, at ANMO these azimuths differ by less than 10°. The difference in apparent origin times for each pair of detections ranges from a fraction of a minute to more than 6 min. If a nominal group velocity of 4.0 km/s is assumed, the origin time differences correspond to an uncertainty in epicenter of as much as 20°. Clearly, the criteria by which detection pairs are judged to be associated or not are inadequate for accurate epicenter determinations.

Table II-10 contains epicenter pairs for a presumed earthquake at a latitude of about 15° with a longitude that is uncertain by as much as 20° in arc distance. Most of the epicenters lie in West Africa, which is consistent with the largest amplitude recorded at BCAO. However, a longitude passing through West Africa would give an epicentral distance to BCAO with the range 10° to 20° which is too close to be consistent with the dispersed wave trains shown for event 2 in Fig. II-14. The dispersion and azimuth are consistent with an earthquake on the mid-Atlantic ridge. Although this association of Rayleigh waves from this azimuth detector has not yet given much encouragement of accurately determining epicenters by this means, a rough origin time and location could be used to search the short-period records for P-waves that have gone undetected in a first pass through the data.

T. J. Fitch

## J. SRO/ASRO RAYLEIGH-WAVE DETECTIONS

The long-period seismograms from the SRO/ASROs contain an abundance of surface waves most of which cannot be associated with events located by the standard technique using short-period P times. Conversely, only a fraction of the events listed in the PDE or ISC bulletins can be correlated with a Rayleigh-wave detection. The detections considered here are from the azimuth detector previously described in this report.

Examples of these raw and processed data from stations ANMO and CHTO, shown in Figs. II-15(a) and (b), illustrate some of the major problems encountered when evaluating individual detections. A signal was considered detected if elliptical particle motion was correlated on the vertical and at least one of the horizontal components to better than 0.7 for more than 60 s. The filtered records for ANMO show that the detector often switches off and on sometimes several times during the passage of what looks like a single wave train to the observer. This problem is exacerbated by multipathing that is seen as a beating pattern on Rayleigh waves that have traveled teleseismic distances.

Parameters of mean azimuth in the detection window, mean amplitude, onset time, and duration were stored for each detection. Table II-11 summarizes the results of a comparison between Rayleigh-wave detections and PDE locations for 4 October 1980. At most, only half of the located events have detectable Rayleigh waves at a given station, and at a sensitive site such as the one for BCAO in Central Africa there will be many times as many detections as there are local events.

These disparities are not surprising because the body phases, of which the P-waves are prime examples, and the surface waves have fundamentally different excitation functions that are strongly depth dependent in the case of fundamental-mode surface waves. P-waves are excited preferentially by underground explosions or earthquakes at subcrustal depths. Of the located events on 4 October, two ($m_b$ 4.7 and 4.8) were placed in the mantle and, as expected, Rayleigh waves from them were not detected at teleseismic distances. In contrast, Rayleigh

TABLE II-11

PDE LOCATIONS FOR 4 OCTOBER 1980
VS RAYLEIGH-WAVE DETECTIONS

| Station | Number of Rayleigh-Wave Detections | Number Correlated With 10 Events of $m_b > 3.5$† |
|---|---|---|
| ANMO | 11 | 3 |
| CHTO | 15 | 4 |
| NWAO | 13 | 3 |
| ANTO | 20 | 4 |
| BOCO | 8 | 2 |
| BCAO | 62 | 3 |

†Station to epicenter azimuth agree within ±30°, and Rayleigh-wave arrival times predicted from locations agree with detector onset times within a few minutes, assuming a group velocity of 3.8 km/s.

waves from a small earthquake ($m_b$ 5.2, O.T. 03:24:49.0) on 4 October were located in the Philippine Islands region but yielded no short-period P-wave detections at even the closer of the SRO/ASROs – CHTO, GUMO, TATO, and NWAO – whereas Rayleigh waves with reasonable onset times and azimuth were detected at these stations. The Rayleigh-wave detections can be formally associated with a particular event if amplitudes, onset times, and azimuths meet certain criteria that are discussed in Sec. III.

T. J. Fitch

## REFERENCES


1. U.S. Contribution to the Data Collection Experiment, US/GSE/13, February 2, 1981.
2. Seismic Discrimination SATS, Lincoln Laboratory, M.I.T. (30 September 1979), DDC AD-A082615/6.
3. Ibid. (30 September 1980), DTIC AD-A097999.
4. W. H. Swindell and N. S. Snell, "Station Processor Automatic Signal Detection System: Phase I Final Report," Texas Instruments Report ALEX(01)-FR-77-01 (1977).
5. R. V. Allen, "Automatic Earthquake Recognition and Timing from Single Traces," Bull. Seismol. Soc. Am. 68, 1521-1523 (1978).
6. Seismic Discrimination SATS, Lincoln Laboratory, M.I.T. (30 September 1980), p. 19, DTIC AD-A097999.
7. J. F. Masso, C. B. Archambeau, and J. M. Savino, "Implementation, Testing, and Specification of a Seismic Event and Discrimination System," Final Report U.S. Arms Control and Disarmament Agency, Report No. SSS-R-70-3963, System, Science and Software, La Jolla, California (1979).

8. A. Dziewonski, S. Bloch, and M. Landisman, "A Technique for the Analysis of Transient Seismic Signals," Bull. Seismol. Soc. Am. 59, 427-444 (1969).

9. G. Stockman, L. Kanal, and M. C. Kyle, "Structural Pattern Recognition of Carotid Pulse Waves Using a General Waveform Parsing System," Commun. ACM 12, 688-695 (1976).

10. T. Lozano-Perez, "Parsing Intensity Profiles," Artificial Intelligence Memo No. 329, M.I.T. (1975).

11. P. Miller, "A Locally Organized Parser for Spoken Input," Commun. ACM 17, 621-630 (1974).

12. T. Pavlidis and F. Ali, "A Hierarchical Syntactic Shape Analyzer," IEEE Trans. Pat. Anal. Mach. Int. PAMI-1, 2-9 (1979).

13. J. P. Thorne, P. Bratley, and H. Dewar, "The Syntactic Analysis of English by Machine," in Machine Intelligence 3, edited by D. Michie (American Elsevier, New York, 1968), pp. 281-309.

14. D. G. Bobrow and J. B. Fraser, "An Augmented State Transition Network Analysis Procedure," Proc. Intl. Joint Conf. on Artificial Intelligence, 1979, pp. 557-567.

15. W. A. Woods, "Transition Network Grammars for Natural Language Analysis," Commun. ACM 13, 591-606 (1970).

16. M. Bates, "The Theory and Practice of Augmented Transition Network Grammars," in Natural Language Communication with Computers (Springer-Verlag, New York, 1978), pp. 191-259.

17. E. Charniak, C. K. Riesbeck, and D. V. McDermott, Artificial Intelligence Programming (Lawrence Erlbaum Associates, Hillsdale, New Jersey, 1980), p. 323.

18. R. W. Ehrich and J. P. Foith, "Representation of Random Waveforms by Relational Trees," IEEE Trans. Comp. C-25, 725-736 (1976).

19. K. R. Anderson, "Automatic Processing of Local Earthquake Data," Ph.D. Thesis, Department of Earth and Planetary Sciences, M.I.T., August 1978.

20. Seismic Discrimination SATS, Lincoln Laboratory, M.I.T. (30 September 1977), DDC AD-A050584/2.

21. Ibid. (31 March 1977), DDC AD-A045453/8.

22. Ibid. (30 September 1978), DDC AD-A065574/6.

23. E. Smart, "A Three-Component, Single-Station, Maximum-Likelihood Surface Wave Processor," Teledyne-Geotech Report Number SDAC-TR-77-14 (1978).

24. A. C. Strauss and L. C. Weltman, "Continuation of the Seismic Research Observatories Evaluation," Texas Instruments Report ALEX(01)-TR-77-02 (1977).

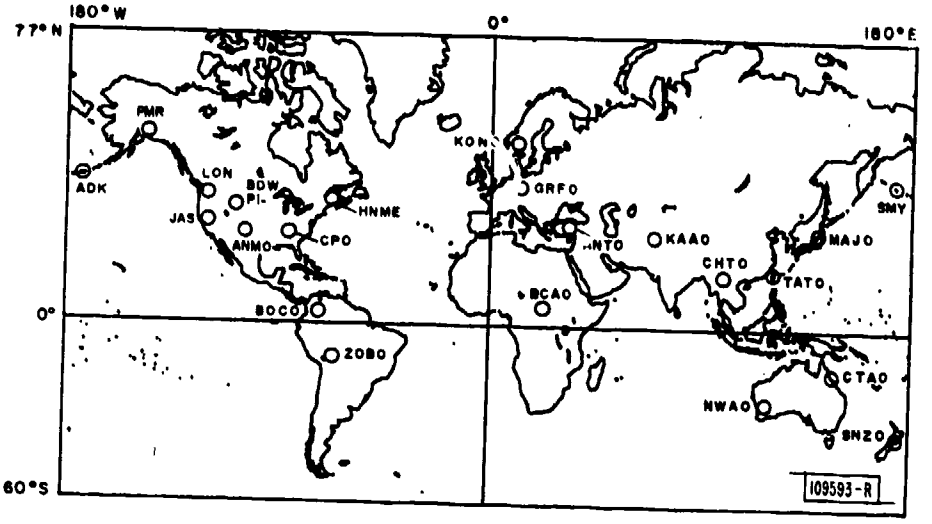


Fig. II-1. Locations of stations from which data were included in U.S. contribution to IDCE.

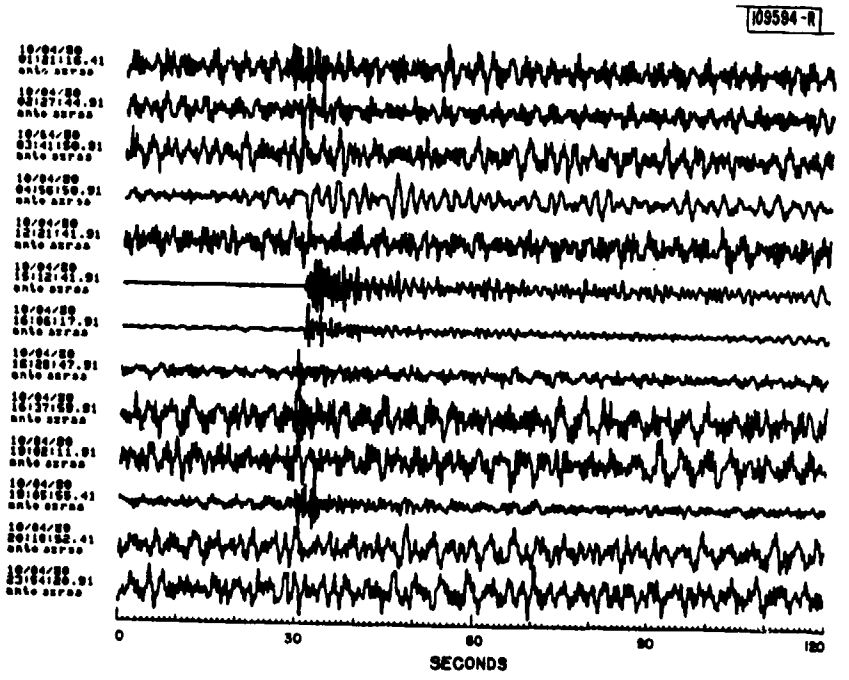


Fig. II-2. Detection windows for station ANTO, for 4 October 1980.

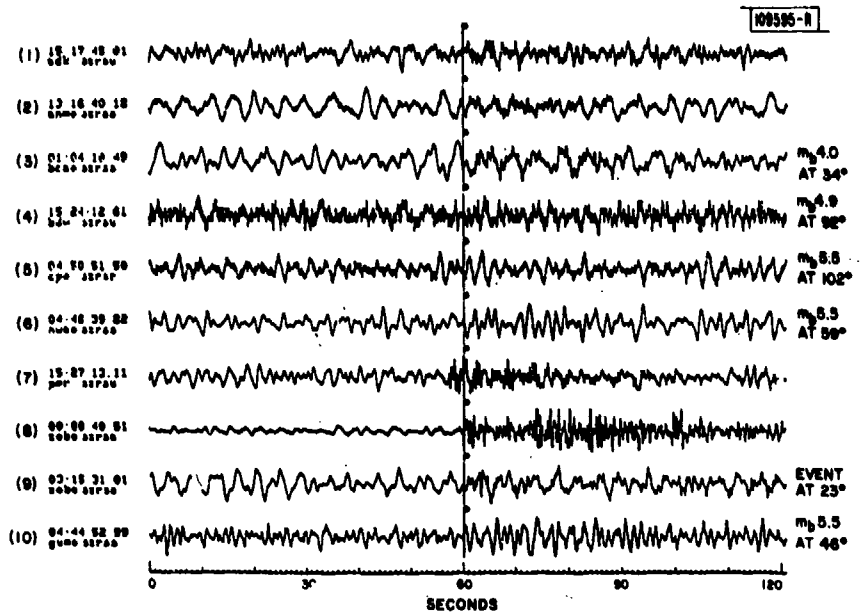


Fig. II-3. Sample seismograms showing analyst time picks for arrivals which were not detected with detector using standard parameters given in Table II-2. P identifies onset time picked by analyst.

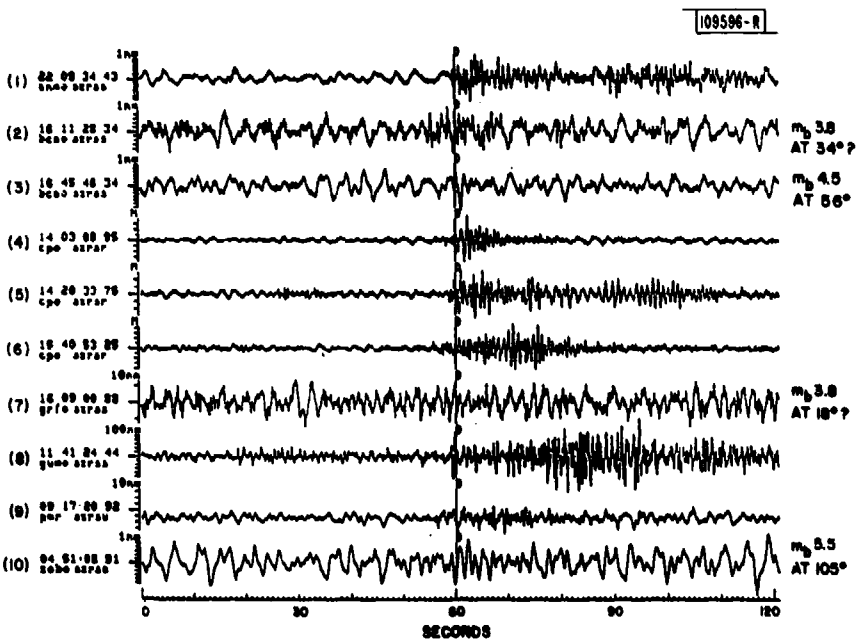


Fig. II-4. Sample seismograms showing signals which were detected but not picked by analyst. D identifies detector onset time which is invariably later than true onset which would be picked by an analyst.

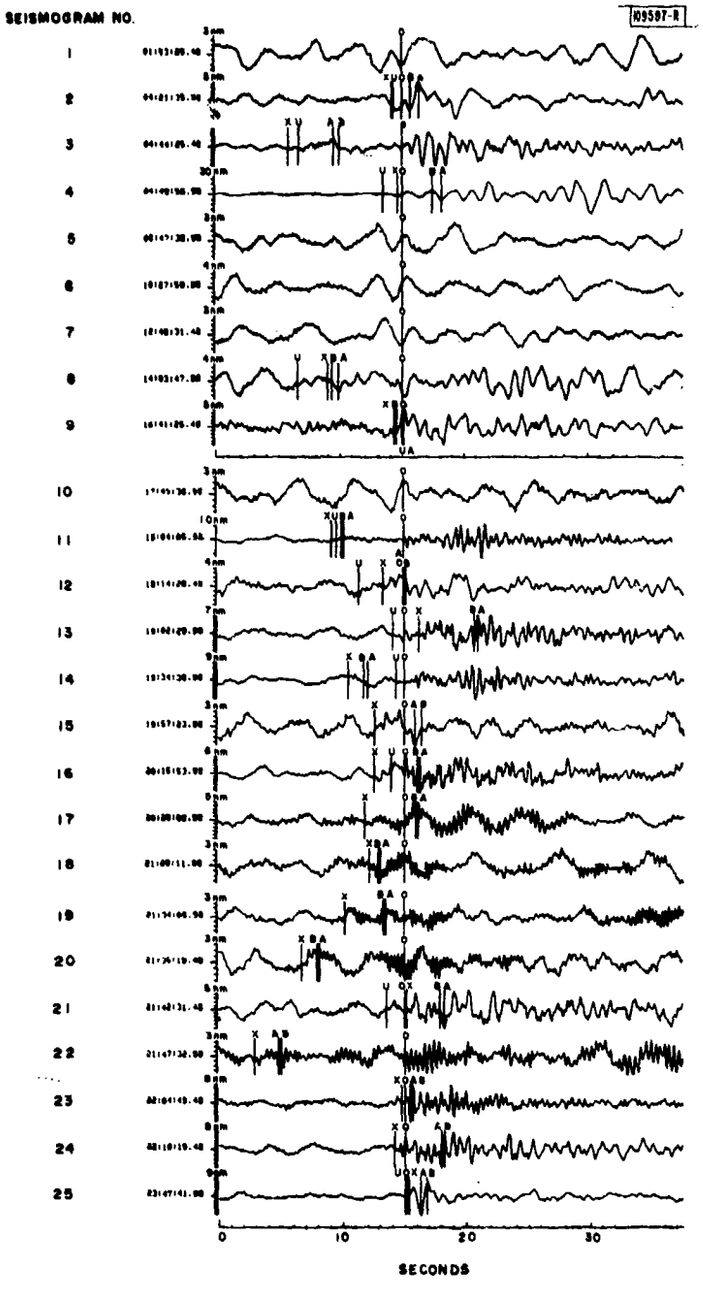


Fig. II-5. 25 detections from ANMO SPZ 4 October 1980. X is program first-arrival pick; U is analyst pick provided with IDCE parameter database; O is detection time; A is largest peak in first 5 s.

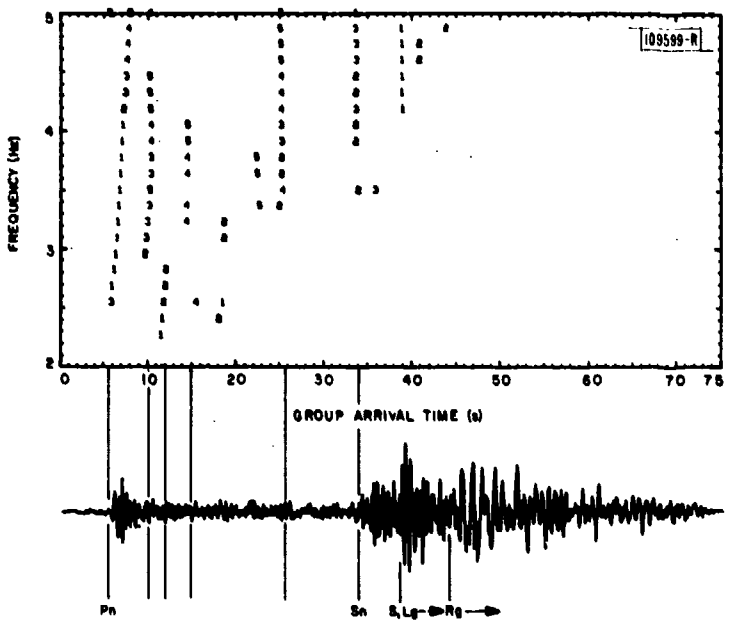


Fig. II-6. The $t_g$-f plane and seismogram for an event recorded by short-period band of CPO. Start time is 4 October 1980, 17:07:10.45 GMT.

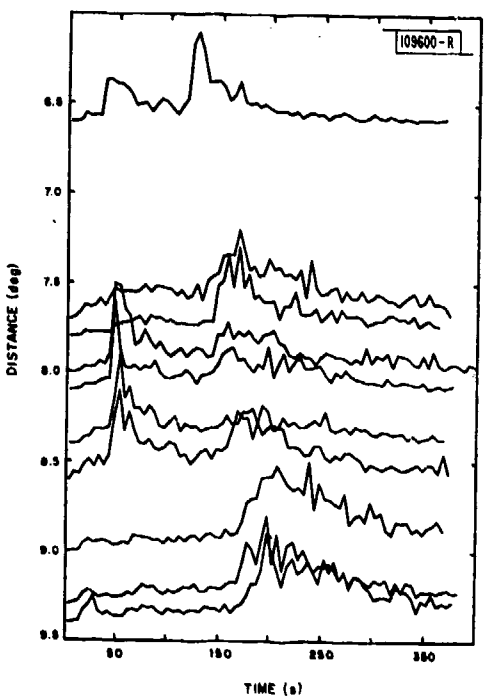


Fig. II-7. Variation of seismic envelope shape between 6° and 9°. Original seismograms were recorded at ANMO.

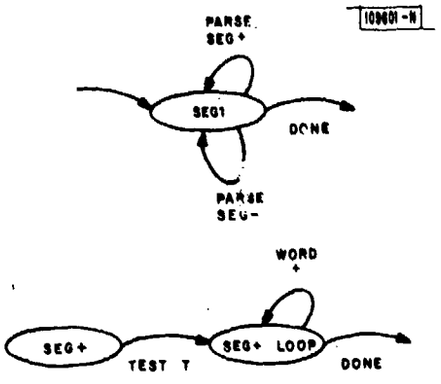


Fig. II-8. A simple ATN grammar. Subnet for SEG– (not shown) is similar to that of SEG+.

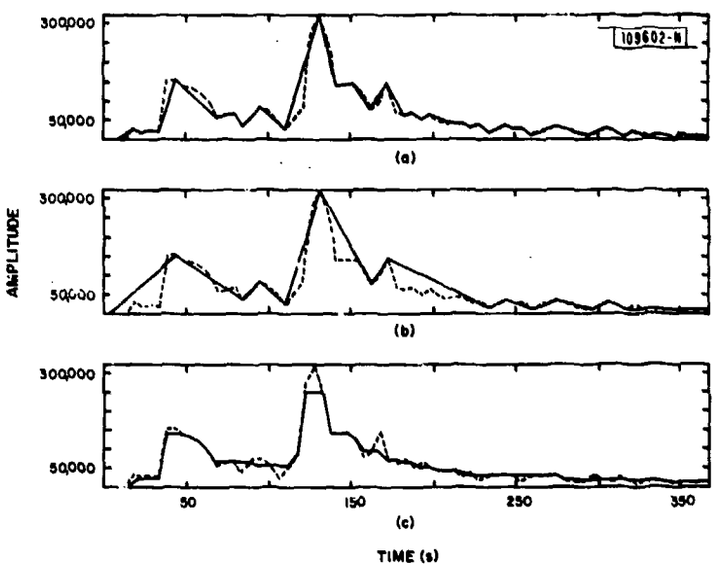


Fig. II-9. Data representation using (a) SEG1 grammar, and (b) SEG2 grammar. Effect of a 25-s running median smoother is shown for comparison in (c).

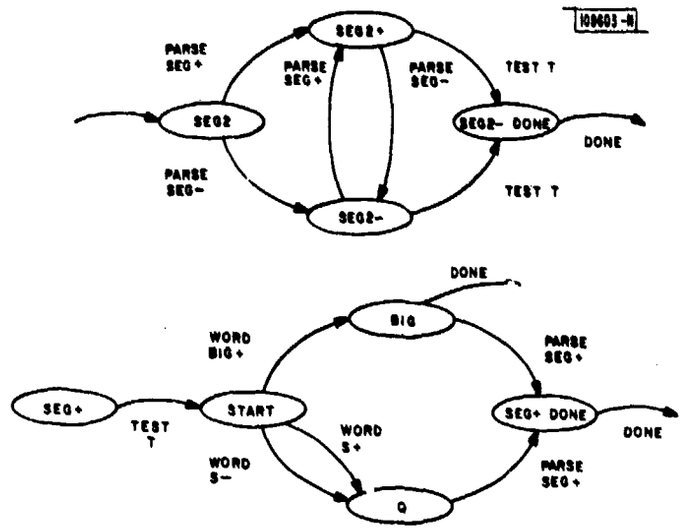


Fig. II-10. SEG2 grammar. Subnet for SEG- (not shown) is similar to that of SEG+.

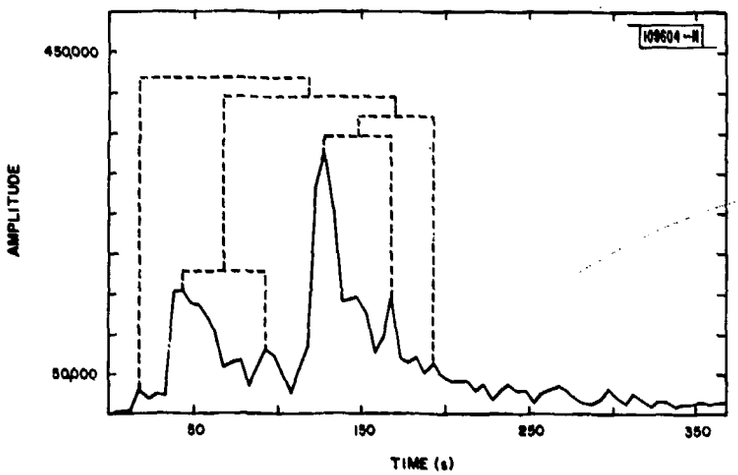


Fig. II-11. Hierarchical structure (dotted lines) imposed by relationships between peaks and valleys in seismic envelope (solid curve).

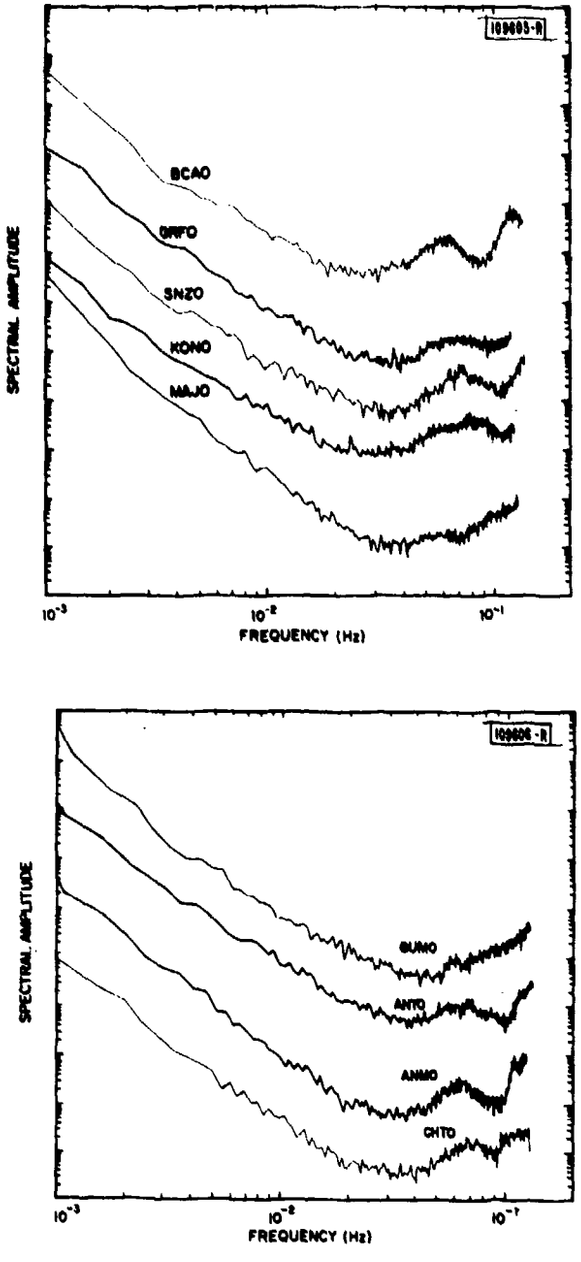


Fig. II-12. SRO/ASRO long-period noise spectra from 1 April 1980. Instrument response and spectra smoothed by averaging over seven to eight 512-point time samples. Sampling interval is 4 s.

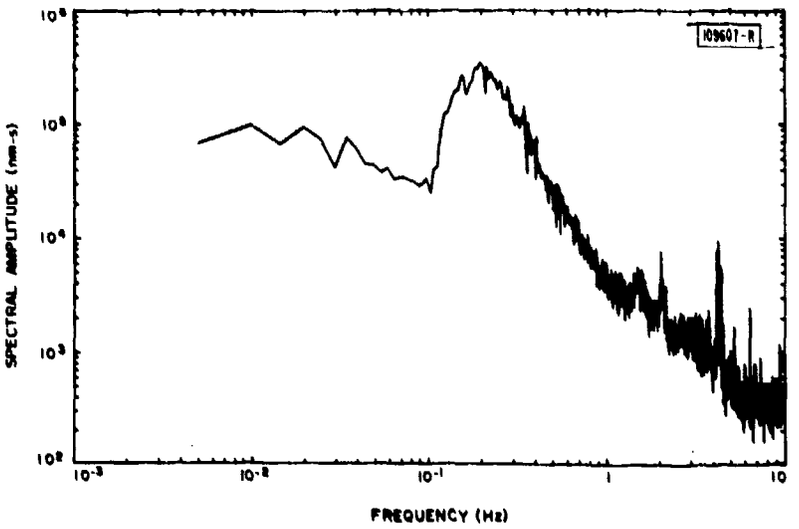


Fig. II-13. Spectra of a broadband SRO recording at ANMO. Spectra smoothed by averaging eight 4096-point time samples. Sampling interval is 1/20 s. Notice spectral lines in band from 1 to Nyquist frequency of 10 Hz.

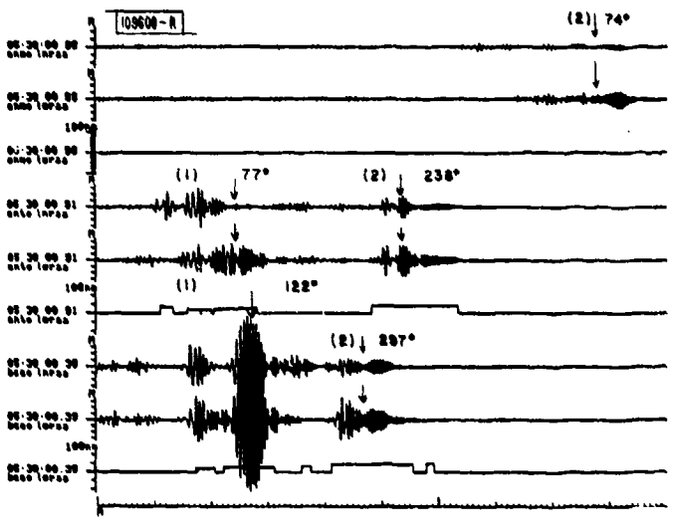


Fig. II-14. Detailed Rayleigh waves – associate wave trains are numbered and apparent azimuth from station to epicenter is given on opposite sides of arrows.

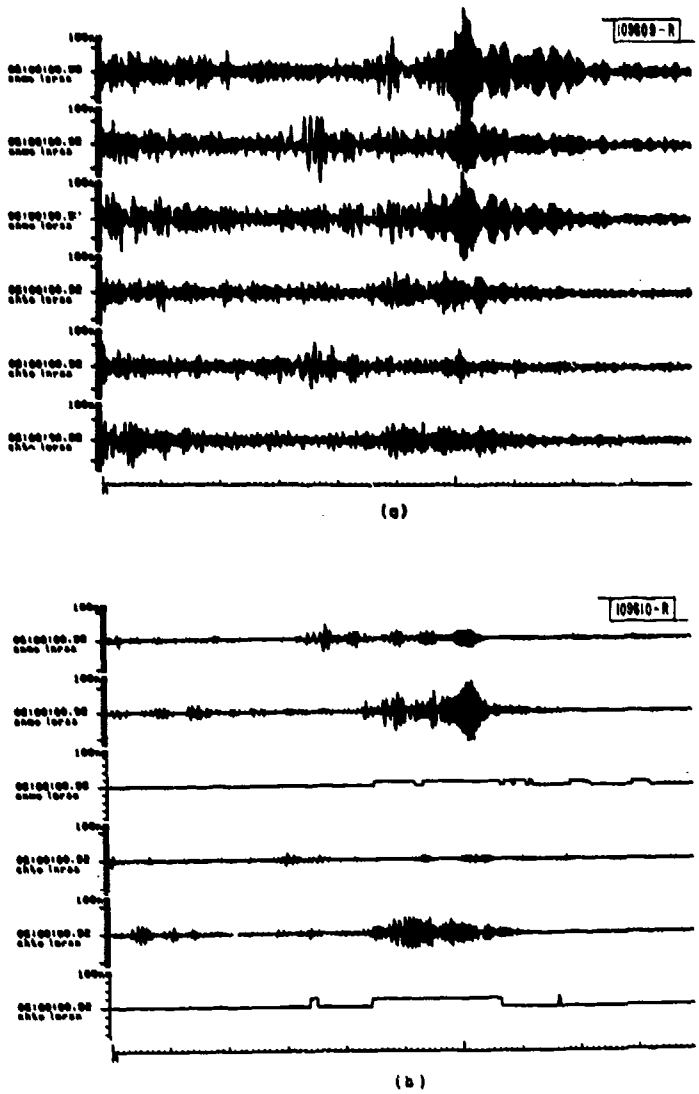


Fig. II-15. (a) Raw seismograms; (b) seismograms processed for Rayleigh-wave detection.

# III. GENERAL SEISMOLOGY

## A. FURTHER SURFACE-WAVE ANALYSIS OF EASTERN KAZAKH PRESUMED EXPLOSIONS

In the two preceding SATSs,[1,2] we studied several presumed explosions in the eastern part of the Soviet test site in Eastern Kazakh. For one of these (on 7/7/79), the Rayleigh waves were reversed in phase compared with the others at all observing stations, with a pronounced non-circular radiation pattern and enhanced Love-wave radiation pattern. We have since extended the number of events studied to those given in Table III-1. A detailed analysis of these events (carried out as before) reveals that, as well as the event on 7/7/79, another event on 8/18/79 generated Rayleigh waves which were reversed in phase at all stations compared with the "normal" events (hereafter called type I), with a similar Rayleigh-wave radiation pattern and enhanced Love-wave amplitudes (type III). In addition, a third event (on 11/4/78) is reversed in phase at two stations only (KAAO and MAJO) which correspond to observation points in opposing quadrants of the radiation pattern (type II).

TABLE III-1

REVISED LOCATIONS AND MAGNITUDES OF EASTERN KAZAKH EVENTS

| Event | Date | Origin Time (h:m:s) | Latitude | E(Lat) (km) | Longitude | E(Lon) (km) | $m_b$ | $M_s$ | SD($M_s$) | N($M_s$) |
|---|---|---|---|---|---|---|---|---|---|---|
| 1 | 9/15/78 | 02:36:57.3 | 49.920 | 2.95 | 78.843 | 3.62 | 6.0 | 3.99 | 0.14 | 5 |
| 2 | 11/4/78 | 05:05:57.5 | 50.050 | 4.18 | 78.918 | 3.07 | 5.6 | 3.75 | 0.12 | 7 |
| 3 | 6/23/79 | 02:56:57.0 | 49.896 | 3.37 | 78.807 | 4.63 | 6.3 | 4.14 | 0.08 | 6 |
| 4 | 7/7/79 | 03:46:57.4 | 50.013 | 4.58 | 78.947 | 4.11 | 5.8 | 3.95 | 0.49 | 5 |
| 5 | 8/4/79 | 03:56:57.2 | 49.887 | 3.51 | 78.838 | 4.23 | 6.1 | 4.23 | 0.07 | 6 |
| 6 | 8/18/79 | 02:51:57.3 | 49.953 | 3.40 | 78.912 | 3.34 | 6.1 | 3.84 | 0.17 | 7 |
| 7 | 10/28/79 | 03:16:56.9 | 49.987 | 4.28 | 78.949 | 3.68 | 6.0 | 4.18 | 0.15 | 5 |
| 8 | 12/2/79 | 04:36:57.5 | 49.903 | 2.81 | 78.817 | 4.26 | 6.0 | 4.25 | 0.05 | 7 |
| 9 | 12/23/79 | 04:56:57.6 | 49.930 | 3.05 | 78.716 | 3.05 | 6.1 | 3.96 | 0.02 | 4 |

Date, origin time, and body-wave magnitude $m_b$ from NEIS bulletin. Locations revised as described in Ref.1, E(Lat) and E(Lon) are standard errors in latitude and longitude. Surface-wave magnitude $M_s$ is mean of N($M_s$) observations at stations of SRO/ASRO networks, with standard deviation of SD($M_s$).

As we have pointed out previously,[2] the surface-wave radiation for the types II and III events can be explained by the addition of induced thrust faulting to the explosion monopole. Induced faulting, though in this case of strike-slip type, has been suggested to explain observations similar to those of the type II event for some explosions at the Nevada Test Site (NTS). Thrust faulting has been proposed independently[3,4] as a possible mechanism for certain features of the elastic-wave radiation from some underground explosions.

In our previous studies[1,2] we noted that the imaginary part of the far-field complex spectrum of both Rayleigh and Love waves is very poorly excited by shallow sources. In our earlier attempts to invert surface-wave data from Eastern Kazakh, we carried out inversion in the time domain for the resolvable parts of the seismic moment tensor in the formulation of Mendiguren.[5] We have subsequently abandoned the time-domain inversion procedure because of its extreme sensitivity to small phase changes, and now invert the data in the frequency domain assuming induced thrust faulting and the explosion monopole to be the only contributors to the surface-wave radiation. This extremely restricted model ignores some proposed features of the seismic source for explosions such as spall, the contribution from which is however inextricably linked with that of the monopole in the surface-wave radiation. There is no clear indication of spall in the short-period P-waves for any of the events studied here, though this need not preclude its occurrence at very short intervals after the explosion itself.

In the absence of the imaginary part, the far-field Rayleigh-wave radiation for a shallow source is given by

$$F_R(\Theta) = A_R S_R (R_1 - R_2 \sin 2\Theta + R_3 \cos 2\Theta)$$

where $F_R(\Theta)$, $A_R$, and $S_R$ are as defined previously[2] (depending additionally upon frequency and source depth), $\Theta$ being the azimuth of observation. Assuming the source to consist only of a monopole of seismic moment E and thrust faulting of moment Q,

$$R_1 = \frac{2}{3} E - \frac{5}{6} Q$$

$$R_2 = Q \sin 2\phi/2$$

$$R_3 = Q \cos 2\phi/2$$

where the strike of the thrust fault is given by $\phi$. Thus E, Q, and $\phi$ are given by

$$Q = 2(R_2^2 + R_3^2)^{1/2}$$

$$E = 1.5\, R_1 + 1.25\, Q$$

$$\phi = \frac{\tan^{-1}(R_2/R_3)}{2} \quad .$$

The data we wish to invert are the real part of the source spectrum: we have observation only of the amplitude variations with azimuth and phase differences between events. To obtain the real part from this information, we make the following assumptions:

(1) The imaginary part of the spectrum cannot be appreciably excited for shallow sources.

(2) The six "normal" events (type I) with the smallest amplitude variation with azimuth are such that the monopole term dominates, and the source initial phase is $\pi$. Observations of phase reversals at a given station compared with these normal events indicate a source initial phase of 0.

(3) The real part of the spectrum is consequently given by (−amplitude spectrum) for unreversed signals and by (+amplitude spectrum) for reversed signals.

We are forced to make assumption (2) and hence (3) by the lack of any calibration of propagation effects for the paths used. The above assumption conveniently sidesteps the problem of calibrating the dispersion for each path, and we are left with the question of attenuation. We have chosen an attenuation coefficient $\gamma$ of $1 \times 10^{-4}$/km over the period range 20 to 45 s to correct the observed amplitudes back to the source. This rather arbitrary choice falls between the largest and smallest Q estimates of Burton[6] and is toward the lower end of the measurements of Patton.[7] We have found that different choices of average $\gamma$ (e.g., 0.5 or $2.0 \times 10^{-4}$/km) result in only marginal changes in the results of the inversion. For such disparate paths as those considered here, any gross average must for some paths be substantially in error, but we are, again in the absence of a calibration event of known mechanism, unable to assign different attenuation coefficients to each path. A very large difference exists between both spectral and time-domain amplitudes at stations CHTO and SHIO, though these differ only slightly in both azimuth and distance from the source. We have somewhat arbitrarily decided to multiply amplitudes at CHTO by 3 in order to bring them into closer agreement with those at SHIO. We believe the amplitudes at CHTO to be low due to defocusing of the ray paths by oblique incidence at the high velocity-contrast boundary between the Tibetan plateau and the structure to its south, and ray-tracing experiments[8] in laterally varying velocity models of this area demonstrate such an effect. It should be noted here that the effects of geometrical spreading over the surface of the globe are incorporated in the term $S_R$ given above.

In the moment tensor inversion schemes as implemented by Mendiguren[5] and Patton,[9] the data to be inverted consist of the real and imaginary parts of the spectrum at a range of frequencies as observed over a number of stations or azimuths. In general, this is necessary because of the differing variation of the excitation functions $A_R$, $B_R$, and $C_R$ with frequency. This is not strictly necessary for very shallow sources since the spectra are determined in this case only by $A_R$, scaled by a factor (which may be negative) depending on the value of Mij and the azimuth. Thus, provided the propagation corrections and various other basic assumptions such as that of a step source time function are correct, the same solution would be provided by observations at a single frequency only. We may thus choose to invert the data in several different forms:

(1) At a single frequency point where we believe that variations in propagation effects such as spreading and attenuation are smallest, such as the longest periods available in the spectrum.

(2) At a number of frequencies, taking advantage of the redundancy thus provided to effectively average several estimates.

(3) Integrate the spectrum over a certain frequency range, the excitation function then being the corresponding integral of $A_R S_R$.

After several experiments, we settled upon method (3) above, integrating over the period range 20 to 45 s, as providing the most stable data for inversion, probably because it averaged out variations which could not otherwise be removed without excessive smoothing. Figure III-1 shows this form of the input data for the inversion, consisting of integrals of the real part over the chosen frequency range. Negative values indicate initial phase of $\pi$ (i.e., for "normal" phase seismograms), and positive values indicate an initial source phase of 0 (reversed compared with normal seismograms).

The results of a least-squares inversion of the data shown in Fig. III-1 are given in Table III-2, where $R_1$, $R_2$, and $R_3$ are the $\Theta$-invariant, $\sin(2\Theta)$, and $\cos(2\Theta)$ coefficients providing the best fit to the data. The number of stations used in each inversion and the ratio of the residual rms to that of the data itself are also given. The latter is smallest for the type I events exhibiting the least azimuthal variation, and larger for the types II and III events. We discovered that the large residual rms for event 2 could be considerably reduced (by 50 percent) by changing the sign of the real part (i.e., reversing the phase) at station ANTO, but such a step is not warranted by the phase difference data. We have, however, no real explanation for the greater difficulty in obtaining a fit, as measured in terms of residual rms, for the types II and III events. Misfits were largest for the stations near the "nodes," i.e., of smallest amplitude: this is a common feature of inversions of radiation patterns since amplitudes in these directions are generally overestimated.

From the results of the inversion we have deduced the seismic moments of the explosion monopole and double-couple components, assuming the latter induced faulting to be of thrust type, and these, together with the ratio of the moment of faulting to explosion (or F-factor), are given in Table III-2. As we could have deduced from Fig. III-1, F is smallest for the type I events and largest for those of type III, for which F exceeds 2.0, as required for phase reversal at all azimuths. We do not really understand the very large F (13.28) obtained for event 6, which is primarily due to the exceptionally low value obtained for the explosive moment. Excluding this, we see that the values of the moment of the explosion range only from 9.06 to $20.38 \times 10^{22}$ dyn-cm, reflecting the small range of explosion yields which can be deduced from the similarly small range of $m_b$ values for these events. Blandford[10] has obtained an expression for corner

TABLE III-2

RESULTS OF RAYLEIGH-WAVE INVERSION

| Event | $R_1$ | $R_2$ | $R_3$ | N | Fit | Q | E | F | Azimuth |
|---|---|---|---|---|---|---|---|---|---|
| 1 | 5.30 | 0.84 | −1.30 | 6 | 0.21 | 3.09 | 11.81 | 0.26 | 73.5 |
| 2 | 0.76 | 3.07 | 0.80 | 8 | 0.49 | 6.34 | 9.06 | 0.79 | 37.7 |
| 3 | 6.39 | 2.76 | 1.96 | 8 | 0.15 | 5.60 | 16.59 | 0.34 | 49.9 |
| 4 | −10.60 | 9.84 | −0.48 | 8 | 0.30 | 21.16 | 10.55 | 2.01 | 34.2 |
| 5 | 7.68 | 2.99 | 3.88 | 8 | 0.17 | 7.09 | 20.38 | 0.35 | 61.2 |
| 6 | −5.16 | 2.83 | −1.90 | 9 | 0.28 | 6.59 | 0.49 | 13.28 | 29.6 |
| 7 | 7.16 | 2.75 | 1.69 | 7 | 0.04 | 6.50 | 18.86 | 0.34 | 28.9 |
| 8 | 9.58 | 0.32 | 1.73 | 9 | 0.21 | 4.43 | 19.91 | 0.22 | 85.8 |
| 9 | 4.23 | 0.65 | −1.59 | 8 | 0.07 | 3.42 | 10.63 | 0.32 | 78.9 |

$R_1$, $R_2$, and $R_3$ are radiation pattern coefficients as defined in text (units $10^{22}$ dyn-cm), N is the number of stations used, and the fit is measured as the ratio of the residual rms to the data rms. Assuming induced thrust faulting, the respective moments of the thrust fault and explosion monopole are given by Q and E (units $10^{22}$ dyn-cm) and their ratio F = Q/E is listed in the next column. The final column gives the strike (measured in degrees West of North) of the assumed thrust fault contribution.

frequency as a function of yield from data for NTS explosions; for 100-kT yield his formula gives a corner frequency of 0.8 Hz which, assuming omega-square scaling, implies a DC seismic moment of $\sim 10^{23}$ dyn-cm, in good agreement with the values we have obtained. It is worth emphasizing that a simple model, such as an omega-square model with such a DC value of moment, is incapable of generating the large short-period P-waves generated by these explosions; and a more complicated source model, such as that of Aki et al.,[11] is required to explain the large differences in the excitation of high- and low-frequency for explosions which leads to the $M_s$:$m_b$ discriminant.

In Fig. III-2(a-b) we show two comparisons of the monopole explosion moment with short-period body-wave amplitudes. Figure III-2(a) compares the average amplitude, obtained from $\log (m_b - 5)$ where $m_b$ is that given in the PDE, with the explosion moment. This is somewhat unconvincing, primarily, we believe, because of the large variations in amplitude from station to station as exemplified in the short-period P-waves observed at the SRO/ASRO sites. To attempt to obtain a more consistent measure of short-period amplitudes we have, for each of the SRO/ASRO stations, calculated the ratio of the P-wave maximum amplitude to that for event 8, and averaged this for the same set of stations for each event. The results are shown in Fig. III-2(b) where a slightly more convincing correlation is obtained. By both measures, however, the explosive moment obtained for event 6 is excessively low.

We have investigated the solution for event 6 in some detail and found no errors in our reduction of the data for this event. The data from KONO are a crucial factor in the solution. By reducing the spectral amplitude given in Fig. III-1 for KONO by two-thirds, an apparently more reasonable solution with F ~ 3 can be obtained, but there is no reason to assume that the data for this station are in error and, in fact, the spectral amplitude variations shown for KONO for each event in Fig. III-1 exactly mirror the time-domain measurements. The spall or slapdown phase may conceivably have been unusually large for this event and largely canceled out the monopole contribution in the long-period part of the spectrum. No indication can be seen of such a phase in the short-period data for this event, but this does not necessarily mean that spall is not a significant factor. It is unfortunately inseparable from the monopole contribution in the long-period surface-wave spectra. We have assumed step-function time dependence for both monopole and faulting contributions. That this is not strictly valid is shown by the well-known observation that the dominant period of the maximum amplitude surface waves, from larger nuclear explosions at least, is much shorter (8 to 12 s) than that for earthquakes at similar distances as seen on the WWSSN instrument, though not on the narrower-band SRO/ASRO systems. Several studies[11-13] have indicated a different source time function for explosions, which is apparently yield-dependent.

The deduced seismic moment of the inferred thrust faulting shows much more variation than that for the explosive component. A possible check on these values is provided by the Love waves, which are of course generated by the faulting component only. We have integrated the Love-wave spectra of each seismogram over the period range 20 to 45 s, as we did previously for the Rayleigh-wave data, correcting for spreading and an attenuation of $2 \times 10^{-4}$/km (twice that used for the Rayleigh waves). An average value of this was determined for each event, and the results are plotted in Fig. III-3 against the predicted maximum value of this amplitude integral, given simply by

$$\int \frac{Q}{2} A_L S_L \quad .$$

We see that the amplitudes of the observed Love waves are well predicted by the values obtained for the moment Q of the (thrust) double-couple component. We have not attempted to compare observed and theoretical amplitude radiation patterns since we do not believe we have sufficient azimuthal resolution to do so.

The strike of the assumed induced thrust faulting, given in Table III-2, is fairly restricted, ranging from 29° to 80° West of North. If we restrict ourselves to events with high F-factors (events 2, 4, and 6), for which the faulting contribution is strongest, the strike varies only from 29° to 38° West of North. While we are not aware of the detailed tectonics of this region of Eastern Kazakh, it is interesting to note that this is very close to the strike (40° W of N) of a large fault clearly visible on Landsat imagery of this general region,[14] located however some 70 km to the west and additionally apparently of strike-slip nature. The consistency of the fault azimuths obtained indicates some fairly large-scale regional tectonic influence governing the orientation of the double-couple component of the source. In this respect we differ from Masse[3] who, while advocating thrust faulting as a significant contribution to seismic radiation from explosions, denies that this represents "induced" faulting governed by tectonics.

We believe that, within the limitations of the source model we have assumed (point source, step-function time dependence for both explosive and faulting contribution, and no consideration of spall), we have been fairly successful in explaining most features of the surface-wave radiation from the 9 explosions we have studied here. That this model is not entirely adequate is illustrated by the ludicrously high F-factor obtained for event 6, but, nevertheless, we feel that we have demonstrated that induced thrust faulting is a major contributor to the surface-wave radiation from Eastern Kazakh explosions.

R. G. North
T. J. Fitch

## B. INDUCED THRUST FAULTING AT NTS?

In Sec. A above, we indicated that Rayleigh-wave observations of Eastern Kazakh explosions in a small area to the north of the Shagan River can be adequately explained by a source model combining an explosion monopole and a double-couple component of thrust faulting type. The amount of such induced faulting can, when sufficiently large, cause phase reversals at some or all azimuths. The moments obtained for the monopole and thrust faulting components of the combined source are well correlated with short-period P-wave amplitudes and long-period Love-wave amplitudes, respectively. These conclusions are in good agreement with an explosion source model suggested by Masse.[3]

Observations of noncircular radiation patterns and phase reversals in some quadrants for some NTS explosions may also be explained by such induced thrust faulting, rather than the strike-slip faulting which was assumed by Toksoz and Kehrer,[14] with little justification from other evidence such as tectonic strain release patterns. We prefer, on purely physical grounds, the inducement of thrust or normal faulting over that of strike-slip faulting, since it seems to us more reasonable that vertical, rather than horizontal, displacements are more likely to occur as a result of an explosion. The thrust faulting hypothesis has the added advantage that the induced faulting is much smaller in fault dimensions, as measured in terms of seismic moment, for thrust rather than strike-slip to explain the same Rayleigh-wave observations. The largest moment that we obtained for the Eastern Kazakh events we have studied, sufficient to reverse phase at all azimuths, is quite small ($2 \times 10^{23}$ dyn-cm). Assuming a shear modulus of $3 \times 10^{11}$ dyn/cm$^2$, this is, for example, equivalent to slip of 10 cm over a fault of dimensions $2 \times 3$ km.

This choice between strike-slip and thrust as the mode of induced faulting could be resolved by the large difference in Love-wave excitation between the two faulting types. Unfortunately, this information cannot be deduced from the data given by Toksoz and Kehrer, and we do not have available high-quality digital data of SRO type with good azimuthal coverage for NTS. A lengthy analysis of LRSM data for earlier events would possibly resolve the question of whether induced faulting at NTS is of strike-slip type, as assumed by Toksoz and Kehrer, or of thrust type, supporting the generality of the model of Masse.

A somewhat cruder method of confirming one or the other mode of induced faulting may be provided by the variation of $M_s$ with yield. Figure III-4 shows the radiation pattern produced by the addition of faulting of strike-slip, thrust, and normal type to the explosion monopole, the amount of faulting being described by the F-factor – here defined as the ratio of the moment of the double couple representing the faulting to that of the monopole. From this, we may see that the radiation pattern produced by the addition of induced strike-slip faulting with F = 3.0 can be reproduced in shape and phase by induced thrust faulting of much smaller moment ($F \sim 0.7$). In the former case the amplitudes are larger than that for monopole only, and in the latter they are smaller. From the radiation patterns shown in Fig. III-4, we calculated the effect upon average $M_s$ of induced faulting of strike-slip, thrust, and normal type as a function of F, the ratio of the fault moment to that of the explosion monopole. Average $M_s$ effect has been determined from the algorithm of the ratio of the azimuthally averaged amplitude for (monopole + fault) to that for the monopole only, and the results are shown in Fig. III-5. We see that the addition of normal faulting sharply increases $M_s$, the addition of strike-slip initially has no net effect then increases $M_s$, and that the addition of thrust faulting initially causes a large decrease (up to 0.5 unit) in $M_s$ and then increases it as F grows larger. An alarming feature of induced normal faulting is that it would be difficult to resolve from surface-wave data, as it can never cause telltale phase reversals and simply enhances amplitudes in two quadrants. If normal faulting can be induced by explosions it can substantially increase $M_s$, and since normal faulting regions often involve high heat flow and other indications of low Q, the P-wave amplitudes may be smaller than usual. A combination of the two effects may defeat the $M_s$:$m_b$ discriminant.

The effects of induced faulting shown in Fig. III-5 are for average $M_s$. For NTS it is difficult, however, to obtain the good azimuthal coverage at teleseismic distances to average the radiation pattern. The radiation patterns and station data shown in the figures of Toksoz and Kehrer[14] indicate that, in fact, the observing stations are concentrated in the azimuths of one of the smaller lobes of the radiation pattern. In the direction of the largest lobes (NW and SE), however, the $M_s$ effect is particularly accentuated, as seen in Fig. III-4. In these directions the addition of strike-slip (F = 3.0) enhances $M_s$ by 0.7 unit, while the addition of thrust to produce the same radiation pattern in shape and phase ($F \sim 0.7$) reduces $M_s$ by 0.2 unit. Such a difference and, in particular, the large enhancement of $M_s$ by strike-slip faulting should be observable in these directions.

We have accordingly measured $M_s$ at WWSSN station COL (College, Alaska), which the figures of Toksoz and Kehrer show to be in the direction of the larger lobe for events with large deduced F-values, for 13 events of known yield in the range 56 to 1200 kT. These events include 7 for which Toksoz and Kehrer deduced F-factors assuming strike-slip faulting, 2 for which they had high F-factors (Piledriver, 56 kT, F = 3.2; and Greeley, 825 kT, F = 1.6) and phase reversals at some azimuths. The other 6 events are included to provide more calibration of $M_s$ as a function of yield; some of these may possibly show, on closer examination, induced

TABLE III-3

YIELDS, SURFACE-WAVE MAGNITUDE, AND F-FACTORS FOR UNDERGROUND NUCLEAR EXPLOSIONS IN NEVADA

| Event | Explosion | Y (kT) | $M_s$ | F |
|---|---|---|---|---|
| 1 | Duryea | 65 | 3.64 | 0.75 |
| 2 | Chartreuse | 70 | 3.75 | 0.90 |
| 3 | Piledriver | 56 | 3.56 | 3.2 |
| 4 | Half Beak | 300 | 4.64 | 0.67 |
| 5 | Greeley | 825 | 4.83 | 1.6 |
| 6 | Scotch | 150 | 4.32 | – |
| 7 | Knickerbocker | 71 | 3.90 | – |
| 8 | Boxcar | 1200 | 5.03 | – |
| 9 | Benham | 1100 | 5.08 | – |
| 10 | Flask | 107 | 3.51 | – |
| 11 | Carpetbag | 220 | 4.02 | – |
| 12 | Miniata | 80 | 3.60 | – |
| 13 | Starwort | 85 | 3.51 | – |

Yields Y (kT) from Springer and Kinnaman,[15] in which dates, locations, and shot medium are given for these events. $M_s$ as measured at WWSSN station COL (College, Alaska). F-factor as determined by Toksoz and Kehrer,[14] assuming induced strike-slip faulting.

faulting effects. Table III-3 lists the events used, their announced yield,[15] and, where determined, the F-factors of Toksoz and Kehrer. Their dates, shot times, depths, and locations may be found in the tables of Springer and Kinnaman.[15]

Figure III-6 shows the $M_s$ values measured at COL as a function of yield. Also shown is the relationship

$$M_s = \log Y + 2.0 \qquad \text{(yield } Y \text{ in kT)}$$

determined by Marshall et al.[16] for explosions in consolidated rock. They found that, for events in unconsolidated rock, $M_s$ values were up to 1 magnitude unit smaller. We see that the above formula fits all the events used here to better than 0.5 magnitude unit; in the cases where our events are the same as those of Marshall et al., the measurements made at COL agree very well with their average $M_s$ values. Both our results and those given in Fig. 1 of Marshall et al. show no anomalously large $M_s$ for Piledriver and Greeley, as would be expected by the addition of large amounts of strike-slip faulting.

Toksoz and Kehrer cite as confirmation of the induced strike-slip faulting that they propose the agreement of many of the fault strikes they obtained with the strike of the nearby Yucca fault.

Unfortunately for their case, most observed displacements on this fault have been dip-slip in character and they were forced to propose that observations of en-echelon fractures across this fault after one underground explosion (Corduroy) indicated strike-slip movement in the underlying basement. Their Figs. 8 and 9 show, however, very large numbers of dip-slip faults of precisely the orientation required of thrust faulting to enhance amplitudes in the NW-SE quadrants and to reduce them (and if strong enough, to reverse the phase) in the two other quadrants. We concede that, in view of the well-known extensional character of this region, the purely tectonic motion along these faults is more likely to have normal, rather than thrust faulting, type; but it is not inconceivable that this original direction of fault movement can be reversed by the compressional motion involved during an explosion.

We thus believe that the observations of azimuthal amplitude variations and phase reversals for some events at NTS are more consistent with induced thrust, rather than strike-slip, faulting. This implies that the explosion source model of Masse, involving explosion monopole and induced thrust faulting, with the possible addition of spall, is substantially correct at least in its prediction of the nature of surface-wave radiation from underground nuclear explosions. Further confirmation should be obtained by an analysis of Love-wave data from NTS explosions.

However, we do not agree with Masse that the thrust faulting component does not imply triggering of an earthquake. The consistency of the fault strikes obtained by this study for Eastern Kazakh events, and by Toksoz and Kehrer for NTS, indicates that the direction of a local or regional tectonic stress field governs that of the induced faulting. Symmetric thrust faulting on a cone above the explosion hypocenter, equivalent to a compensated linear vector dipole source, produces Rayleigh waves reversed in initial phase compared with the explosion itself. If sufficiently large, this conical faulting may reverse the phase at all azimuths: it cannot, however, produce the enhanced radiation in some directions, and phase reversals at some azimuths only, that are seen for both NTS and Eastern Kazakh explosions. Phase reversals at all azimuths have not, to our knowledge, been observed for NTS events – this may be due to the low competency of the surficial layers of volcanically derived sediments, that are pervasive in the Basin and Range province of the Western U.S., being unable to support or transmit large local or regional stresses.

R. G. North
T. J. Fitch

## C. CRUST AND UPPER-MANTLE STRUCTURE OF THE MIDDLE EAST AND SOUTH CENTRAL ASIA

In this study, we invert the available Rayleigh-wave phase- and group-velocity data to determine crust and upper-mantle structure in the Middle East and South Central Asia.

Figure III-7 shows some of the paths for which velocities are available. The data come from our measurements (Tubman and Toksoz[17]) as well as those of other investigators.

Figures III-8 to III-10 show phase and group velocities for Iran, the Arabian Peninsula, and Tibet, respectively. The path in Iran is between stations SHI and MSH. Arabian Peninsula velocities are for the path Red Sea – SHI. Velocities for Tibet are from Bird,[18] Patton,[19] and Chen and Molnar.[20]

Phase and group velocities were inverted simultaneously in order to determine crust and upper-mantle structure. A maximum-likelihood method weighted in both data and model space was used. Inversions were done for shear velocities only. Compressional velocities, densities, and layer thicknesses were held constant during the iterations. They were adjusted separately

when starting further iterations with a new starting model. Iterations were continued until the theoretical dispersion curves matched the observed velocities to within a specified rms error.

The structures for Arabia, Iran, and Tibet are shown in Fig. III-11. The model for Tibet is based on a refraction study which displays a low-velocity zone in the middle crust.[21] The surface-wave data do not have sufficient resolution to indicate the presence of this low-velocity layer.

Iran and Tibet exhibit thickened crusts and low velocities. Both regions have been deformed extensively by collisional processes. The Arabian Peninsula is on the other side of the collisional zone from Iran and remains relatively unaffected. Crustal thicknesses determined are 38, 47, and 70 km for Arabia, Iran, and Tibet, respectively.

Figures III-8 to III-10 show the fit of the theoretical dispersion curves predicted by these models to the data. As can be seen in the figures, theoretical and observed velocities agree quite well.

K. M. Tubman

## D. NUMERICALLY STABLE CALCULATION OF MODE EIGENFUNCTIONS

The solution to the numerical problems associated with evaluating the dispersion function for P-SV in a layered medium has been elaborated by Abo-Zena[22] and computational improvements given by Menke[23] and Harvey.[24] These methods avoid the evaluation of propagator products that can have exponentially large terms that algebraically cancel but cannot be successfully machine-canceled without loss of precision. Synthesis of seismograms for a buried source, however, entails not only evaluation of the dispersion function but also evaluation of mode eigenfunctions. This process again encounters the numerical problem associated with evaluating products of propagators. Harvey[24] introduces pseudolayers and the constraint imposed by an exponentially decaying boundary condition to avoid this numerical problem. This method still relies on machine cancellation of exponentially positive terms, but the pseudolayers are kept sufficiently thin that these terms are small.

The exponentially decaying boundary condition, however, can be used to construct an algorithm for eigenfunction calculation that completely avoids the use of pseudolayers. This algorithm preserves the advantage of the asymptotic fundamental matrix method given by Cormier[25] in minimizing the number of vertically inhomogeneous layers needed to describe an Earth model. The outline of the computational technique that follows can be applied to a homogeneously layered model as well as an inhomogeneously layered model.

The stress-displacement eigenfunctions at radius $r_{i-1}$ are related to those at radius $r_i$ by

$$\begin{bmatrix} e_1 \\ e_2 \\ e_3 \\ e_4 \end{bmatrix}^{i-1} = P \begin{bmatrix} e_1 \\ e_2 \\ e_3 \\ e_4 \end{bmatrix}^{i} \qquad \text{(III-1)}$$

where P is the propagator matrix from $r_{i-1}$ to $r_i$. Following Harvey,[24] by using Abo-Zena's Y matrix elements and the Sommerfeld radiation condition, the two traction eigenfunctions can be expressed in terms of the two displacement eigenfunctions:

$$e_3 = -Y_{14}/Y_{34}e_1 - Y_{24}/Y_{34}e_2$$

$$e_4 = Y_{13}/Y_{34}e_1 + Y_{23}/Y_{34}e_2 \qquad \text{(III-2)}$$

where the Y matrix elements and eigenfunctions are evaluated at the same depth. Substituting Eq. (III-2) into Eq. (III-1) shows that the eigenfunctions $e_1^{i-1}, e_2^{i-1}$ at radius $r_{i-1}$ are related to $e_1^i, e_2^i$ at $r_i$ by a 2 × 2 propagator matrix E:

$$\begin{bmatrix} e_1 \\ e_2 \end{bmatrix}^{i-1} = E \begin{bmatrix} e_1 \\ e_2 \end{bmatrix}^{i} \qquad \text{(III-3)}$$

where the elements of E are given by

$$E_{11} = (P_{11}Y_{34} - P_{13}Y_{14} + P_{14}Y_{13})/Y_{34}$$

$$E_{12} = (P_{12}Y_{34} - P_{13}Y_{34} + P_{14}Y_{23})/Y_{34}$$

$$E_{21} = (P_{21}Y_{34} - P_{23}Y_{14} + P_{24}Y_{13})/Y_{34}$$

$$E_{22} = (P_{22}Y_{34} + P_{23}Y_{24} + P_{24})/Y_{34} \qquad \text{(III-4)}$$

Y elements being evaluated at radius $r_i$, and P being the propagator from $r_{i-1}$ to $r_i$. For an Earth model having n − i discontinuities between radius $r_i$ and the free surface, Eq. (III-3) can be generalized by

$$\begin{bmatrix} e_1 \\ e_2 \end{bmatrix}^{i-1} = E^i E^{i+1} \cdots E^n \begin{bmatrix} 1 \\ \epsilon \end{bmatrix} \qquad \text{(III-5)}$$

where the index $\epsilon$ is the ellipticity at the free surface, and E is the eigenfunction propagator from the first model boundary below the free surface to the free surface. At any depth the traction eigenfunctions $e_3$, $e_4$ can be found by Eq. (III-3). By substituting specific expressions for the Y elements and propagator elements in Eq. (III-4) and exploiting all the algebraic cancellations that occur, it can be shown that the numerator of each element of an $E^i$ matrix consists of four terms of different exponential order. The order of each of these terms is always less than or equal to the exponential order of the denominator $Y_{34}$. When each numerator term is normalized by the same factor as $Y_{34}$, numerical stability is insured without need of inserting pseudolayer boundaries.

V. F. Cormier

## E. THE WAVEGUIDE OF Lg

The regional seismic phase termed "Lg" refers to surface shear waves having a dominant period 0.5 to 6 s and an average group velocity of 3.5 km/s (Press and Ewing[26]). Lg can be observed on all three components of ground motion, although it is commonly largest on the horizontal component (e.g., see Street et al.[27]). Because Lg is often the largest arrival at regional distances, seismic discriminants based on Lg have particular value for smaller events. Gupta et al.[28] tested an earthquake-explosion discriminant formed from the ratio of the maximum

P-wave amplitude to the maximum Lg amplitude ($P_{max}/Lg_{max}$). Chen and Pomeroy[29] tested a discriminant given by the ratio of the energies of Lg in two group-velocity windows ($E_h/E_l$, where $E_h$ is the energy in the window 4.0 to 3.4 km/s and $E_l$ is the energy in the window 3.4 to 2.8 km/s). Given that the properties of Lg can be successfully predicted from a superposition of higher-mode Rayleigh and Love waves in the appropriate group-velocity window (Oliver and Ewing[30]; Knopoff et al.[31]; Panza and Calcagnile[32]), a study of the waveguide of higher surface-wave modes combined with an examination of their group-velocity dispersion can be used to optimize discriminants based on Lg amplitudes. One result of such a study would be a prediction of the group-velocity and frequency windows of Lg that are best excited by a deep source vs those windows best excited by a near-surface source.

As a first step in such a study, the relative amplitudes and eigenfunction depth behavior of the higher Rayleigh modes were computed for a crustal model. The computational techniques used are described in the preceding section of this report. Figure III-12 shows the group velocities of Rayleigh modes of the Southern California model of Kanamori and Hadley[33] in the window appropriate for the Lg phase. (This crustal model is same as that used by Harvey[24] in a test of seismogram synthesis. The model calculated here, however, includes the effects of Earth sphericity by the use of asymptotic wave functions as discussed in Cormier.[25]) In Fig. III-12 one can see narrow bands of group velocity in which the stationary phases of groups of higher modes cluster. This clustering of stationary phases may account for the observations of multiple Lg phases described by Bath.[34] For the discussion that follows, the modes in the frequency window 1.3 to 2 Hz will be referred to as $Lg_1$ in the group-velocity window 3.35 to 3.50 km/s, $Lg_2$ in the window 3.24 to 3.32 km/s, and $Lg_3$ in the window 2.96 to 3.06 km/s.

Panza et al.[35] define the normalized energy density of a mode in terms of the density function $\rho(z)$, the vertical and horizontal displacement functions u(z), w(z), and their values at the free surface:

$$E = \rho(z) \{[u(z)/u(o)]^2 + [w(z)/w(o)]^2\} \quad . \tag{III-6}$$

In terms of ellipticity and displacement eigenfunctions, the energy density is given by

$$E = \rho(z) [e_1^2 + (e_2/\epsilon)^2] \quad . \tag{III-7}$$

The frequencies at which the mode energy densities of $Lg_1$, $Lg_2$, and $Lg_3$ were calculated were chosen to be at or near points of stationary phase in the mode group-velocity curves. In each energy-depth plot (Figs. III-13 to III-15), the S-velocity profile is shown for comparison.

Figure III-13 shows the energy of a mode member of $Lg_1$ to be maximum in the depth range 5 to 30 km. Mode members of $Lg_2$ (Fig. III-14) and $Lg_3$ (Fig. III-15), in contrast, have large energy throughout the depth range 0 to 35 km and maximum energy in the uppermost crustal layer. From these results it can be concluded that the crustal layers form the waveguide of Lg – the free surface forming the upper boundary of the waveguide, and the moho forming the lower boundary. The thinness of oceanic crust implies that if an oceanic phase analogous to Lg does exist, it will have a characteristic frequency much higher than that of continental Lg. For continental models having a sedimentary layer, the earliest portion of the Lg wavetrain in the highest group-velocity window has most of its energy concentrated in the crustal layer lying beneath the sedimentary layer. The waveguide of this portion of the Lg wavetrain is consistent with Press and Ewing's[26] idea that Lg propagates in the granitic layer of the crust.

The waveguide of $Lg_1$ is also consistent with the success of the seismic discriminant constructed by Chen and Pomeroy using the ratio of Lg energies in different group-velocity windows. That study found $E_h/E_l$ to be smallest for the Salmon explosion compared with $E_h/E_l$ for earthquakes in eastern North America. From Fig. III-13, it is apparent that an explosion at or near the free surface of a sedimentary layer will be less efficient in exciting the modes that $E_h$ measures compared with an earthquake beneath the sedimentary layer. If this interpretation is correct, the $E_h/E_l$ discriminant would not perform as well for Lg propagating in a crust lacking a sedimentary layer. These results suggest the feasibility of using the energy depth behavior of Lg modes to optimize seismic discriminants. Once the average crustal structure that characterizes an Lg path is known, optimal frequency and group-velocity filters can be constructed to discriminate source depth.

V. F. Cormier

## F. INVERSION FOR MULTIPLE SOURCES

This section describes generalization of the method of centroid location[1,36] to the problem of searching for the source parameters (moment tensor, hypocentral location) of either independent events closely spaced in time or events of finite spatial and temporal dimensions. In particular, we shall demonstrate application of this method in a numerical experiment in which the mechanism of a strike-slip earthquake and explosion of commensurate moments are fully resolved. The following describes the principle of the approach.

Assume that there are N point sources at starting locations $(r_n, \Theta_n, \phi_n)$ and origin times $t_n$. In the starting iteration, an attempt is made to determine their moment tensors $f_{in}^{(0)}$; for the $k^{th}$ record of our data set, the equation of condition is:

$$u_k(\underline{r}, t) = \sum_{n=1}^{N} \sum_{i=1}^{G} f_{in}^{(0)} \cdot \psi_{in}^{(0)}(\underline{r}, \underline{r}_n, t_n, t) \quad . \tag{III-8}$$

After the appropriate system of normal equations is solved for the initial estimates of $f_{in}^{(0)}$, the elements of the moment tensor and location parameters are refined in successive iterations:

$$u_k(\underline{r}, t) - u_k^{(0)}(r, t) = \sum_{n=1}^{N} \Bigg[ a_n^{(0)}(t)\, \delta r_n + b_n^{(0)}(t)\, \delta\Theta_n + c_n^{(0)}(t)\, \delta\phi_n + d_n^{(0)}(t)\, \delta t_n + \sum_{i=1} \psi_{in}^{(0)} \cdot \delta f_{in} \Bigg] \quad . \tag{III-9}$$

The appropriate definitions and derivatives are given for a single source in Ref. 36.

In Table III-4 we give a synthetic example of application of this approach to the resolution of two sources approximately 150 km apart and activated within 10 s of each other. The first source was a strike-slip earthquake ($f_2 = 1$, $f_3 = -1$; see Ref. 1 or 36 for explanation of notation); the second was an explosion ($f_1 = f_2 = f_3 = 1$). The starting locations are quite remote from the true ones, and the initial iteration yields moment tensors that have little in common with the true source mechanism of the individual events. However, after several iterations, both sources are fully resolved and their locations, origin times, as well as the moment tensors agree very well with the exact values. Although this has been a synthetic example, the result is of some interest, as we are not aware of any other method that would allow such resolution with a comparably sparse receiver network.

TABLE III-4

RESOLUTION OF A DOUBLE SOURCE*

| | Iteration 0 | | Iteration 1 | | Iteration 2 | | Iteration 3 | | Iteration 4 | |
|---|---|---|---|---|---|---|---|---|---|---|
| | S.1 | S.2 | S.1 | S.2 | S.1 | S.2 | S.1 | S.2 | S.1 | S.2 |
| Latitude | 35.50 | 37.50 | 36.02 | 36.50 | 35.95 | 36.91 | 36.02 | 37.00 | 36.00 | 37.00 |
| Longitude | 77.50 | 79.50 | 78.42 | 78.81 | 78.04 | 78.91 | 78.06 | 79.01 | 78.01 | 79.00 |
| $\delta t_0$ | −3.00 | 6.00 | 0.28 | 11.22 | 1.31 | 12.50 | −0.26 | 10.43 | 0.02 | 10.03 |
| $f_1$ | −0.561 | 0.963 | 0.371 | 0.436 | 0.034 | 0.947 | −0.009 | 0.983 | −0.002 | 0.997 |
| $f_2$ | 0.517 | 1.016 | 1.296 | 0.508 | 1.027 | 0.975 | 0.992 | 0.990 | 0.999 | 1.002 |
| $f_3$ | −1.542 | 1.256 | −0.271 | 0.140 | −0.943 | 0.928 | −0.997 | 0.989 | −1.001 | 0.998 |
| $f_4$ | 0.738 | −0.911 | −1.007 | 0.755 | −0.066 | −0.032 | −0.012 | 0.008 | −0.002 | 0.001 |
| $f_5$ | 0.559 | −0.565 | −0.627 | 0.493 | −0.043 | −0.005 | −0.003 | −0.002 | 0.000 | −0.002 |
| $f_6$ | 0.191 | −0.106 | −0.169 | 0.123 | −0.031 | 0.001 | −0.003 | −0.002 | 0.001 | 0.000 |

*An experiment with synthetic data. Seismograms were computed for a network of 13 SRO/ASRO stations assuming the following source parameters: (1) Strike-slip earthquake ($f_2 = 1$, $f_3 = -1$, $f_1 = f_4 = f_5 = f_6 = 0$) at location 36°N, 78°E, and origin time 0 s; and (2) an explosion ($f_1 = f_2 = f_3 = 1$, $f_4 = f_5 = f_6 = 0$) at location 37°N, 79°E, and origin time 10 s. The sum of these two sets of seismograms represented the data set in inversion. The starting coordinates are given in the column for Iteration 0 (only moment tensor is obtained in the zeroth iteration). S.1 and S.2 represent sources 1 and 2, respectively.

Another potential application of this approach is in studies of sources of finite size. Imagine that an earthquake can be approximated by a propagating line source, with the fault length L and duration 2T. The centroid method[36] for a single source would yield a point at the center of the fault and shift in the origin time equal to T. As discussed in the next section (Sec. G), this information is sufficient to resolve the fault parameters, provided that neither the location of the point of origin nor the centroid location are biased by the effect of lateral heterogeneities. Our current experience indicates that such bias is probable, and thus the estimates of the fault length velocity and direction of rupture propagation could be grossly erroneous. If the propagating fault were to be represented by two point sources, their locations, ideally, should fall on the fault at points distant by 1/4 and 3/4L from the point of origin, and at times 1/2 and 3/2T after the origin time. However, even if due to the large-scale heterogeneities the absolute locations are biased, in this case the estimate of the source dimensions should be much more accurate, as the ray-paths from both point sources to the receiver are very similar.

Even though our current experience with the analysis of actual data is limited, the initial results are encouraging, or at least intriguing. The main difficulty appears to be associated with assuring the stability of the solution by imposing physically plausible smoothing conditions.

A. M. Dziewonski

## G. ROUTINE DETERMINATION OF SOURCE PARAMETERS FROM THE ANALYSIS OF WAVEFORMS RECORDED BY THE GLOBAL DIGITAL NETWORK

In 1980, Chou and Dziewonski[1] proposed a method of derivation of the elements of the seismic moment tensor through linear inversion of the body-wave sections of records of the SRO/ASRO digital seismograph network. The fundamental mode data are excluded from the analysis, because of their sensitivity to the lateral variations in the Earth's structure. Derivation by Woodhouse[1] of the differential kernels for perturbation of synthetic seismograms with respect to changes in the geographical coordinates, depth, and the origin time of an event allowed joint inversion for the source mechanism and location of the centroid of the stress glut.[37] The detailed description of the procedure with numerous examples of application to studies of global and regional seismicity has been given by Dziewonski, Chou, and Woodhouse.[36] Since that report has been completed, we have analyzed approximately 100 events ranging in seismic moment from $2 \times 10^{24}$ to $2 \times 10^{27}$ dyn-cm. The ability to cover this wide a spread of earthquake sizes using exactly the same procedure is the result of the wide dynamic range of the SRO/ASRO network.

It is possible to think of extending the current lower limit of the seismic moment to $2 \times 10^{23}$ dyn-cm ($M_s \sim 4.5$) by calibrating the source-receiver paths for dispersion and attenuation of the fundamental-mode surface waves. This requires occurrence of earthquakes with $M_s \sim 6$ in a given region. The suggested procedure is as follows. Once the source mechanism is determined for a large event, using the approach of Ref. 36, the phase velocity and apparent attenuation can be determined for the Rayleigh-wave train contained in the same set of records. These calibration curves can be used to determine moments and source mechanism of considerably smaller events in the vicinity of the master earthquake. Substantial effort will be necessary to establish the range of distances from the master event over which the calibration curves are valid. Most likely, there will be strong dependence on the tectonic nature of the source-receiver path; one would anticipate that paths along continental margins, mid-ocean ridges, or trenches could be rather unstable.

The next subject to be discussed in this report has to do with rather large-magnitude (6.5 to 8) events. Because of the response of the SRO/ASRO network, the energy of the signals used in our analysis is strongly concentrated near a 60-s period (the spectrum is tapered and truncated at a 45-s period). For the events of magnitude above 7, or events with anomalous time function ("slow" earthquakes), it is possible that our results could seriously underestimate the seismic moment. For this reason, we have expanded our procedure to incorporate information contained in records of the ultra-long period IDA (International Deployment of Accelerometers[38]) network. The dynamic range of these instruments is rather small (2048 digital counts), and following a major earthquake the initial portion of the record is distorted. However, these records contain excellent-quality information on excitation of waves with periods greater than 100 s which, depending on the Q of the given mode, may be detected from hours to months (only ${}_0S_0$, really) after an event. In reaching the decision how long a section of record to use, one should recognize the fact that our knowledge of the elastic and anelastic structure of the Earth is imperfect. If, for a $k^{th}$ normal mode, the difference between the actual and computed frequency and attenuation factors of a particular normal mode is $\delta\omega_k$ and $\delta\alpha_k$, the difference between predicted and observed displacements is:

$$\delta u_k \sim t(\delta\omega_k \sin\omega_k t + \delta\alpha_k \cos\omega_k t)\, e^{-\alpha_k t}$$

Thus, for small perturbations, the difference increases linearly with time. The conclusion is that one should use time series beginning as close to the origin time as possible, and minimize their length, providing that all pertinent information about the source properties has been included. In case of IDA data, this minimum length is approximately 3 h: the time required by the slowest mantle waves to travel once around the world. With an unimportant exception of the modes that correspond to nearly vertical ScS reflections, all other modes propagate with higher group velocities, and we are assured that their contributions from both minor and major arc propagation will be included in a 3-h-long segment of a record. It is worthwhile to note that quite different strategy would be advantageous if the purpose of data analysis were to measure functionals of the Earth's structure such as periods of normal modes and their attenuation.

Another important decision is related to the problem of scaling of the information contained in the data from two sets of instruments of very different response. Decision has been made to weigh the records from the IDA network in such a way that, on average, contribution to the system of normal equations of the data from an IDA record would be the same as that of data from a record from an ASRO or SRO station.

Figure III-16 shows distribution of SRO/ASRO and IDA stations that were used in studying the Irpinia earthquake of 23 November 1980. This magnitude 7 earthquake in southern Italy caused death of at least 3,000 persons and destroyed living quarters of 300,000 people. The map is an equidistant azimuthal projection centered on the epicenter. The short-broken lines connect to the epicenter the SRO (squares), ASRO (up-triangles), and DWWSSN stations (down-triangle). The long-broken lines are full great-circles passing through an appropriate IDA station, as, in this case, information on the waves excited in both minor and major arc directions is included.

Figures III-17(a) through (c) show examples of comparison between the observed records (upper trace) and synthetics computed for our solution for the source parameters. The parameter AMAX indicates the SRO digital count for the maximum amplitude for a given pair of stations; the response of DWWSSN and ASRO stations has been appropriately normalized.

The observed and computed traces for the IDA records are shown in Fig. III-18. The parameter DELAY represents the time interval (in hours) between the origin time and beginning of a particular record shown in the figure. The agreement is very good. The dispersion of surface waves in the selected records does not exhibit major differences with respect to the reference model [1066B (see Ref. 39)], but cases of major shifts have been encountered on other occasions.

The very good match of both SRO/ASRO as well as the long-period IDA data has been achieved, in part, by introducing a finite duration of the source: half-time duration of 15 s. The apparent shifts in the origin time of 17 s are very large for an event of this magnitude. This indicates the possibility that this might have been a multiple event.

Table III-5 summarizes our results of inversion for the Irpinia earthquake. Also included in the table are results for the Yugoslavian earthquake of 15 April 1979. This earthquake had a seismic moment very similar to the Irpinia earthquake, but its mechanism was entirely different. While the Irpinia event was a normal fault, the Yugoslavian earthquake was a thrust event. The strikes of both earthquakes are nearly parallel. One might speculate that there is a link between these events on the opposite sides of the Adriatic micro-plate. Figures III-19(a) through (c) and III-20 show comparison between the data and synthetics for the event of 15 April 1979.

TABLE III-5

SOURCE PARAMETERS OF TWO EARTHQUAKES*

| | | 23 November 1980 | 15 April 1979 |
|---|---|---|---|
| NEIS | Origin Time | 18:34:53.3 | 6:19:44.1 |
| | Latitude (°N) | 40.89 | 42.10 |
| | Longitude (°E) | 15.33 | 19.21 |
| Relocation | $\delta t_0$ (s) | 17.1 | 16.6 |
| | Latitude (°N) | 40.73 | 42.12 |
| | Longitude (°E) | 14.97 | 18.68 |
| | Depth (km) | 25 | (10) |
| | Half-Duration (s) | 15 | 15 |
| Scale Factors | $f_1$ | $-3.05 \pm 0.05$ | $2.75 \pm 0.05$ |
| | $f_2$ | $1.08 \pm 0.07$ | $-1.32 \pm 0.06$ |
| | $f_3$ | $1.97 \pm 0.04$ | $-1.43 \pm 0.05$ |
| | $f_4$ | $0.96 \pm 0.16$ | $1.24 \pm 0.14$ |
| | $f_5$ | $-0.94 \pm 0.16$ | $-1.16 \pm 0.17$ |
| | $f_6$ | $-0.48 \pm 0.06$ | $0.77 \pm 0.06$ |
| Principal Axes T-Axis | Moment | 2.47 | 3.28 |
| | Plunge/AZM | 13°/62° | 73°/41° |
| Principal Axes N-Axis | Moment | 0.92 | −0.61 |
| | Plunge/AZM | 6°/331° | 1°/136° |
| Principal Axes P-Axis | Moment | −3.39 | −2.68 |
| | Plunge/AZM | 76°/218° | 17°/226° |

* Relocation parameters and the elements of the moment tensor for the Irpinia earthquake of 23 November 1980 and Yugoslavian earthquake of 15 April 1979. Note that the two earthquakes are of similar size but the elements of their moment tensors are, essentially, opposite in sign. The elements of the moment tensors and the principal values are multiplied by a scale factor of $10^{26}$ dyn-cm. The focal depth of the Yugoslavian earthquake was held fixed at 10 km.

It is interesting to note that the relative contribution of overtones is different for the Italian (depth 25 km) and Yugoslavian (depth 10 km) earthquakes. Even though the difference in depth is relatively small, the actual recordings, as well as synthetics, show substantial increase in the relative amplitude of overtones for the Italian earthquake.

One interesting conclusion of the analysis of these two large, damaging earthquakes is that highly reliable information on the source properties can be obtained from a relatively sparse network. If, in the future, data from globally distributed digital stations were transmitted in real time, it is possible, I think, to obtain information on the size and mechanism of important earthquakes within a few hours after an event. In cases of tsunamogenic earthquakes, this could be used for issuing appropriate warnings. For earthquakes occurring near densely populated areas, estimates of the earthquake size, direction, and length of the fault could be used for early estimates of potential damage and needed aid.

A. M. Dziewonski

## H. EXACT NUMERICAL SOLUTION FOR A PROPAGATING LINE SOURCE AND THE METHOD OF CENTROID LOCATION

The most commonly used mathematical model of an earthquake of finite spatial and temporal dimensions is a propagating line source. This approximation is justified for earthquakes with the fault lengths significantly exceeding their widths. In addition to its practical applications, the model is attractive from a theoretical point of view, because for a radially (vertically) symmetric Earth model variation of displacements in the horizontal plane is described by analytical functions. Thus, it is possible to derive relatively simple expressions for excitation of surface waves or free oscillations generated by such a source. On the other hand, numerical integration is necessary to consider the effect of source propagation in the vertical plane and it is difficult, if not impossible, to examine the functional dependence between the source parameters and radiation of seismic waves.

Generation of surface waves by a propagating line source was first considered by Ben-Menahem,[40] who showed that the spectrum of a wavetrain due to a point source is modified by the directivity factor:

$$\frac{\sin X}{X}\, e^{-iX} \qquad \text{(III-10)}$$

where

$$X = \frac{L\omega}{2C}\left(\frac{C}{v} - \cos\gamma\right) \qquad \text{(III-11)}$$

and L is the fault length, $\omega$ is the frequency, C is phase velocity, v is the velocity of rupture propagation, and $\gamma$ is the angle between the direction of rupture propagation and direction to the receiver.

This expression has been utilized in numerous studies, most notably by Kanamori, who first applied it to the analysis of the excitation of mantle waves generated by the Kurile Islands earthquake of 1963 (Ref. 41) and the Alaskan earthquake of 1964 (Ref. 42), and subsequently to records of many major events of this century.

As the expression (III-10) applies to contribution of a wavegroup for a particular dispersion branch (most frequently fundamental modes) and a specific orbit ($R_3$, for example), it is difficult to use it in the analysis of waveforms corresponding to superposition of numerous, strongly dispersed overtone branches. This used to impose limitations on the type of data that could be applied in studies of the effect of finiteness of the source.

In 1977, Dziewonski and Romanowicz[43] derived an exact solution to the problem of excitation of normal modes by horizontal line source representing a fragment of a great circle. If the coordinate system is rotated such that the fault lies in the equatorial plane with the direction of rupture propagation coincident with the increasing longitude, then the expressions of Gilbert and Dziewonski[39] for the strain at the source can be integrated analytically along the fault length. There is a simple relationship between excitation of a normal mode due to a point source and the line source. The displacement spectrum of the $k^{th}$ mode of angular order number $\ell$ excited by the point source is:

$$\hat{\underline{u}}_k(\underline{r},\omega) = \hat{h}_k(\omega) \sum_{m=-\ell}^{\ell} \underline{s}_k^m \psi_k^m \qquad \text{(III-12)}$$

where $\hat{h}_k(\omega)$ is the spectrum of $h_k(t) = 1 - e^{\alpha_k t} \cos \omega_k t$, and

$$\psi_k^m = \sum_{i=1}^{G} \bar{\epsilon}_{ki}^m(\underline{r}_o) \cdot f_i \qquad \text{(III-13)}$$

with $f_i$ being the six independent elements of the moment tensor, and the strains $\epsilon$ defined by Gilbert and Dziewonski[39] in Eqs. (2.1.19) for spheroidal modes and (2.1.20) for toroidal modes; the vector $\underline{s}$ is defined in Eq. (2.1.1) of that paper. Dziewonski and Romanowicz have shown that the effect of the line source is to modify the excitation parameters $\psi_k^m$ by a frequency-dependent factor:

$$\hat{\psi}_k^m(\omega) = \frac{\sin X_m}{X_m} e^{-iX_m} \psi_k^m \qquad \text{(III-14)}$$

where

$$X_m = \frac{1}{2} \Phi \left( \frac{\omega r_o}{v} + m \right) \qquad \text{(III-15)}$$

and $\Phi$ is the angular extent of the fault, $r_o$ is the source radius, and $v$ is the velocity of rupture propagation. They have also pointed out the similarity between the directivity terms in Eqs. (III-10) and (III-12).

While Eqs. (III-12) and (III-14) provide the means for the exact evaluation of the spectra of normal modes excited by a line source, the frequency-domain representation would be very inefficient in the calculation of synthetic seismograms in applications considered by Dziewonski, Chou, and Woodhouse,[36] who add contributions from roughly 5000 normal modes to obtain a wavetrain composed of long-period body waves.

It may be noted that the spectrum

$$\frac{\sin X_m}{X_m} e^{-iX_m}$$

is the Fourier transform of a function f(t):

$$f(t) = \begin{cases} 0 & , \quad \text{for } t < 0 \\ \frac{1}{2T} \exp[-imvt/r_o] & , \quad \text{for } 0 \leqslant t \leqslant 2T \\ 0 & , \quad \text{for } t > 2T \end{cases}$$

where $T = (1/2)\,\Phi r_o/v$ is the half-duration of the source.

Thus, to account for the finite size of the source, one needs to evaluate the convolution integral:

$$g_m(t) = \frac{1}{2T} \int_o^{\min(t,\,2T)} e^{-imv\tau/r_o} \left[ 1 - e^{-\alpha_k(t-\tau)} \cos \omega_k(t-\tau) \right] d\tau \quad . \tag{III-16}$$

This integral may be readily evaluated analytically. For reasons of numerical efficiency, it is expedient to consider excitation at times greater than 2T (that is, after the fault has stopped), disregard contributions of permanent displacements, approximate through linearization the effect of attenuation during the process of fault propagation, and to change the limits of integration to $(-T, T)$. The result is:

$$g_m(t - T) = e^{-\alpha_k(t-T)} [(A_k^m + B_k^m) \cos \omega_k(t - T) + i(A_k^m - B_k^m) \sin \omega_k(t - T)]$$

where

$$A_k^m = \frac{\sin(\omega_k + \beta_m)\,T}{2(\omega_k + \beta_m)\,T}$$

$$B_k^m = \frac{\sin(\omega_k - \beta_m)\,T}{2(\omega_k - \beta_m)\,T}$$

with $\beta_m = mv/r_o$.

The displacement vector associated with the $k^{th}$ normal mode is thus:

$$\underline{u}_k(\underline{r}, t - T) = e^{-\alpha_k(t-T)} [\underline{C}_k \cos \omega_k(t - T) + \underline{S}_k \sin \omega_k(t - T)] \tag{III-17}$$

where

$$\underline{C}_k = \mathrm{Re} \sum_{m=0}^{\ell} \delta_m \underline{S}_k^m (A_k^m + B_k^m)\, \psi_k^m$$

$$\underline{S}_k = -\mathrm{Im} \sum_{m=0}^{\ell}{}' \delta_m \underline{S}_k^m (A_k^m - B_k^m)\, \psi_k^m \tag{III-18}$$

where $\delta_m$ is the Newman's delta ($\delta_m = 1$ for $m = 0$; $\delta_m = 2$ for $m > 0$) and $\psi_k^m$ are the excitation coefficients of Eq. (III-13) for a point source in the "equatorial" coordinate system. The time shift of T can be applied to the final synthetic seismogram. The advantage of the procedure implied by Eqs. (III-17) and (III-18) over that associated with Eq. (III-14) is that, in the former case, it is necessary to apply summation to $(\ell + 1)$ scalar values while, in the latter case, it would be necessary to add $(\ell + 1)$ spectra, each represented by several hundred values.

The execution time needed for computation of a set of synthetic seismograms for a propagating line source assuming typical coverage of an event by 12 SRO/ASRO three-component stations and 10 IDA vertical component gravimeters is about 25 min. on an Interdata 8/32 computer, some four to five times greater than for the point source – a substantial but not formidable difference.

Equation (III-16) may be modified to evaluate excitation for source time functions other than a boxcar. In general:

$$g_m(t) = \int_0^{\min(t,2T)} a(\tau)\, e^{-im v\tau/r_o} \left[1 - e^{-\alpha_k(t-\tau)} \cos\omega_k(t-\tau)\right] d\tau \qquad \text{(III-19)}$$

where the source function $a(\tau)$ is normalized such that:

$$\int_0^{2T} a(\tau)\, d\tau = 1 \quad .$$

There is a wide class of functions appropriate for representation of the source (i.e., triangle, trapeze) for which integral (III-19) can be evaluated analytically.

It should also be pointed out that, for a given set of parameters related to the rupture propagation, excitation of normal modes remains linear with respect to the zero-frequency components of the moment tensor. Thus, the equations presented here can be readily used, after obvious modifications, in formulation of an inverse problem for the moment tensor of a propagating line source.

The solid lines in Fig. III-21 represent a set of synthetic seismograms for a lone source of a length of 1° of arc (111.2 km) propagating due east with a velocity of 3.3 km/s. The source mechanism is a 45° normal fault at a depth of 15 km with the strike along the east-west axis. All receivers spaced with a 45° step in azimuth are located at a distance of 90° and have response of the SRO instruments. The dotted lines are the difference between the result for propagating line source and the point source at the centroid location, corrected for the finite duration. The effect of the direction of source propagation on amplitudes is clearly discernible. However, the zero-crossings of the difference traces coincide with those of the signal. Thus, a point source at the centroid location accounts very well for the phase shifts associated with the propagating line source. This is explained by the following consideration.

The change in the travel time of a wave with a phase velocity C from the point of origin to a receiver at a distance x is the sum of the perturbation in the origin time: $\delta t_o = L/v$; and the change in the travel time due to the perturbation in the epicentral distance. To the first order: $\delta x = -(1/2)\, L \cos\gamma$, where $\gamma$ is the angle between direction of rupture propagation and direction to the receiver. Thus, the total change in the travel time is

$$\delta t = \frac{L}{2C}\left(\frac{C}{v} - \cos\gamma\right)$$

and the phase shift at a frequency $\omega$:

$$\delta\phi = \omega\,\delta t = \frac{L\omega}{2C}\left(\frac{C}{v} - \cos\gamma\right)$$

an expression identical with Eq. (III-11).

This indicates that the method of centroid location[36] can be used, in principle, to resolve the highly nonlinear problem of the propagating line source, that is to determine the fault length,

velocity, and direction of rupture propagation. This conclusion has been verified by experiments on synthetic data using realistic distribution of receivers. However, in processing actual seismograms one should be aware that the epicentral location as well as the parameters of the centroid may be biased by the effect of lateral heterogeneities.

Perhaps the effects of mislocation and the source size could be resolved by studying many earthquakes of a wide range of magnitudes from the same source region, thus developing an equivalent master event technique. Another possible approach is outlined in Sec. G above.

A. M. Dziewonski

## I. THE EXCITATION OF SEISMIC WAVES BY A SOURCE SPANNING A SURFACE OF DISCONTINUITY

The displacement seismograms due to any seismic source may be written as a function of spatial coordinates $\underline{x}$ and time t (see Refs. 37, 39, and 44)

$$\underline{s}(\underline{x}, t) = \sum_k \underline{s}_k(\underline{x})\, h_k(t) * \psi_k(t) \qquad \text{(III-20)}$$

where the summation is over all normal modes, and where * denotes convolution. The vector fields $\underline{s}_k(\underline{x})$ are the normal mode eigenfunctions, and the time functions $h_k(t)$ are given by

$$h_k(t) = 1 - e^{-\alpha_k t} \cos \omega_k t \qquad \text{(III-21)}$$

where $\omega_k$ and $\alpha_k$ are the eigenfrequency and attenuation constant of the $k^{th}$ mode. The excitation coefficients $\psi_k(t)$ in Eq. (III-20) are

$$\psi_k(t) = \int_{V_s} \bar{\underline{\underline{e}}}^k(\underline{x}') : \dot{\underline{\underline{\Gamma}}}(\underline{x}', t)\, d^3\underline{x}' \qquad \text{(III-22)}$$

where $\underline{\underline{e}}^k$ is the elastic strain in the $k^{th}$ mode (overbar indicates complex conjugation), and $\dot{\Gamma}$ is the glut rate distribution of the source. The spatial integration in Eq. (III-22) is over the source region $V_s$.

This representation of the seismograms, in terms of a superposition of normal modes, is, of course, under suitable approximations, equivalent to representations more often used in body-wave seismology, as has recently been explicitly shown by Chapman and Woodhouse.[45] The results to be presented here are generally applicable and are not restricted to the normal-mode representation.

If the source region $V_s$ is sufficiently small compared with the wavelengths of modes included in Eq. (III-20), it will be an adequate approximation to assume $\underline{\underline{e}}^k(\underline{x})$ to be constant in $V_s$, and Eq. (III-22) then gives the point source approximation

$$\psi_k(t) = \bar{\underline{\underline{e}}}^k(\underline{x}_0) : \underline{\underline{M}}(t) \qquad \text{(III-23)}$$

where $\underline{x}_0$ is a point in $V_s$, and $\underline{\underline{M}}(t)$ is the moment rate tensor of the source

$$\underline{\underline{M}}(t) = \int_{V_s} \dot{\underline{\underline{\Gamma}}}(\underline{x}', t)\, d^3\underline{x}' \quad . \qquad \text{(III-24)}$$

It is the purpose of this contribution to point out that this argument fails if the source region $V_s$ spans a surface of discontinuity, such as the moho, and to investigate the effect of such a circumstance on the excitation of seismic waves and upon the interpretation of moment tensors obtained from inversion. The results presented below show that the seismic radiation from a source spanning a discontinuity is equivalent, in the point source approximation, to that for a particular source placed on one side of the discontinuity, or to that of a different source placed on the other side, and that significantly different moment tensors can be obtained from inversion, depending upon which side of the discontinuity the source is assumed to lie. Neither of these equivalent sources corresponds to the moment rate tensor defined in Eq. (III-24), and it is not possible, in general, to recover the true moment rate tensor unless further assumptions about the source are made. A set of assumptions, which seem reasonable for certain physical situations and which make the inverse problem determinate, is suggested below. An important consequence of this indeterminacy is that constraints, such as that the moment tensor be trace free or that it represent a double-couple, cannot be applied unless one makes such further assumptions, since the constraints will have different effects, depending upon which side of the discontinuity one assumes the source to lie.

Consider a small source region $V_s$ which is divided into two subregions $V_+$, $V_-$ by the surface $\Sigma$, across which the elastic moduli are discontinuous. We shall define a local Cartesian coordinate system in which the $x_1$ direction is normal to $\Sigma$ and denote the six independent components of $\underline{e}^k$ and $\underline{M}(t)$ by[39]

$$e_1 = \bar{e}_{11} \ , \quad e_2 = \bar{e}_{22} \ , \quad e_3 = \bar{e}_{33} \ , \quad e_4 = \bar{e}_{12} \ , \quad e_5 = \bar{e}_{13} \ , \quad e_6 = \bar{e}_{23}$$

$$f_1 = M_{11} \ , \quad f_2 = M_{22} \ , \quad f_3 = M_{33} \ , \quad f_4 = M_{12} \ , \quad f_5 = M_{13} \ , \quad f_6 = M_{23} \ .$$

In place of Eq. (III-23) we now have

$$\psi_k(t) = \underline{e}^+ \cdot \underline{f}^+ + \underline{e}^- \cdot \underline{f}^- \tag{III-25}$$

where $\underline{e}^\pm$ are the strains evaluated on each side of $\Sigma$, and $\underline{f}^\pm$ are source vectors corresponding to the moment rate tensors

$$\underline{M}^\pm = \int_{V_\pm} \dot{\Gamma}(x', t) \, d^3x' \ . \tag{III-26}$$

Because of the required continuity of the modal displacements and tractions across $\Sigma$, $\underline{e}^\pm$ must satisfy certain continuity conditions; the tangential strains $e_2, e_3, e_6$ must be continuous, together with the normal tractions $(\lambda + 2\mu)e_1 + \lambda(e_2 + e_3)$, $2\mu e_4$, $2\mu e_5$, where $\lambda, \mu$ are the Lame parameters. It follows that $\underline{e}^\pm$ in Eq. (III-25) satisfy

$$\underline{A}^+ \underline{e}^+ = \underline{A}^- \underline{e}^-$$

where $\underline{A}^\pm$ are the matrices with nonvanishing elements

$$A^\pm_{11} = \lambda_\pm + 2\mu_\pm \ , \quad A^\pm_{22} = A^\pm_{33} = A^\pm_{66} = 1$$

$$A^\pm_{44} = A^\pm_{55} = 2\mu_\pm \ , \quad A^\pm_{12} = A^\pm_{13} = \lambda_\pm \ .$$

Equation (III-25) may now be written in such a way that it depends only upon $\underline{e}^+$ or only upon $\underline{e}^-$, i.e.,

$$\psi_k(t) = \underline{e}^+ \cdot \underline{F}^+ = \underline{e}^- \cdot \underline{F}^- \tag{III-27}$$

where

$$\left.\begin{aligned} \underline{F}^+ &= \underline{f}^+ + (\underline{A}^{--1}\underline{A}^+)^T \underline{f}^- \\ \underline{F}^- &= \underline{f}^- + (A^{+-1}A^-)^T \underline{f}^+ \end{aligned}\right\} \tag{III-28}$$

where superscript T indicates matrix transposition. It is clear from Eq. (III-27) that the true source is equivalent to the source $\underline{F}^+$ placed on the plus side of $\Sigma$ or to the source $\underline{F}^-$ placed on the minus side of $\Sigma$. $\underline{F}^+$ and $\underline{F}^-$ represent the two different sources which would be obtained from inversion of seismic data under the assumption that the source lay on the plus or the minus side of the discontinuity surface $\Sigma$. Neither of these sources represents the true moment rate tensor components

$$\underline{f} = \underline{f}^+ + \underline{f}^-$$

corresponding to the moment tensor defined in Eq. (III-24). From Eq. (III-27), we find that the equivalent sources $\underline{F}^+, \underline{F}^-$ are related to each other by

$$\underline{A}^{+T-1}\underline{F}^+ = \underline{A}^{-T-1}\underline{F}^- = \underline{A}^{+T-1}\underline{f}^+ + \underline{A}^{-T-1}\underline{f}^- \quad . \tag{III-29}$$

Specifically,

$$\left.\begin{aligned} F_1^+ &= A F_1^- \\ F_2^+ &= F_2^- - B F_2^- \\ F_3^+ &= F_3^- - B F_1^- \\ F_4^+ &= C F_4^- \\ F_5^+ &= C F_5^- \\ F_6^+ &= F_6^- \end{aligned}\right\} \tag{III-30}$$

where

$$\left.\begin{aligned} A &= (\lambda_+ + 2\mu_+)/(\lambda_- + 2\mu_-) \\ B &= (\lambda_- - \lambda_+)/(\lambda_- + 2\mu_-) \\ C &= \mu_+/\mu_- \quad . \end{aligned}\right\} \tag{III-31}$$

For a major discontinuity, such as the moho, or an interface between slow sedimentary strata and basement rocks, the sources $\underline{F}^+, \underline{F}^-$ can differ quite appreciably, both in magnitude and in geometry. Using, for instance, the parameters from the model $1066B^2$ appropriate for the moho, and taking T to indicate above the moho, we find

$$A = 0.545 \quad , \quad B = 0.027 \quad , \quad C = 0.434 \quad .$$

If two solutions are obtained for the moment tensor of a seismic source, one assuming it to lie just above the moho and the other assuming it to lie just below, they are only directly comparable if transformed by the above relations. Furthermore, if $\underline{F}^+$, say, is constrained to represent a source without volume change ($F_1^+ + F_2^+ + F_3^+ = 0$), or to represent a double-couple, then $F^-$ will not have the corresponding property. If the source is explosive, but is near a major discontinuity, it can appear to have a significant deviatoric part.

The true moment tensor components $\underline{f} = \underline{f}^+ + \underline{f}^-$ cannot be determined from the seismic radiation without making further assumptions about the source. One possible assumption would be that $\underline{f}^+, \underline{f}^-$ are proportional, as would be the case, for example, if a single fault cut across the discontinuity. Let us assume, then, that

$$\underline{f}^- = \beta \underline{f} \quad , \quad \underline{f}^+ = (1 - \beta)\, \underline{f} \tag{III-32}$$

where $\beta$ is a parameter representing the fraction of the total moment lying on the minus side of the discontinuity. In this case, we have from Eq. (III-28)

$$\left.\begin{aligned} \underline{F}^+ &= [\bar{\beta} + \beta(\underline{A}^{-1}\underline{A}^+)^T]\, \underline{f} \\ \underline{F}^- &= [\beta + \bar{\beta}(A^{+-1}A^-)^T]\, \underline{f} \end{aligned}\right\} \tag{III-33}$$

where $\bar{\beta} = 1 - \beta$.

Let us suppose that $\underline{F}^+$ is the source obtained from inversion under the assumption that the source lies on the plus side of the discontinuity. Then, Eq. (III-33) gives

$$\left.\begin{aligned} f_1 &= (\bar{\beta} + A\beta)^{-1}\, F_1^+ \\ f_2 &= F_2^+ + \beta B(\bar{\beta} + A\beta)^{-1}\, F_1^+ \\ f_3 &= F_3^+ + \beta B(\bar{\beta} + A\beta)^{-1}\, F_1^+ \\ f_4 &= (\beta C + \bar{\beta})^{-1}\, F_4^+ \\ f_5 &= (\beta C + \bar{\beta})^{-1}\, F_5^+ \\ f_6 &= F_6^+ \end{aligned}\right\} \tag{III-34}$$

where A, B, and C are those given in Eq. (III-31). If it is required to constrain f to represent a source without volume change ($f_1 + f_2 + f_3 = 0$), then the inversion for $\underline{F}^+$ should be carried out under the corresponding constraint

$$(1 + 2\beta)\, F_1^+ + (\bar{\beta} + A\beta)\, (F_2^+ + F_3^+) = 0 \quad . \tag{III-35}$$

Similarly, if $\underline{f}$ is to represent a double-couple the corresponding nonlinear constraint must be translated into a constraint on $\underline{F}^+$.

With the above prescription, inversion for the true moment tensor $\underline{f}$ may be carried out by making only minor modifications to existing inversion algorithms. The result, however, will depend upon the specified parameter $\beta$. If a least-squares procedure is used, these modifications can be performed during the final stage of inversion in which only the inner product matrix

and the corresponding vector are required; thus, many values of $\beta$ may be tried at little computational cost.

J. H. Woodhouse

## J. A LINEAR APPROXIMATION TO THE EFFECT OF FINITE RUPTURE LENGTH AND RUPTURE VELOCITY ON THE RADIATION FROM SEISMIC SOURCES

In our ongoing effort to retrieve from long-period waveform data as much information as possible about seismic sources, it is desirable to incorporate the effect of a finite rupture length and rupture velocity. It should be possible to obtain direct estimates of these quantities by including the extra parameters in our inversion procedure. In order to begin the linearization inversion for the rupture velocity, it is necessary first to have a linear approximation to its effect on the predicted waveforms; it is our purpose here to derive such an approximation.

The extra solution for a rupture of infinitesimal vertical and lateral, but of arbitrary, length, propagating along a great circle, has been given by Dziewonski and Romanowicz[43] and was discussed in Sec. H above. This exact solution, however, does not provide a convenient starting point to obtain the linearized result sought here.

We shall consider a "line source," viewed in a Cartesian coordinate frame in which the rupture propagates along the x-axis. The source will be represented by the glut rate distribution[37]

$$\dot{\underline{\Gamma}}(\underline{x},t) = \frac{1}{2T}\,\delta(x - vt)\,\delta(y)\,\delta(z)\,H(t + T)\,H(T - t)\,\underline{M} \qquad \text{(III-36)}$$

where $\underline{M}$ is the total moment tensor, v is the rupture velocity, assumed constant, and 2T is the source duration. In Eq. (III-36), $\delta(x)$ and $H(x)$ are the Dirac $\delta$-function and the Heaviside step function, respectively. The excitations of free oscillations for this source are obtainable directly from Eq. (III-22) above. On performing the spatial integrations we find, simply,

$$\psi_k(t) = \begin{cases} \frac{1}{2T}\,\underline{M} : \underline{\bar{e}}^k(\underline{x})\Big|_{x=vt,\,y=0,\,z=0} & |t| < T \\ 0 & |t| > T \end{cases} . \qquad \text{(III-37)}$$

We shall now make the approximation that the modal strains $\underline{e}^k(x)$ are sufficiently well approximated along the rupture by the first two terms in their Taylor expansions about the midpoint. We then have

$$\psi_k(t) \simeq \frac{1}{2T}\,M : \left[\underline{\bar{e}}^k(\underline{0}) + vt\,\frac{\partial}{\partial x}\,\underline{\bar{e}}^k(\underline{x})\Big|_{\underline{x}=\underline{0}}\right] \qquad |t| < T \quad . \qquad \text{(III-38)}$$

Convolving with the modal time functions $h_k(t)$, as in Eq. (III-36), we find

$$h_k(t) * \psi_k(t) = \left(1 - \frac{\sin\omega_k T}{\omega_k T}\,e^{-\alpha_k t}\cos\omega_k t\right)\underline{M} : \underline{\bar{e}}^k(\underline{0}) - \frac{v}{\omega}\left(\frac{\sin\omega_k T}{\omega_k T} - \cos\omega_k T\right)e^{-\alpha_k t}\sin\omega_k t\,\underline{M} : \frac{\partial \underline{\bar{e}}^k}{\partial x}(\underline{x})\Big|_{\underline{x}=\underline{0}} \qquad \text{(III-39)}$$

where terms proportional to the small quantity $\alpha_k$ have been neglected.

$$h_k(t) * \psi_k(t) = \left(1 - \frac{\sin \omega_k T}{\omega_k T} e^{-\alpha_k t} \cos \omega_k t\right) \underline{M} : \underline{e}^k$$

$$-\left(\frac{\sin \omega_k T}{\omega_k T} - \cos \omega_k T\right) e^{-\alpha_k t} \sin \omega_k t \frac{v_i}{\omega_k} \underline{M} : \underline{e}^k_{,i} \qquad \text{(III-40)}$$

where $v_i$ are the three components of the rupture propagation velocity vector (summation over i assumed) and where the modal strains $\underline{e}^k$ and strain gradients $\underline{e}^k_{,i}$ are those evaluated at the midpoint of the rupture, which is also the source centroid.[1,37] Similarly, time in Eq. (III-39) is measured relative to the centroid time, namely a time T after the onset of rupture.

A successful inversion procedure for the estimation of the centroid location and time from waveform data has been described in an earlier issue of SATS[1] and the formulas for the strain gradients $\underline{e}^k_{,i}$ in Eq. (III-40) have also been given previously.[1,36] By virtue of Eq. (III-20), Eq. (III-39) provides a direct linear relationship between the predicted waveforms and the components of the rupture velocity vector, and will form the basis for a linearized inversion for these quantities together with an iterative inversion for the half-duration T of the source. This technique will be applied first to synthetic data calculated from the exact solution for a line source as discussed in Sec. H above. It will then be applied to a combined data set consisting of long-period body waves (~16 MHz) from SRO and ASRO records and long-period surface waves (~6 MHz) in IDA records, for a number of earthquakes.

J. H. Woodhouse

## K. THE CALCULATION OF THE COMPLETE NORMAL-MODE SPECTRUM OF THE EARTH USING FINITE DIFFERENCE METHODS

The synthesis of complete long-period seismograms by the superposition of normal modes forms the basis of many seismological studies, and, in particular, forms the basis of some of the studies of the seismic source reported here and in an earlier SATS.[46] Clearly, it is desirable to extend such studies to higher frequencies. The major advantage of this method of synthesis is that it is completely automatic and omits no part of the theoretically predictable seismic signal. To use the method, however, one must have previously calculated a complete catalog of normal-mode eigenfrequencies and eigenfunctions, up to some preassigned limit in frequency. At present, only two complete catalogs are available, comprising the modal data up to 22 MHz for the models 1066A and 1066B,[39] calculated by Buland[47] using a Rayleigh-Ritz procedure.

It is, of course, possible to calculate normal-mode eigenfrequencies and eigenfunctions by solving numerically the radial differential equations, but this method has been incapable of producing a complete catalog of modes in a reasonable computation time since no systematic way of searching for roots of the secular equation has been devised. Simply to scan all frequencies requires such a small frequency step as to make the method quite impracticable. The major advantage of the Rayleigh-Ritz technique is that it converts the problem into a matrix eigenvalue problem, for which a Sturm count can be calculated. Thus, given any two frequencies it is possible to say, without an exhaustive search, how many roots of the secular equation lie between those frequencies. This allows all the roots to be bracketed very efficiently, and convergence on the bracketed roots is then relatively straightforward.

Here, we report that a similar scheme is now available for the differential-equation procedure (if the gravitational perturbation due to the oscillations is neglected) since, as with the Rayleigh-Ritz procedure, we are now able to calculate how many roots of the secular equation lie between two given frequencies simply by integrating twice the system of ordinary differential equations. It is well known that for second-order Sturm-Liouville boundary-value problems, such a count of eigenvalues may be established in terms of the number of zero crossings of some combination of the eigenfunction and its derivative. This method is applicable to toroidal and radial modes, but in these cases the modes are sufficiently well and predictably separated in frequency that it need not be used. Until now there has been no corresponding result for spheroidal modes, which are often extremely closely and unevenly spaced in frequency.

In addition to the difficulty of finding all roots of the secular equation, a further difficulty in using the differential-equation approach is an essential numerical instability in the calculation of the secular determinant. This difficulty has been solved by several authors in different contexts[22,48-50]; the general solution of the problem is to perform calculations in terms of the "minor vectors" of pairs (or triplets) of solutions.[48] A technique for calculating eigenfunctions entirely in terms of such solutions of the minor equations has recently been given by Woodhouse.[51]

The technique to be described here has, as yet, been developed only for the case in which the gravitational perturbation due to the oscillations is neglected. This approximation is probably entirely adequate for frequencies exceeding, say, 10 MHz. At lower frequencies, corrections may be applied for the effects of self-gravitation, or the modal eigenfunctions may be rediagonalized to account for the gravitational perturbation. In practice, the catalogs of Buland[47] were also calculated in this way for reasons of computational economy. The new technique has been used to calculate all spheroidal modes up to a frequency of 35 MHz for the Preliminary Reference Earth Model[52] of Dziewonski and Anderson, including the effects of transverse isotropy in the upper mantle and the frequency-dependent corrections to elastic moduli due to attenuation.[53] The dispersion diagram for angular orders up to 100 is shown in Fig. III-22. The calculation was performed for all angular orders for which the fundamental mode lies below 35 MHz in frequency, namely up to order $\ell = 360$.

We will not go into detail here about how the algorithm for counting eigenvalues was derived. In fact, a rigorous proof of the result is still lacking though we can show that it has several of the properties required of such a count. Here, we shall simply give a recipe for its calculation.

Neglecting the gravitational perturbation, the equations governing spheroidal eigenfunctions may be written[54]

$$\frac{d\underline{b}}{dr} = A(r, \omega, \ell)\, \underline{b} \quad . \tag{III-41}$$

In solid regions of the Earth, Eq. (III-41) is a fourth-order system of ordinary differential equations, and in fluid regions (core and ocean) it is a second-order system. In Eq. (III-41), $r$ is radius, $\omega$ is angular frequency, and $\ell$ is angular order; and the components of $\underline{b}$ are: in solid regions, $b_1 = U$, $b_2 = [\ell(\ell+1)]^{1/2} V$, $b_3 = P$, $b_4 = [\ell(\ell+1)]^{1/2} S$; and in fluid regions, $b_1 = U$, $b_2 = P$ — where U, V, P, and S are functions of $r$ such that the components of the vector displacement field in the Earth are given by†

† The factors of $r$ in these equations differ from the conventions of Phinney and Burridge.[54]

$$
\left.
\begin{aligned}
rs_r &= U(r)\, Y_\ell^m(\Theta,\phi) \\
rs_\Theta &= V(r)\,[\ell(\ell+1)]^{-1/2}\, \partial_\Theta Y_\ell^m(\Theta,\phi) \\
rs_\phi &= -V(r)\,[\ell(\ell+1)]^{-1/2}\, \operatorname{cosec}\Theta\, \partial_\phi Y_\ell^m(\Theta,\phi)
\end{aligned}
\right\} \qquad \text{(III-42)}
$$

and $r, \Theta, \phi$ are spherical polar coordinates. The components of radial traction are

$$
\left.
\begin{aligned}
r\tau_{rr} &= P(r)\, Y_\ell^m(\Theta,\phi) \\
r\tau_{r\Theta} &= S(r)\,[\ell(\ell+1)]^{-1/2}\, \partial_\Theta Y_\ell^m(\Theta,\phi) \\
r\tau_{r\phi} &= -S(r)\,[\ell(\ell+1)]^{-1/2}\, \partial_\phi Y_\ell^m(\Theta,\phi)
\end{aligned}
\right\} \qquad \text{(III-43)}
$$

where $\tau$ is the stress tensor.

At the center of the Earth are two linearly independent solutions $\underline{b}(r)$ which satisfy the appropriate conditions of regularity.[55] When these solutions are integrated to the inner-outer core boundary, there will be a single 2-vector solution in the core satisfying the conditions of continuity of U, P at the inner-core boundary. When this solution is integrated to the core-mantle boundary, there will be two linearly independent solutions in the mantle satisfying the same conditions. Similarly, a single solution in the ocean will satisfy these conditions at the ocean floor, and the secular equation is then obtained by requiring that the normal traction P(r) vanishes at the ocean surface. At other interfaces, $\underline{b}(r)$ is continuous. In solid regions, let us define the minor vector of the two allowable solutions $\underline{b}_1(r), \underline{b}_2(r)$ as

$$
\left.
\begin{aligned}
m_1 &= b_{11} b_{22} - b_{12} b_{21} \\
m_2 &= b_{11} b_{23} - b_{13} b_{21} \\
m_3 &= b_{11} b_{24} - b_{14} b_{21} \\
m_4 &= b_{12} b_{23} - b_{13} b_{22} \\
m_5 &= b_{12} b_{24} - b_{14} b_{22} \\
m_6 &= b_{13} b_{24} - b_{14} b_{23}
\end{aligned}
\right\} \qquad \text{(III-44)}
$$

where the second subscript is used to specify individual elements of $b_1, b_2$.

It may be shown[51] that

$$
m_2(r) + m_5(r) = 0 \qquad \text{(III-45)}
$$

and $\underline{m}(r)$ satisfies a 6th-order system of equations of the form

$$
\frac{d\underline{m}}{dr} = A(r, \omega, \ell)\, \underline{m} \qquad \text{(III-46)}
$$

which, by virtue of Eq. (III-45), immediately reduces to 5th order. It may be shown[51,55] that the eigenvalue problem may be stably solved by integrating Eq. (III-46) in solid regions of the Earth, subject to the requirement of continuity at welded interfaces and to suitable boundary conditions at fluid-solid interfaces. On passing from a solid to a fluid, these are

$$\left.\begin{aligned} b_1 &= m_3 \\ b_2 &= m_6 \end{aligned}\right\} \qquad \text{(III-47)}$$

and on passing from a fluid to a solid

$$\left.\begin{aligned} m_1 &= b_1 \\ m_4 &= -b_2 \\ m_2 &= m_3 = m_5 = m_6 = 0 \end{aligned}\right\} \qquad \text{(III-48)}$$

Let us now define the two functions of radius

$$f_1(r) = \begin{cases} m_6(r) & \text{in solid regions} \\ b_2(r) & \text{in fluid regions} \end{cases} \qquad \text{(III-49)}$$

$$f_2(r) = \begin{cases} m_3(r) - m_4(r) & \text{in solid regions} \\ b_1(r) & \text{in fluid regions} \end{cases} \qquad \text{(III-50)}$$

We can now define the function

$$n(\omega, \ell) = \sum_{r_i} \operatorname{sgn}[f_2(r_i)\, f_1'(r_i)] + \sigma_c + \sigma_\ell \qquad \text{(III-51)}$$

where the summation is over all zeros of $f_1(r)$, and sgn takes values $\pm 1$ according to the sign of its argument. $\sigma_c$ is defined to be 0 or 1 dependent on $f_1^-(b)$, $f_1^{+\prime}(b)$ being positive or negative, where b is the radius of the outer core and superscripts plus and minus indicate that $f_1$ or $f_1'$ is evaluated just outside or just inside the core. The additional quantity $\sigma_\ell$ in Eq. (III-51) is simply unity if $\ell = 1$, and zero otherwise, and is included simply to make this equation concordant with the conventional designation of overtone number.

It is our contention, well validated in numerical tests and indicated by theoretical considerations, that $n(\omega, \ell)$ is the spectral function for the spheroidal mode spectrum. That is to say, $n(\omega, \ell)$ is equal to the overtone number of the mode of largest frequency less than $\omega$. Consequently, the number of eigenfrequencies between two frequencies $\omega_1, \omega_2$ $(\omega_2 > \omega_1)$ is given by $n(\omega_2) - n(\omega_1)$. It is this property which is invaluable in enabling all eigenperiods to be rapidly bounded, and, consequently, a complete catalog to be constructed.

In the calculations for the PREM[52] model, approximately 1.3 evaluations of $n(\omega, \ell)$ per mode were necessary to bracket all roots. A straightforward procedure of linear interpolation and bisection was then employed, using the values of the secular determinant to converge on the roots. This is the more-time-consuming part of the process. The calculation of some 9000 modes took approximately 50 h using an Interdata 8/32 computer. A part of the dispersion diagram is shown in Fig. III-22.

J. H. Woodhouse

## REFERENCES


1. Seismic Discrimination SATS, Lincoln Laboratory, M.I.T. (31 March 1980), DTIC AD-A091107.
2. Ibid. (30 September 1980), DTIC AD-A097999.
3. R. P. Masse, "A Seismic Source Model for Underground Nuclear Explosions," Special Report AFTAC-TR-80-26 (1980).
4. H. J. Patton, "Surface Wave Generation by Underground Nuclear Explosions Releasing Tectonic Strain," Lawrence Livermore Laboratory Report UCRL-53062 (1980).
5. J. A. Mendiguren, "Inversion of Surface Wave Data in Source Mechanism Studies," J. Geophys. Res. 82, 889-894 (1977).
6. P. Burton, "Estimates of 1/Q from Seismic Rayleigh Waves," Geophys. J. R. Astr. Soc. 36, 167-189 (1974).
7. H. Patton and R. G. North, "Crustal and Upper Mantle Structure of the Eurasian Continent from the Phase Velocity and Q of Surface Waves," Rev. Geophys. 18, 605-625 (1980).
8. Seismic Discrimination SATS, Lincoln Laboratory, M.I.T. (31 December 1975), DDC AD-A025777/4.
9. H. Patton, "Reference Point Equalisation Method for Determining the Source and Path Effects of Surface Waves," J. Geophys. Res. 85, 821-848 (1979).
10. R. Blandford, "Experimental Determination of Scaling Laws for Contained and Cratering Explosions," Technical Report SDAC-TR-76-3, Teledyne Geotech, Alexandria, Virginia (1976).
11. K. Aki and M. Bouchon, "Seismic Source Function for an Underground Nuclear Explosion," Bull. Seismol. Soc. Am. 64, 131-148 (1974).
12. D. G. Harkrider, M. N. Toksoz, and A. Ben-Menahem, "Determination of Source Parameters of Explosions and Earthquakes by Amplitude Equalisation of Seismic Surface Waves, I. Underground Nuclear Explosions," J. Geophys. Res. 69, 4355-4365 (1964).
13. H. C. Rodean, "ISC Events from 1964 to 1976 at and Near the Nuclear Testing Ground in Eastern Kazakhstan," Lawrence Livermore Laboratory Report UCRL 52856 (1979).
14. M. N. Toksoz and H. H. Kehrer, "Tectonic Stress Release by Underground Nuclear Explosions and Its Effect on Seismic Discrimination," Geophys. J. R. Astr. Soc. 31, 141-161 (1972).
15. D. L. Springer and R. L. Kinnaman, "Seismic Source Summary for U.S. Underground Nuclear Explosions 1961-70," Bull. Seismol. Soc. Am. 61, 1073-1098 (1971).
16. D. P. Marshall and J. Hudson, "Surface Waves from Underground Nuclear Explosions," Nature 234, 8-9 (1971).
17. K. M. Tubman and M. N. Toksoz, "Structure and Seismic Properties of the Alpine-Himalayan Convergence Zone," in "Research in Seismology (Attenuation and Source Mechanisms)," Final Technical Report, AFOSR Contract #F44620-75-C-0064 (1981).
18. G. P. Bird, "Thermal and Mechanical Evolution of Continental Convergence Zones: Zagros and Himalayas," Ph. D. Thesis, Department of Earth and Planetary Sciences, M.I.T. (1976).
19. H. J. Patton, "Source and Propagation Effects of Rayleigh Waves from Central Asian Earthquakes," Ph.D. Thesis, Department of Earth and Planetary Sciences, M.I.T. (1978).
20. W. P. Chen and P. Molnar, "Constraints on the Seismic Wave Velocity Structure Beneath the Tibetan Plateau and Their Tectonic Implications," J. Geophys. Res. (in press, 1981).

21. J.-W. Teng et al., "Explosion Seismic Study for Velocity Distribution and Structure of the Crust and Upper Mantle from Damxung to Yadong of Xizang Plateau," Proc. Symp. on Qimghai-Xizang Plateau, Peking, 25 May – 1 June 1980, pp. 81-82.

22. A. M. Abo-Zena, "Dispersion Function Computations for Unlimited Frequency Values," Geophys. J. R. Astr. Soc. 58, 91-105 (1979).

23. W. Menke, "Comment on 'Dispersion Function Computations for Unlimited Frequency Values' by Anas Abo-Zena," Geophys. J. R. Astr. Soc. 59, 315-324 (1979).

24. D. Harvey, "Seismogram Syntheses Using Normal Mode Superposition: The Locked Mode Approximation Method," Geophys. J. R. Astr. Soc. (in press, 1981).

25. V. F. Cormier, "The Synthesis of Complete Seismograms in an Earth Model Specified by Radially Inhomogeneous Layers," Bull. Seismol. Soc. Am. 70, 691-716 (1980).

26. F. Press and M. Ewing, "Two Slow Surface Waves Across North America," Bull. Seismol. Soc. Am. 42, 219-228 (1952).

27. R. L. Street, R. B. Herrmann, and O. W. Nuttli, "Spectral Characteristics of the Lg Wave Generated by Central United States Earthquakes," Geophys. J. R. Astr. Soc. 11, 51-64 (1975).

28. I. N. Gupta, B. W. Barker, J. A. Burnetti, and Z. A. Der, "A Study of Regional Phases from Earthquakes and Explosions in Western Russia," Bull. Seismol. Soc. Am. 70, 851-872 (1980).

29. T. C. Chen and P. W. Pomeroy, "Regional Seismic Wave Propagation," Semiannual Technical Report No. 5, Roundout Associates, Stone Ridge, New York (30 June 1980).

30. J. Oliver and M. Ewing, "Higher Modes of Continental Surface Waves," Bull. Seismol. Soc. Am. 18, 33-49 (1958).

31. L. F. Knopoff, F. Schwab, and K. Kausel, "Interpretation of Lg," Geophys. J. R. Astr. Soc. 33, 389-414 (1973).

32. G. F. Panza and G. Calcagnile, "Lg, Li and Rg from Rayleigh Modes," Geophys. J. R. Astr. Soc. 40, 475-487 (1975).

33. H. Kanamori and D. Hadley, "Crustal Structure and Temporal Velocity Change in Southern California," Pageoph. 113, 280-285 (1975).

34. M. Bath, "The Elastic Waves Lg and Rg Along Euroasiatic Paths," Arkiv. Geofys. 2, 295-324 (1954).

35. G. F. Panza, F. A. Schwab, and L. Knopoff, "Channel and Crustal Rayleigh Waves," Geophys. J. R. Astr. Soc. 30, 273-280 (1972).

36. A. M. Dziewonski, T.-A. Chou, and J. H. Woodhouse, "Determination of Earthquake Source Parameters from Waveform Data for Studies of Global and Regional Seismicity," J. Geophys. Res. (in press, 1981).

37. G. E. Backus and M. Mulcahy, "Moment Tensors and Other Phenomenological Descriptions of Seismic Sources – I. Continuous Displacements," Geophys. J. R. Astr. Soc. 46, 341-361 (1976).

38. D. Agnew, J. Berger, R. Buland, W. Farell, and F. Gilbert, "International Deployment of Accelerometers: A Network of Very Long Period Seismology," Trans. Am. Geophys. Union 57, 180-188 (1976).

39. F. Gilbert and A. M. Dziewonski, "An Application of Normal Mode Theory to the Retrieval of Structural Parameters and Source Mechanisms from Seismic Spectra," Philos. Trans. R. Soc. London, Ser. A: A278, 187-269 (1975).

40. A. Ben-Menahem, "Radiation of Seismic Surface Waves from Finite Moving Sources," Bull. Seismol. Soc. Am. 51, 401-435 (1961).

41. H. Kanamori, "Synthesis of Long-Period Surface Waves and Its Applications to Earthquake Source Studies – Kurile Islands Earthquake of October 13, 1963," J. Geophys. Res. 75, 5011-5028 (1970).

42. H. Kanamori, "The Alaskan Earthquake of 1964: Radiation of Long-Period Surface Waves and Source Mechanism," J. Geophys. Res. 75, 5029-5040 (1970).

43. Seismic Discrimination SATS, Lincoln Laboratory, M.I.T. (31 March 1977), DDC AD-A045453/8.

44. F. Gilbert, "Excitation of the Normal Modes of the Earth by Earthquake Sources," Geophys. J. R. Astr. Soc. 22, 223-226 (1971).

45. C. M. Chapman and J. H. Woodhouse, "Symmetry of the Wave Equation and Excitation of Body Waves," Geophys. J. R. Astr. Soc. (in press, 1981).

46. Seismic Discrimination SATS, Lincoln Laboratory, M.I.T. (31 March 1978), DDC AD-A057279.

47. R. P. Buland, "Retrieving the Seismic Moment Tensor," Ph.D. Thesis, University of California, San Diego (1976).

48. J. F. Gilbert and G. E. Backus, "Propagation Matrices in Elastic Wave and Vibration Problems," Geophys. 31, 326 (1966).

49. F. A. Schwab and L. Knopoff, "Fast Surface Wave and Free Mode Computations," Methods in Computational Phys. 11, 87-180 (1972).

50. J. W. Dunkin, "Computation of Modal Solutions in Layered, Elastic Media at High Frequencies," Bull. Seismol. Soc. Am. 55, 335-358 (1965).

51. J. H. Woodhouse, "Efficient and Stable Methods for Performing Seismic Calculations in Stratified Media," in Physics of the Earth's Interior, A. M. Dziewonski and E. Boschi, Eds. (North-Holland, Amsterdam, 1980).

52. A. M. Dziewonski and D. L. Anderson, "Preliminary Reference Earth Model," Phys. Earth Planet. Inter. (in press, 1981).

53. H.-P. Liu, D. L. Anderson, and H. Kanamori, "Velocity Dispersion Due to Anelasticity: Implications for Seismology and Mantle Composition," Geophys. J. R. Astr. Soc. 47, 41-58 (1976).

54. R. A. Phinney and R. Burridge, "Representation of the Elastic-Gravitational Excitation of a Spherical Earth Model by Generalized Spherical Harmonics," Geophys. J. R. Astr. Soc. 34, 451-487 (1973).

55. M. Takeuchi and M. Saito, "Seismic Surface Waves," Methods in Computational Physics 11, 217-295 (1972).

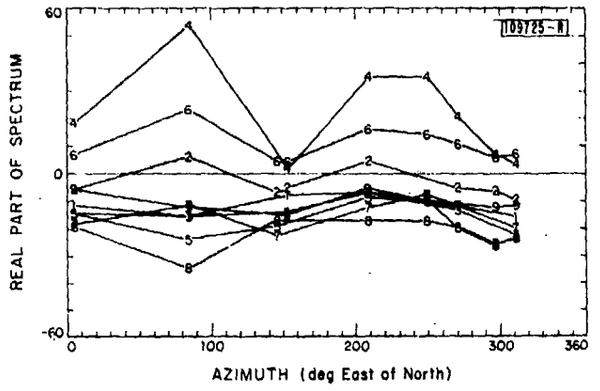


Fig. III-1. Data used in inversion scheme. Real part of spectrum integrated over period range 20 to 45 s after correction back to source, as a function of station azimuth. Numbers correspond to events given in Table III-1.

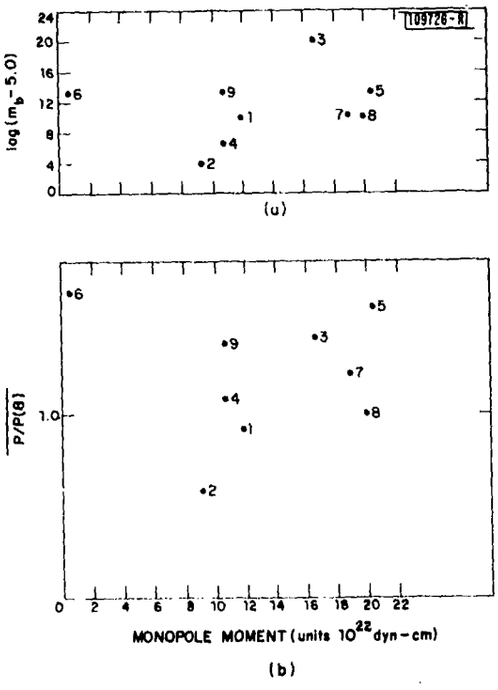


Fig. III-2(a-b). Two comparisons of short-period P-wave amplitudes with deduced monopole component of source (see text).

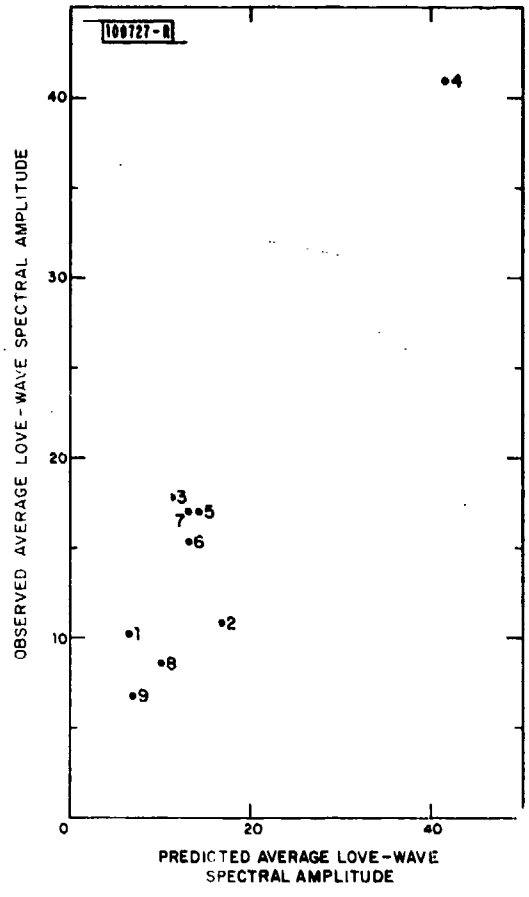


Fig. III-3. Observed azimuthally averaged Love-wave spectral amplitudes compared with that predicted by deduced thrust faulting component of source.

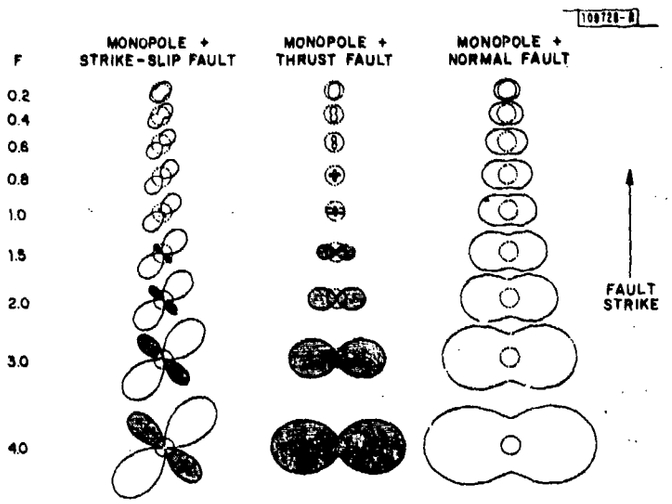


Fig. III-4. Rayleigh-wave patterns resulting from addition of various fault types of moment Q = FE to a monopole of strength E, for different values of F. Dashed circles denote radiation from monopole only. Shaded portions have phase reversed compared with monopole.

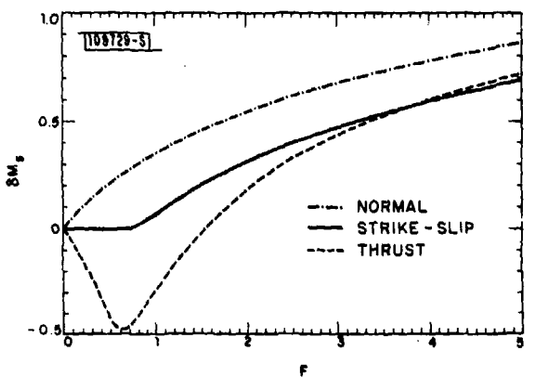


Fig. III-5. Azimuthally averaged effect upon $M_S$ ($M_S$ units) caused by addition of strike-slip, normal, and thrust faulting to a monopole of moment E, as a function of fault moment Q = FE.

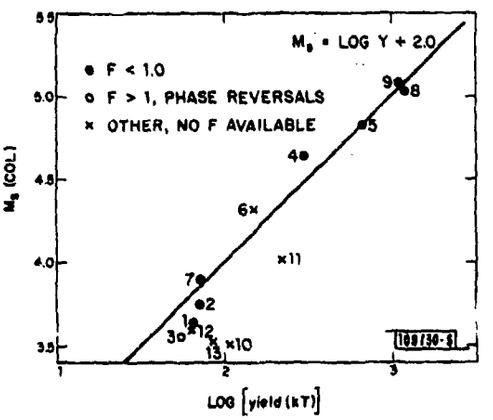


Fig. III-6. $M_S$ measured at COL (College, Alaska) as a function of yield for 13 NTS explosions.

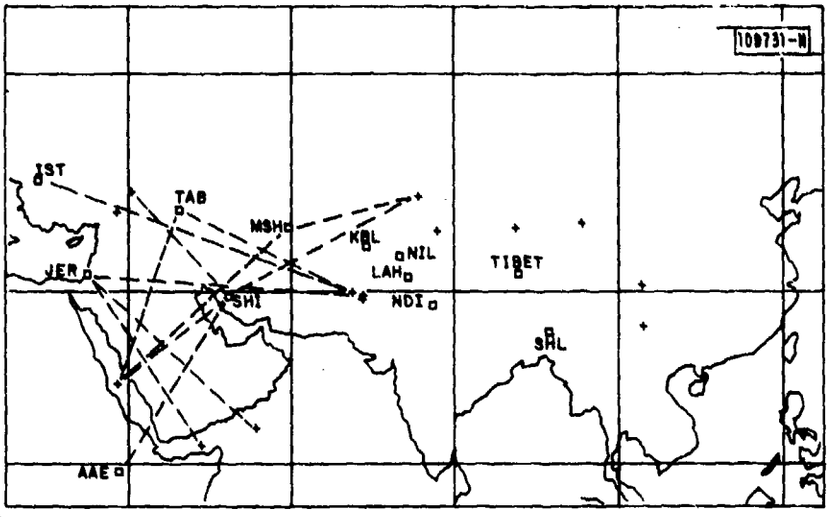


Fig. III-7. Map showing some paths for which velocities are available.

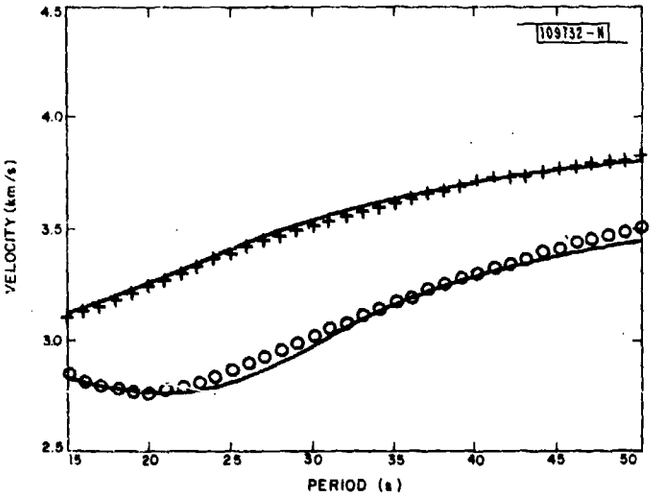


Fig. III-8. Observed phase velocities (+) and group velocities (o) for Iran. Lines are theoretical velocities predicted by derived model.

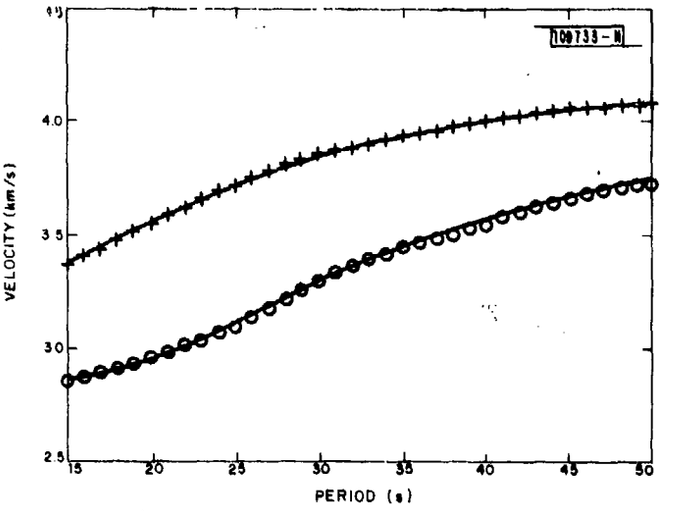


Fig. III-9. Same as Fig. III-8 for Arabian Peninsula.

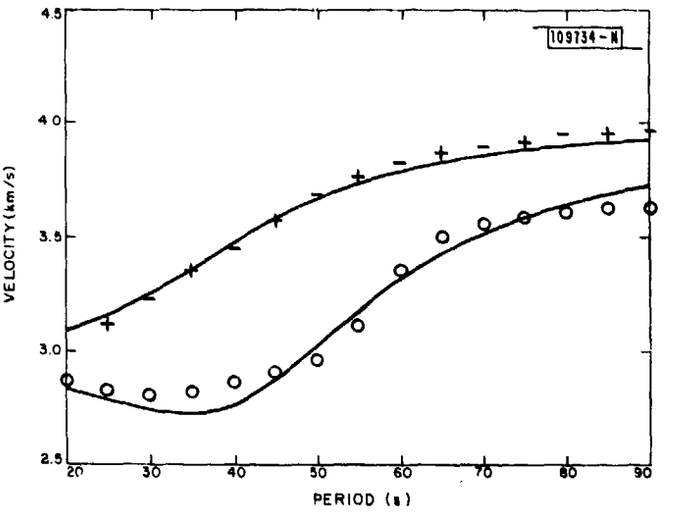


Fig. III-10. Same as Fig. III-8 for Tibet.

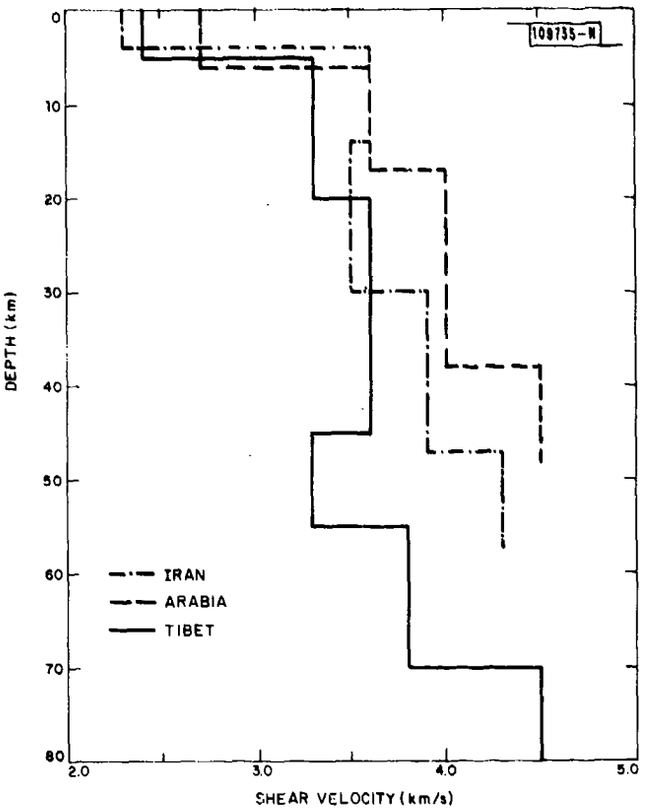


Fig. III-11. Velocity profiles for Iran, Arabia, and Tibet.

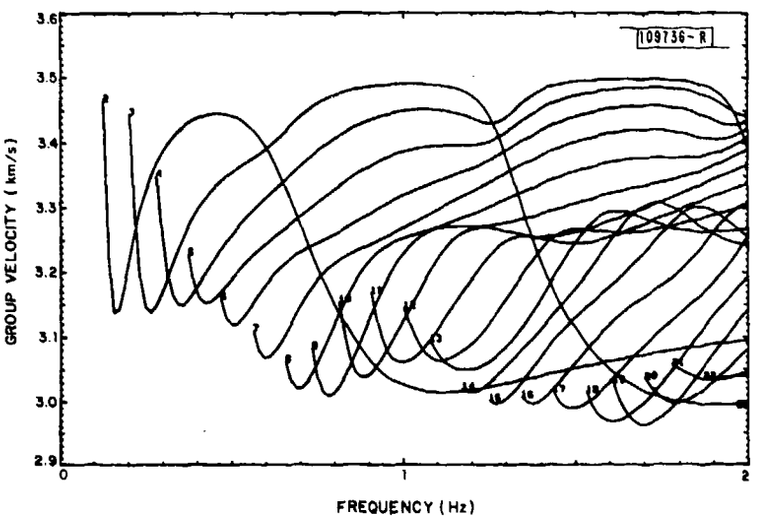


Fig. III-12. Group-velocity dispersion of Lg modes of a Southern California crustal model. Rayleigh-mode numbers are given for each curve.

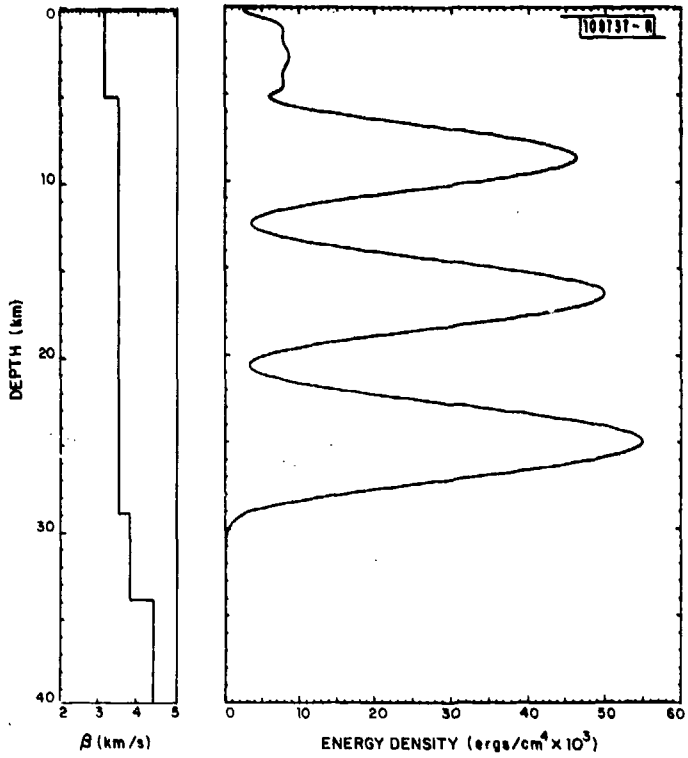


Fig. III-13. Energy density as a function of depth for Rayleigh-mode 6 at 1.6875 Hz. S-velocity profile is shown for comparison.

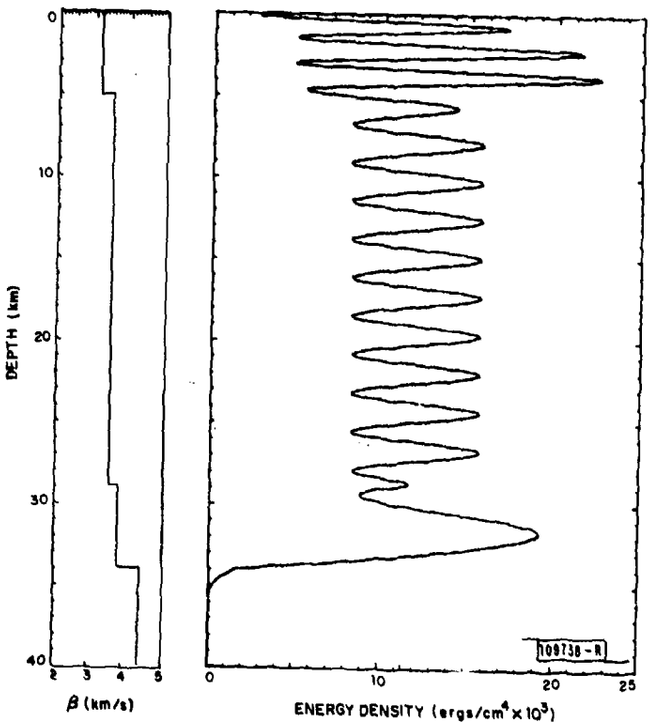


Fig. III-14. Energy density for Rayleigh-mode 15 at 1.75 Hz.

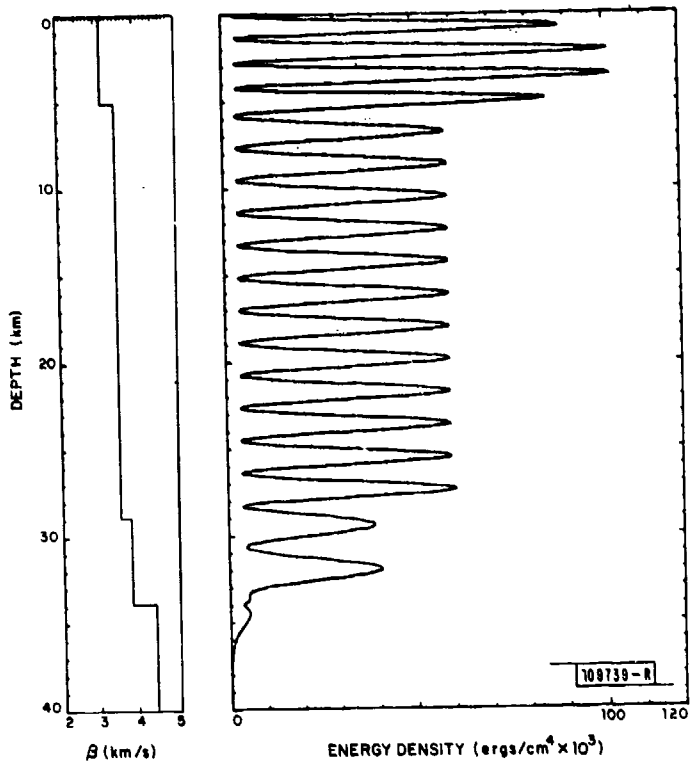


Fig. III-15. Energy density for Rayleigh-mode 19 at 1.6875 Hz.

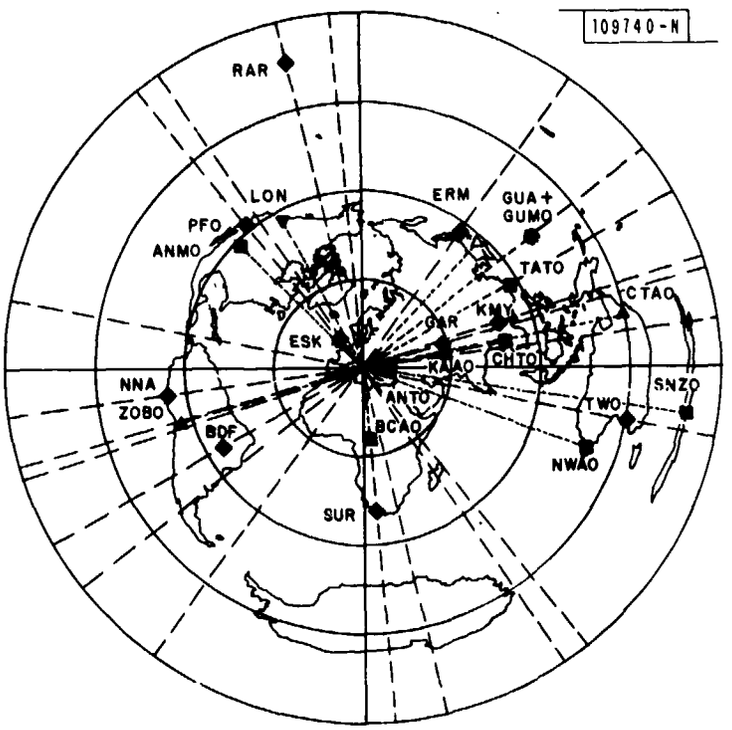


Fig. III-16. Digital network coverage of Irpinia event of 23 November 1980. Squares are SRO stations; upward-pointing triangles, ASRO stations; downward-pointing triangle, first operational DWWSSN station (Longmire, Washington); and diamonds, IDA gravimeters. Both SRO and IDA instruments are operational on Guam.

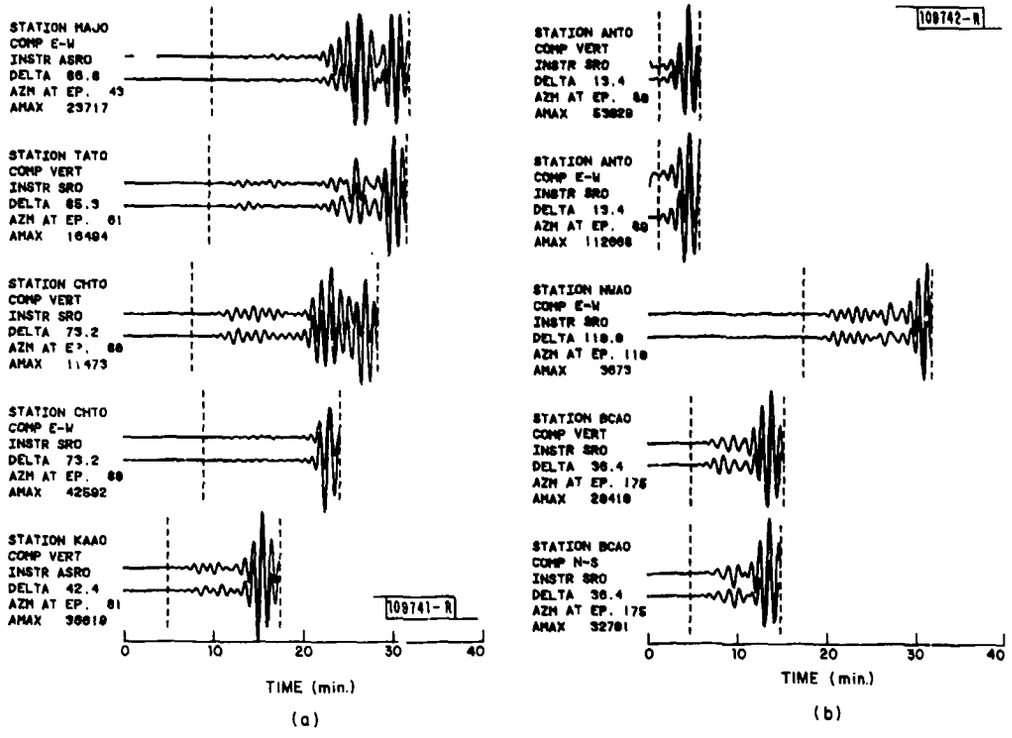


Fig. III-17(a-c). Comparison of observed (top trace) and synthetic seismograms from SRO/ASRO/DWWSSN networks for Irpinia earthquake of 23 November 1980; see Table III-5 for source parameters used to construct the synthetic seismograms. Parameter AMAX is maximum amplitude for a given pair of traces in terms of digital counts of an SRO receiver.

Fig. III-17(a-c). Continued.

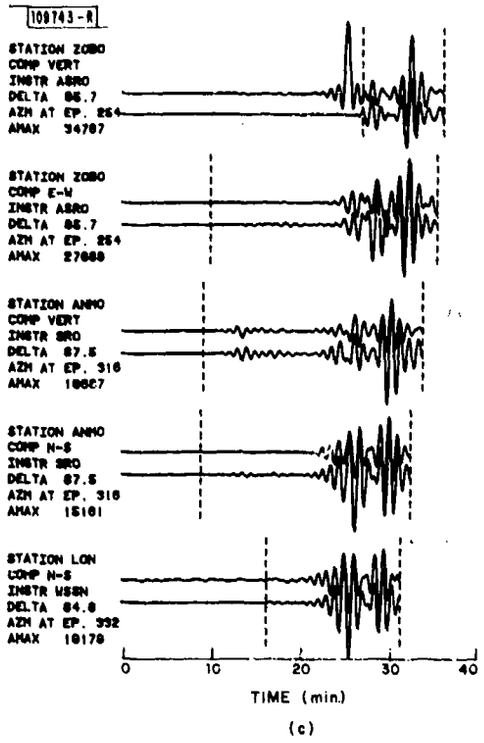


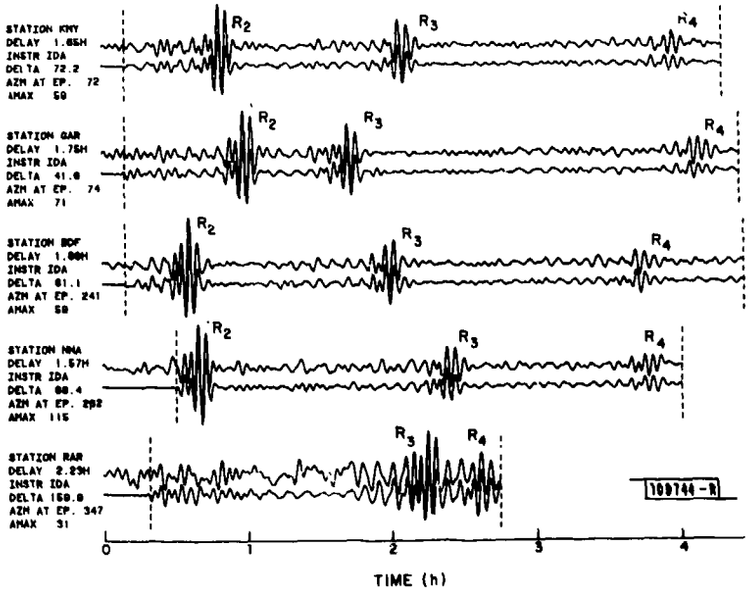


Fig. III-18. Comparison of observed (top trace) and synthetic seismograms from IDA network for Irpinia earthquake. Parameter DELAY is time elapsed between origin and beginning of traces shown. Symbols $R_2$, $R_3$, and $R_4$ describe specific orbits of mantle Rayleigh waves.

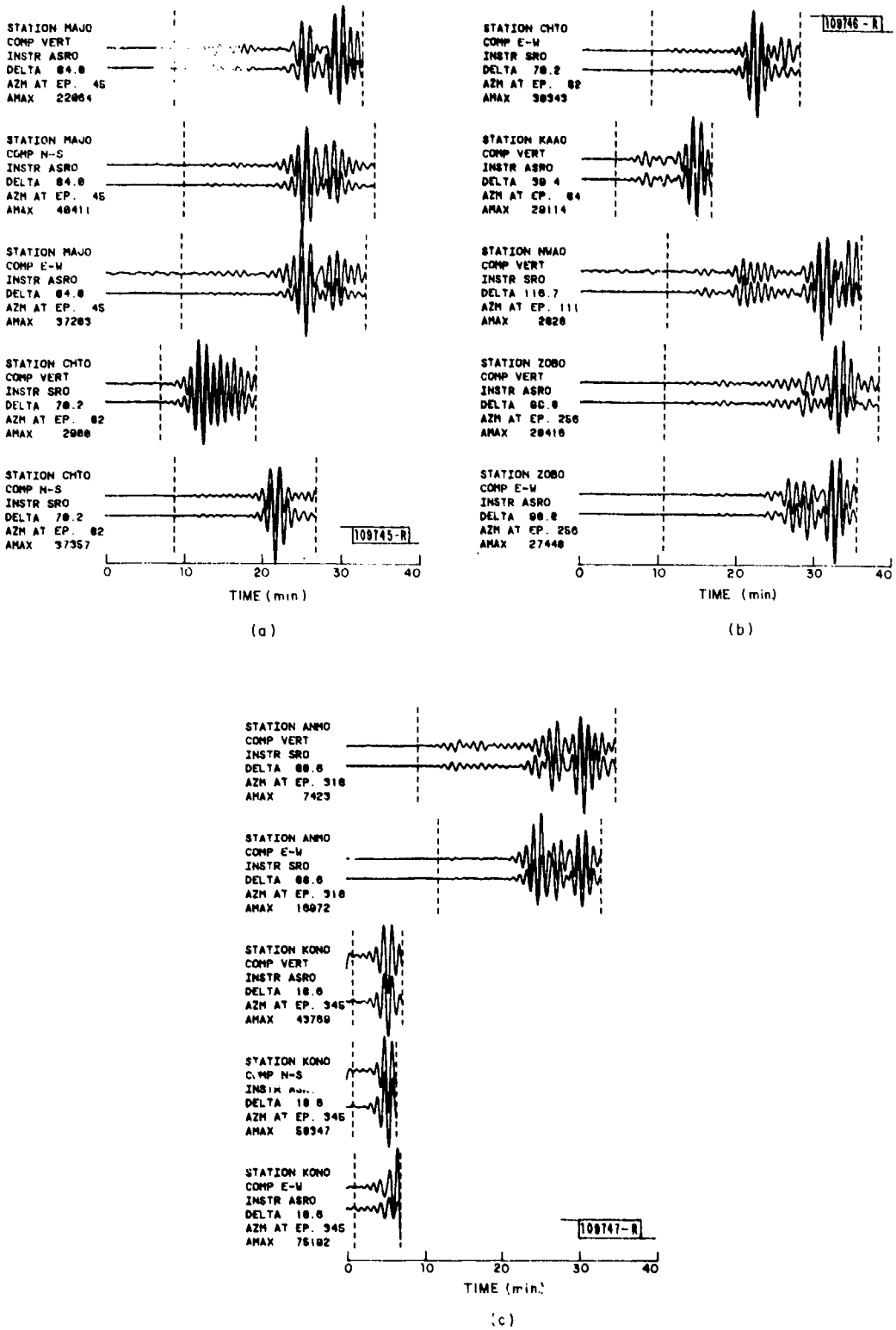


Fig. III-19(a-c). Same as Fig. III-17(a-c) but for event of 15 April 1979.

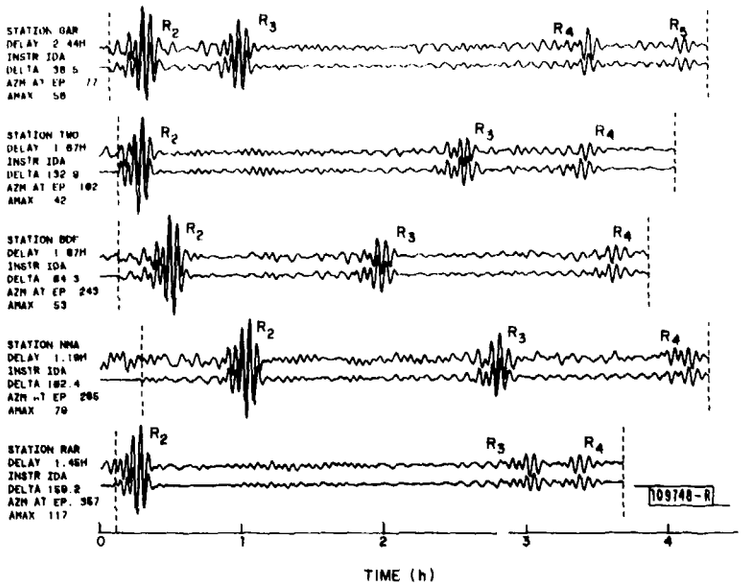


Fig. III-20. Same as Fig. III-18 but for event of 15 April 1979. Because this earthquake was shallower than Irpinia event, relative contribution of overtones is less than that in Fig. III-18.

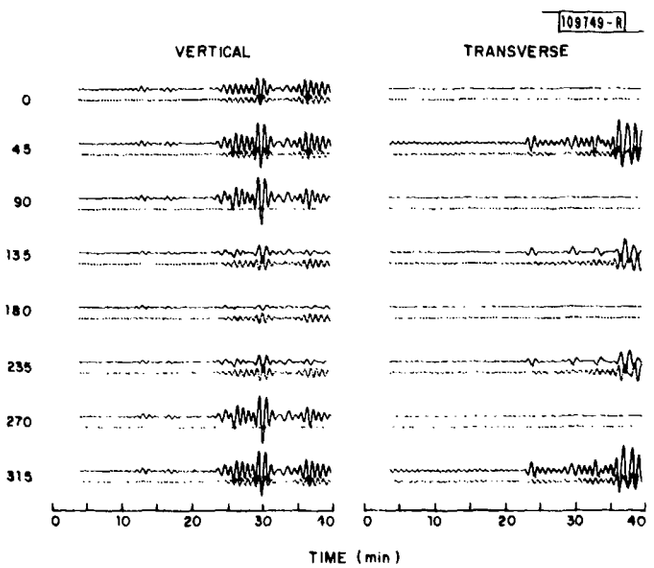


Fig. III-21. Solid lines are synthetic seismograms of long-period body waves (truncated just before the arrival of fundamental modes) for a propagating line source evaluated according to exact method described in text. All modes, except for fundamentals, in periods greater than 45 s were used in calculation (roughly 5000 modes). Dotted line represents difference between exact solution and a solution obtained for point source located at midpoint of fault. Spectrum of point source has been corrected for finite duration. Numbers adjacent to traces indicate azimuth of a receiver in respect to direction of fault propagation. See text for details.

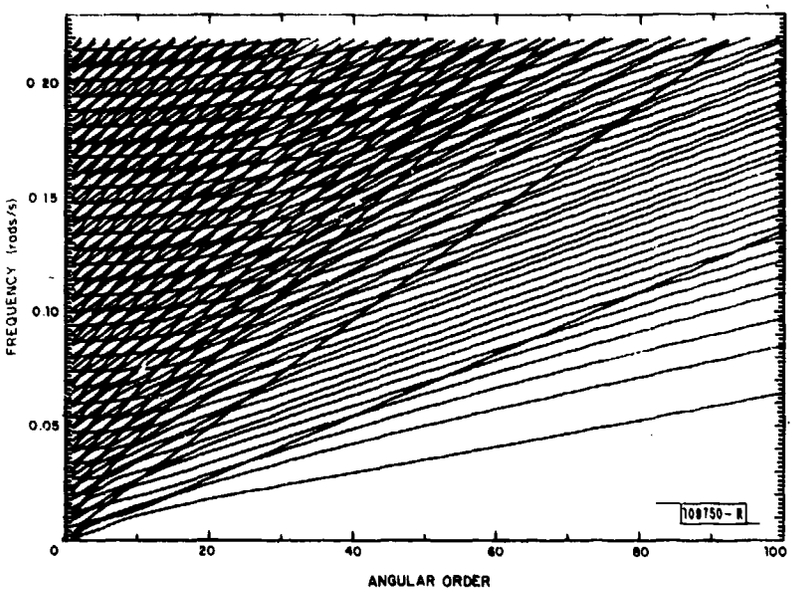


Fig. III-22. Spheroidal dispersion diagram for PREM Earth model.

## GLOSSARY

| | |
|---|---|
| AA | Automatic Association |
| ABAR | Arrival Based Analyst Review |
| A/D | Analog/Digital |
| ASRO | Abbreviated Seismic Research Observatory |
| ATN | Augmented Transition Network |
| bpi | Bits per Inch |
| CCS | California Computer Systems, Inc. |
| CPU | Control and Processing Unit |
| DC | Zero Frequency |
| DEC | Digital Equipment Corporation |
| DOE | Department of Energy |
| DP | Detection Processing |
| DWWSSN | Digital World-Wide Standard Station Network |
| EBAR | Event Based Analyst Review |
| GDSN | Global Digital Seismograph Network |
| GTS | Global Telecommunications System |
| IDA | International Deployment of Accelerometers |
| IDCE | International Data Collection Experiment |
| IESD | International Exchange of Seismic Data |
| I/O | Input-Output |
| ISC | International Seismological Center |
| LRSM | Long-Range Seismic Measurements |
| LTA | Long-Term Average |
| MARS | Multiple-Arrival Recognition System |
| NEIS | National Earthquake Information Service |
| NSS | National Seismic Station |
| NTS | Nevada Test Site |
| PDE | Preliminary Determination of Epicenters |
| RAM | Random Access Memory |
| rms | Root Mean Square |
| RST | Remote Seismic Terminal |
| RSTN | Regional Seismic Test Network |

| | |
|---|---|
| SAS | Seismic Analysis Station |
| SATS | Semiannual Technical Summary |
| SDAC | Seismic Data Analysis Center |
| SDC | Seismic Data Center |
| SDCS | Seismic Data Collection System |
| SDC-V1 | Version 1 of Prototype SDC |
| SPZ | Short-Period, Vertical Component |
| SRO | Seismic Research Observatory |
| STA | Short-Term Average |
| UC | University of California |
| USGS | U. S. Geological Survey |
| WMO | World Meteorological Organization |
| WWSSN | World-Wide Standard Station Network |

UNCLASSIFIED

SECURITY CLASSIFICATION OF THIS PAGE *(When Data Entered)*

| REPORT DOCUMENTATION PAGE | | READ INSTRUCTIONS BEFORE COMPLETING FORM |
|---|---|---|
| 1. REPORT NUMBER<br>ESD-TR-81-84 | 2. GOVT ACCESSION NO.<br>AD-A109 184 | 3. RECIPIENT'S CATALOG NUMBER |
| 4. TITLE *(and Subtitle)*<br>Seismic Discrimination | | 5. TYPE OF REPORT & PERIOD COVERED<br>Semiannual Technical Summary<br>1 October 1980 31 March 1981 |
| | | 6. PERFORMING ORG. REPORT NUMBER |
| 7. AUTHOR*(s)*<br>Michael A. Chinnery | | 8. CONTRACT OR GRANT NUMBER*(s)*<br>F19628-80-C-0002 |
| 9. PERFORMING ORGANIZATION NAME AND ADDRESS<br>Lincoln Laboratory, M.I.T.<br>P.O. Box 73<br>Lexington, MA 02173 | | 10. PROGRAM ELEMENT, PROJECT, TASK AREA & WORK UNIT NUMBERS<br>ARPA Order 512<br>Program Element No. 62714E<br>Project No. 1A10 |
| 11. CONTROLLING OFFICE NAME AND ADDRESS<br>Defense Advanced Research Projects Agency<br>1400 Wilson Boulevard<br>Arlington, VA 22209 | | 12. REPORT DATE<br>31 March 1981 |
| | | 13. NUMBER OF PAGES<br>106 |
| 14. MONITORING AGENCY NAME & ADDRESS *(if different from Controlling Office)*<br>Electronic Systems Division<br>Hanscom AFB<br>Bedford, MA 01731 | | 15. SECURITY CLASS. *(of this report)*<br>Unclassified |
| | | 15a. DECLASSIFICATION DOWNGRADING SCHEDULE |

16. DISTRIBUTION STATEMENT *(of this Report)*

Approved for public release; distribution unlimited.

17. DISTRIBUTION STATEMENT *(of the abstract entered in Block 20, if different from Report)*

18. SUPPLEMENTARY NOTES

None

19. KEY WORDS *(Continue on reverse side if necessary and identify by block number)*

| | | |
|---|---|---|
| seismic discrimination | surface waves | NORSAR |
| seismic array | body waves | ARPANET |
| seismology | LASA | |

20. ABSTRACT *(Continue on reverse side if necessary and identify by block number)*

This Semiannual Technical Summary describes the Lincoln Laboratory Vela Uniform program for the period 1 October 1980 through 31 March 1981. Section I describes progress in the development of a prototype Seismic Data Center. This development is on schedule, and a first version of the prototype will be operational during the next six months. Section II describes a series of activities in the development and implementation of the seismic processing techniques that will be utilized in the prototype system. Section III describes a series of investigations in General Seismological Research.

DD FORM 1 JAN 73 1473 EDITION OF 1 NOV 65 IS OBSOLETE

UNCLASSIFIED

SECURITY CLASSIFICATION OF THIS PAGE *(When Data Entered)*

☆ U.S. GOVERNMENT PRINTING OFFICE: 1981 500-000/38